



FAKULTÄT FÜR VERFAHRENS-
UND SYSTEMTECHNIK



MAX-PLANCK-INSTITUT
FÜR DYNAMIK KOMPLEXER
TECHNISCHER SYSTEME
MAGDEBURG



PHYSIKALISCH-CHEMISCHE
GRUNDLAGEN
DER PROZESSTECHNIK

Exploitation of temperature and solvent gradients in preparative liquid chromatography

Dissertation

zur Erlangung des akademischen Grades

Doktoringenieur (Dr. -Ing.)

von **M. Eng. Xinghai An**

geb. am 27. Jan. 1989 in Jilin, China

genehmigt durch die Fakultät für Verfahrens- und Systemtechnik
der Otto-von-Guericke-Universität Magdeburg

Promotionskommission:

Prof. Dr. rer. nat. Jan von Langermann	(Vorsitz)
Prof. Dr. -Ing. Andreas Seidel-Morgenstern	(Gutachter)
Prof. Dr. -Ing. Christof Hamel	(Gutachter)
Prof. Dr. -Ing. Dorota Antos	(Gutachter)

eingereicht am 05.09.2023

Promotionskolloquium am 11.12.2023

Abstract

Despite chromatography has become a relatively mature separation technology, progress has never stopped, e.g. via exploiting new degrees of freedom to improve performance and cost-effectiveness. Among them, gradients are considered as attractive options to deal with difficult separation problems when normal approaches are not able to meet desired performance. Owing to simplicity and controllability, solvent gradients are widely used in liquid chromatography and temperature gradients in gas chromatography. However, the potential of applying temperature gradients in liquid chromatography has not been fully explored.

This work focuses on theoretical design and experimental validation of temperature and solvent gradients in preparative liquid chromatography followed by an evaluation of the potential for gradient combinations. A ternary separation characterised by a relative wide retention time spectrum was chosen as the model problem. In this scenario, a component falls behind in the chromatogram compared to the other two components, which leads to a rather long cycle time connected with a low productivity. By applying gradients, migration velocities of components can be individually manipulated in order to reduce this long cycle time and, thus, to increase the productivity.

In this study, a rapid and general design tool for gradients based on equilibrium theory was utilised to generate graphical solutions. Space-time diagrams illustrate migration paths of components under the isocratic/isothermal conditions and influence of gradients. These paths are governed by thermodynamics and can be quantified by adsorption isotherms. As a key information, characteristic times can be identified for gradients to be applied in the repetitive batch chromatography mode. These specific switch times are crucial to optimise the separation regimes to reduce the cycle time.

In the first part, isotherm parameters of the three components of a model system were determined focusing on the linear range for certain ranges of temperatures and modifier fractions. These equilibrium constants allow predicting ideal separation performance using the physical planes based on equilibrium model. For more realistic predictions, the equilibrium dispersion model was used to generate numerically chromatograms by taking experimentally determined kinetic parameter into account. To be close to reality, the nonideality of implementing gradients was analysed for both temperature and

solvent gradients using simplified sub-models. Kinetic effects and gradient nonidealities provide criteria to introduce safety margins regarding the operating parameters.

In a second part, the model was validated through experiments by finding a good agreement between predicted and measured retention behaviour under gradient conditions.

Finally, an overall comparison between temperature and solvent gradients was given. Each gradient has its own merits and drawbacks, and therefore, a proper combination can have a synergistic effect. Some potential combinations were suggested. The approaches and tools developed in this thesis were found to be useful. They can be extended to other gradient types, isotherm courses and mixtures.

Zusammenfassung

Chromatographie ist als Trenntechnologie bereits relativ ausgereift. Dennoch hat der Fortschritt niemals aufgehört, z. B. hinsichtlich der Nutzung neuer Freiheitsgrade zur Verbesserung von Leistung und Kosteneffektivität. Insbesondere Gradienten gelten als attraktive Option zur Lösung vieler Trennprobleme, wenn normale Ansätze die gewünschte Leistung nicht ermöglichen. Aufgrund ihrer Einfachheit und Steuerbarkeit werden Lösungsmittelgradienten in der Flüssigchromatographie und Temperaturgradienten in der Gaschromatographie häufig eingesetzt. Das Potenzial von Temperaturgradienten in der Flüssigchromatographie ist jedoch noch nicht ausreichend erforscht worden.

Diese Arbeit konzentriert sich auf die theoretische Auslegung und die experimentelle Validierung von Temperatur- und Lösungsmittelgradienten in der präparativen Flüssigkeitschromatographie, gefolgt von einer Bewertung des Potenzials von Gradientenkombinationen. Eine Trennung dreier Komponenten, die durch ein relativ breites Retentionszeitspektrum charakterisiert sind, wurde als Modellproblem gewählt. In dem betrachteten Szenario fällt eine Komponente im Vergleich zu den anderen beiden Komponenten im Chromatogramm zurück, was zu einer großen Zykluszeit und damit verbunden zu einer geringen Produktivität führt. Durch die Anwendung von Gradienten kann die Migrationsgeschwindigkeit jeder Komponente individuell beeinflusst werden, um lange Zykluszeiten zu reduzieren und somit Produktivitäten zu erhöhen.

Im Rahmen dieser Arbeit wurde ein schnelles und allgemein gültiges Entwurfswerkzeug, das auf dem Gleichgewichtsmodell der Chromatographie basiert, für die Beschreibung von Gradienten verwendet, um grafische Lösungen zu entwickeln. Geeignete Darstellungen in Raum-Zeit-Koordinaten veranschaulichen die Migrationswege von Komponenten unter den isokratischen/isothermen Bedingungen und dem Einfluss von Gradienten. Diese Wege werden durch die Thermodynamik bestimmt, welche mittels Adsorptionsisothermen beschrieben wird. So können Schlüsselinformationen bezüglich der charakteristischen Zeiten bei Gradientenentwürfen für einen repetitiven Batch-Chromatographie-Modus identifiziert werden. Insbesondere die spezifischen Schaltzeiten sind entscheidend für die Optimierung der Trennprozesse, vor allem für die Reduktion von Zykluszeiten.

Im ersten Teil der Arbeit wurden die Isothermenparameter für drei Modellkomponenten im linearen Bereich für bestimmte Temperatur und Lösungsmittelzusammensetzungen ermittelt. So gelang es, den Prozessverlauf in der physikalische Ebenen auf Basis des Gleichgewichtsmodells vorherzusagen. Für realistische Vorhersagen wurde das Gleichgewichts-Dispersionsmodell verwendet, um Chromatogramme numerisch zu erzeugen. Dabei wurden experimentell bestimmte kinetische Parameter berücksichtigt. Nichtidealitäten von umgesetzten Temperatur- und Lösungsmittelgradienten wurden analysiert, um der Realität näher zu kommen. Kinetische Effekte und Nichtidealitäten von Gradienten liefern wichtige Kriterien, um erforderliche Sicherheitsparameters abzuschätzen.

Im zweiten Teil wurde das Modell validiert durch Experimente, in denen eine gute Übereinstimmung zwischen vorhersagtem und gemessenem Retentionsverhalten unter Gradientenbedingungen gefunden wurde.

Abschließend wurde ein Vergleich zwischen Temperatur- und Lösungsmittelgradienten gegeben. Dabei hat jeder Gradient seine Vor- und Nachteile. Daher kann eine geeignete Kombination eine synergistische Wirkung haben. Es wurden einige potenzielle Kombinationen vorgeschlagen. Die entwickelten Ansätze und Werkzeuge in dieser Arbeit erwiesen sich als anwendbar und können auf andere Gradiententypen, Isothermenverläufe und Gemische erweitert werden.

Preface

The reported thesis work was financially supported by Max Planck Society and carried out in the group Physical and Chemical Foundations of Process Engineering at Max Planck Institute for Dynamics of Complex Technical Systems Magdeburg in Germany.

This work was partly performed in collaboration with Adnan Hayat, a PhD candidate from the Institute for Analysis and Numerics at Otto von Guericke University. The analytical solutions and numerical solutions were contributed by this partner. A fruitful collaboration has been reached to understand temperature gradients in liquid chromatography both in theoretical and experimental aspects.

Parts of outcomes and findings in this work have been published in the following two scientific journals, where cited reference numbers are given. The former was focused on theoretical parts, whereas the latter on experimental parts.

[81] A. Hayat, X. An, S. Qamar, G. Warnecke, A. Seidel-Morgenstern, Theoretical analysis of forced segmented temperature gradients in liquid chromatography, *Processes*. 7 (2019) 1–19.

[83] X. An, A. Hayat, J.W. Lee, S. Qamar, G. Warnecke, A. Seidel-Morgenstern, Analysis and experimental demonstration of temperature step gradients in preparative liquid chromatography, *J. Chromatogr. A*. 1665 (2022) 462831.

Contents

List of figures	i
List of tables	ix
Nomenclature	xi
Chapter 1. Introduction	15
1.1 Developments in chromatography	15
1.2 Gradient chromatography	16
1.3 Goal of study and structure of the thesis	20
Chapter 2. Theoretical background	23
2.1 Basic concepts in chromatography and phases involved	23
2.2 Adsorption isotherm.....	25
2.3 Mass balances of chromatographic columns.....	26
2.3.1 Equilibrium model.....	27
2.3.2 Trajectories of chromatograms in the physical plane	28
2.3.3 Equilibrium dispersion model	30
2.3.4 Kinetics: Plate number and efficiency	30
2.3.5 Nonideality of implementing stepwise solvent profiles	33
2.4 Energy balances of chromatographic columns	34
2.4.1 Ideal model	34
2.4.2 Complete energy balance	34
2.4.3 Short-cut energy balance	35
2.5 Cycle time and productivity	38
Chapter 3. Case study and experimental system	43
3.1 Model components and adsorption system	43
3.2 Experimental setup for implementing gradients.....	45
3.3 Measurement of extra-column parameters	49
3.4 Calibrating sensors	51
3.4.1 UV Detector calibration	51
3.4.2 Calibrating measured temperature.....	53
3.5 Estimation of kinetic effect in column.....	54
3.6 Estimation of Henry's constants.....	54
Chapter 4. Determined parameters for the case study	55
4.1 Extra-column parameters of the chromatographic system.....	55
4.2 Calibration parameters	57
4.3 Kinetic parameters of column	58

4.4 Thermodynamic parameters	59
4.4.1 Effect of temperature on Henry's constant	59
4.4.2 Effect of modifier fraction on Henry's constant	60
4.4.3 Combined effect of temperature and modifier fraction	61
4.5 Parameters of short-cut model in energy balance	64
4.5.1 Plausibility test for X_1	66
Chapter 5. Quantitative description of chromatograms under gradient conditions	69
5.1 Isothermal and isocratic operations of ternary mixture	69
5.2 Repetitive chromatography under gradient operations	71
5.3 Temperature gradient	72
5.3.1 Ternary separation by certain operating regimes	72
5.3.2 Nonideality of implementing stepwise temperature profiles	79
5.4 Solvent gradient	80
5.4.1 Linear solvent gradients	80
5.4.2 Stepwise solvent gradients	81
5.5 Protocol to predict chromatograms using EM and EDM	86
5.6 Summary of procedure for predicting chromatograms	87
Chapter 6. Experimental demonstration and model validation	89
6.1 Illustration of selected chromatograms under certain conditions	89
6.2 Chromatograms under reference condition	90
6.3 Temperature gradients	91
6.3.1 Single component wide injection	91
6.3.2 Ternary mixture separation	96
6.4 Solvent gradients	100
6.5 Summary of performance evaluation	104
Chapter 7. Further improvements and productivity comparison	107
7.1 Improved gradients based on simulation	107
7.2 Overall performance comparison	110
Chapter 8. Conclusion and outlook	113
References	117
Appendix	129
Appendix 1 Single component behaviour under gradient conditions	129
Appendix 2 Henry's constants	132
Appendix 3 Derivation of analytical solution for short-cut energy balance	134
Appendix 4 Characteristic times	135

List of figures

Figure 1-1 Classification of gradients according to different criteria. Bold texts indicate the selected options for the presented system.	17
Figure 1-2 Possible functional dependences of solvent gradients expressed via x_{mod}	18
Figure 1-3 Demonstration of the effect of a linear solvent gradient [50].	18
Figure 1-4 General applications of gradients by taking ternary separations as an example. The Scenarios 1 and 2 are termed as partly lagged separations.	20
Figure 2-1 Demonstration of the chromatographic process. The three different colours indicate the ternary mixture.	23
Figure 2-2 Internal structure of in a chromatographic column characterised by various volumes [29].	23
Figure 2-3 Chromatogram characterised by various times connected with system column and component.	24
Figure 2-4 Typical isotherms and their elution profiles [29]. Effect of volume overload is also shown.	25
Figure 2-5 Single component behaviour under isothermal and isocratic conditions. Bottom: physical plane, which is the solution of Eq. (2-10); Top: corresponding ideal chromatogram (dashed) and real chromatogram (solid) at column outlet.	28
Figure 2-6 Migration behaviour under temperature gradient (left) and solvent gradient (right). Green and red blocks refer to reference temperature at $TR = 25\text{ }^{\circ}\text{C}$ and a higher temperature, respectively. White and grey blocks refer to the reference modifier fraction at $x_{mod,R} = 0.5$ and a higher value, respectively. The black dashed lines indicate the gradient lines at switch time t_i^*	29
Figure 2-7 Demonstration of the Van Deemter curve [116].	31
Figure 2-8 Demonstration of an elution profile following Gaussian distribution.	32
Figure 2-9 Approximation of nonideal stepwise solvent profile.	33
Figure 2-10 Effect of X_1 on the temperature profile at outlet by Eq. (2-57). $V=0.3$ ml/min, $X_2=0.003\text{ s}^{-1}$	37
Figure 2-11 Effect of X_2 on the temperature profile at outlet by Eq. (2-57). $V=0.3$ ml/min, $X_1=0.13$	37

Figure 2-12 Effect of the flow rate V on the temperature profile at outlet by Eq. (2-57). $X_1=0.13, X_2=0.003 \text{ s}^{-1}$	37
Figure 2-13 Illustration of the cycle time in a ternary mixture.....	39
Figure 2-14 Effect of theoretical plate number on the cycle time. The chromatograms are generated by Eq. (2-34).....	39
Figure 2-15 Demonstration of various separation scenarios.....	40
Figure 3-1 Results of volume overload experiments for checking linearity of isotherm. $c_{inj,n}=[0.949, 0.948, 0.956] \text{ g/L}$, $V_{inj}=50, 400 \mu\text{L}$. An injection volume of 1500 μL C7 was injected as single solute (solid line). $V=0.3 \text{ ml/min}$	45
Figure 3-2 Schematic diagram of experimental set-up for solvent and segmented temperature gradients. It is an extension of a typical HPLC with an external temperature modulation unit consisting of water jacket and thermostats. The modifier fraction x_{mod} is modulated by a proportioning valve built in the HPLC. The temperature is modulated at the second segment in the water jacket to low or high temperatures, $T_{segment II} = T \in \{TL, TH\} \text{ } ^\circ\text{C}$. The temperatures are measured in real time at a position inside the water jacket inlet T_w , and at the other position on the outer surface of the column outlet line T_{mes} . Both modulations are characterised by switch times t_i^*, k . As already mentioned above, the flow rates provided by the pump was fixed at $V=0.3 \text{ ml/min}$	47
Figure 3-3 Real experimental set-up for solvent and segmented temperature gradients. 1- Thermostats; 2-Switching valves; 3- T_w ; 4- T_{mes}	48
Figure 3-4 Schematic diagram for various times of extra-column. The entire path includes from the confluence point of mixer to the detector flow cell.	51
Figure 3-5 Demonstration of different ranges of detector response [29].....	52
Figure 3-6 Schematic temperature profile along the column in case of heating. The measured outlet temperature is not equal the true temperature so that a calibration procedure is required.....	53
Figure 3-7 Experimental set-up for calibrating measured temperature.....	54
Figure 4-1 Marker experiments to determine t_{plant} , t_0 and ε_t at $V=0.3 \text{ ml/min}$. $V_{inj}=50 \mu\text{L}$	55
Figure 4-2 Step response experiment to determine t_{delay} . The responses at injection valve positions of mainpass and bypass are compared. The flow rate was fixed at $V=0.3 \text{ ml/min}$	56

Figure 4-3 Illustration of solvent profile after step changes and fitted curve by Eq. (2-35) for determining gradient deviation time ΔtG in Figure 2-9.	56
Figure 4-4 Detector calibration using a staircase plateau method for C7 as an example. Blue, red, green, purple and yellow correspond to the wavelength 240, 260, 280, 300, 320 nm, respectively.....	58
Figure 4-5 Theoretical plate number N_p according to temperature at $x_{mod,R}=0.5$ (left) and modifier fraction at $T_R=298$ K (right) using Eq. (2-33).....	59
Figure 4-6 Van't Hoff plot, $\ln(k_H/k_{H,R})$ vs $1/T$, for C5 (triangle), C6 (circle) and C7 (square). $V=0.3$ ml/min, $V_{inj}=50$ μ L, $x_{inj}=0.1$ vol%, $x_{mod}=0.5$	60
Figure 4-7 LSS plot, $\ln(k_H)$ vs x_{mod} , for C5 (triangle), C6 (circle) and C7 (square). $V=0.3$ ml/min, $V_{inj}=50$ μ L, $x_{inj}=0.1$ vol%, $T=298$ K.	61
Figure 4-8 Combined dependence of temperature and modifier fraction by Eq. (2-9) for C5. Left: function of temperature; Right: function of modifier fraction. The temperature range from 278 K to 333 K whereas the modifier fraction from 0.3 to 0.5. The arrow indicates the increasing direction.	62
Figure 4-9 Combined dependence of temperature and modifier fraction by Eq. (2-9) for C6. Left: function of temperature; Right: function of modifier fraction. Applied ranges are same as in Figure 4-8.....	62
Figure 4-10 Combined dependence of temperature and modifier fraction by Eq. (2-9) for C7. Left: function of temperature; Right: function of modifier fraction. Applied ranges are same as in Figure 4-8.....	63
Figure 4-11 Comparison of temperature profiles before and after calibration, heating (left) and cooling (right) between 278 K and 333 K. The normalised time tau (τ) is defined in Eq. (2-54). The profile by analytical solution using Eq. (2-57) with $X_1=0.5$, $X_2=0.003$ s ⁻¹ was also plotted.	65
Figure 4-12 Influence of flow rate V on the temperature profile. Left: $X_1=0.13$ from experiments; Right: $X_1=0.24$ from physical data. The normalised time tau (τ) is defined in Eq. (2-54). The profile is generated by Eq. (2-57) with $X_2=0.003$ s ⁻¹	67
Figure 4-13 Effect of X_1 and V on γ_{end} in Eq. (4-12).	68
Figure 5-1 Trajectories of chromatograms in the physical plane for ternary separation under isothermal and isocratic operation with two consecutive injections. Middle: Physical plane. Red, green and blue pathways correspond to component C5, C6 and C7, respectively. Each component has two pathways for front and rear bands, and their difference is injection period	

Δt_{inj} . The cycle time is denoted above. The left axis at top and bottom subplots correspond to solvent profile (black line) at column inlet and outlet, respectively. The right axis at top subplot is temperature profile (purple line). The right axis at bottom is flow rate profile (cyan line). $T=25$ °C, $x_{mod}=0.5$. Henry's constants are from Table 4-7. $V=0.3$ ml/min, $V_{inj}=400$ μ L. $\Delta t_b=[2.0, 5.4, 0, 2.0, 5.4]$ min, $\Delta t_{cyc}=11.4$ min..... 70

Figure 5-2 Trajectories of chromatograms in the physical plane for ternary separation under isothermal and isocratic operation at $T_H=60$ °C, $x_{mod,R}=0.5$ with two consecutive injections. $V=0.3$ ml/min, $V_{inj}=400$ μ L. $\Delta t_b=[1.0, 3.0, 0, 1.0, 3.0]$ min, $\Delta t_{cyc}=8$ min. 71

Figure 5-3 Illustration of chromatograms in the physical plane according to the boundary of Henry's constants. Left: temperature gradients at $x_{mod,R}=0.5$; Right: solvent gradients at $T_R=298$ K. 72

Figure 5-4 Temperature gradients by conservative regime. The green, blue and red blocks indicate modulated temperature at T_R , T_L and T_H , respectively. 73

Figure 5-5 Possible routes of the last eluting component in conservative regime for temperature gradients..... 74

Figure 5-6 Temperature gradients by improved regime. The green, blue and red blocks indicate modulated temperature at T_R , T_L and T_H , respectively. 76

Figure 5-7 Possible routes of the first eluting component in improved regime for temperature gradients..... 76

Figure 5-8 Possible routes of the last eluting component in improved regime for temperature gradients..... 78

Figure 5-9 Temperature gradients by conservative regime using nonideal temperature profile. The non-ideal temperature profile at outlet (purple line) is shown at the top. Henry's constants are calculated by Eq. (2-9). Temperature profile is generated by Eq. (2-57). 79

Figure 5-10 Example of linear solvent gradient. The solvent profiles at inlet and outlet are shown at bottom and top, respectively. $T=25$ °C, $x_{mod}=[0.5, 0.7]$. Henry's constants are calculated by Eq. (2-9). $V=0.3$ ml/min, $V_{inj}=400$ μ L. $t_i^*=[0, 8]$ min, $\Delta t_b=[0.8, 1.5]$ min, $\Delta t_{cyc}=4.4$ min..... 81

Figure 5-11 2-step solvent gradient. The white and grey blocks indicate modulated modifier fraction at $x_{mod,1}$ and $x_{mod,2}$ respectively..... 82

Figure 5-12 3-step solvent gradient. The white and darkening grey blocks indicate modulated modifier fraction at $x_{mod,1}$, $x_{mod,2}$ and $x_{mod,3}$ respectively..... 84

Figure 5-13 Summary of tasks to predict chromatograms and performance for gradient and isocratic/isothermal conditions.....	88
Figure 6-1 Illustration of chromatograms for three selected isothermal and isocratic conditions. Top: T_R and $x_{mod,R}$; Middle: T_H and $x_{mod,R}$; Bottom: T_R and $x_{mod,H}$	90
Figure 6-2 Chromatograms under isothermal and isocratic operation. Left: EM (solid line) and EDM (dashed line); Right: EDM (dashed line) and experimental profile (black solid line). The corresponding physical plane is in Figure 5-1. $T=T_R=25$ °C, $x_{mod}=x_{mod,R}=0.5$, $V=0.3$ ml/min, $V_{inj}=400$ µL. Henry's constants are from Table 4-7.	90
Figure 6-3 Migration behaviour under temperature gradients when $tRf < t^* < tRr$. Right bottom: physical plane. Green, blue and red colours refer to the temperature at T_R , T_L and T_H , respectively. The grey block indicates modulated temperature. Top: chromatogram at column outlet; Left: column internal profile showing solute distribution between mobile and stationary phases.....	92
Figure 6-4 Experimental validation of single component (C7) retention behaviours under temperature gradients. Top: $t^*=0$ corresponding to scenario in A. Fig. 1; Middle: $tRr(z = fzLc) < t^* \leq tRf(z = Lc)$ corresponding to scenario in A. Fig. 3; Bottom: $tRf < t^* < tRr$ corresponding to scenario in Figure 6-3. Solid lines: experimental profiles; dashed lines: numerical solutions. The lines in green, blue and red indicate the temperature at $T_R=25$ °C, $T_L=5$ °C and $T_H=60$ °C. $x_{mod}=0.5$, Henry's constants are from Table 4-7. $V=0.3$ ml/min, $V_{inj}=1500$ µL.	95
Figure 6-5 Experimental validation of ternary separation under temperature gradients by conservative regime. Lines in red, green and blue correspond to component C5, C6 and C7, respectively. Elution profiles: EM and EDM; Temperature profiles: ideal step gradients. Coloured solid lines: EM; Coloured dashed lines: EDM; Black solid lines: experiment (EXP). Top: profiles from EM and EDM; Middle: trajectories of chromatograms in the physical plane. The blocks in green, blue and red indicate the temperature at $T_R=25$ °C, $T_L=5$ °C and $T_H=60$ °C; Bottom: profiles from EDM and EXP. $x_{mod}=0.5$, Henry's constants are from Table 4-7. $V=0.3$ ml/min, $V_{inj}=400$ µL.	97

Figure 6-6 Experimental validation of ternary separation under temperature gradients by improved regime. Lines in red, green and blue correspond to component C5, C6 and C7, respectively. Elution profiles: EM and EDM; Temperature profiles: ideal step gradients. Coloured solid lines: EM; Coloured dashed lines: EDM; Black solid lines: experiment (EXP). Top: profiles from EM and EDM; Middle: trajectories of chromatograms in the physical plane. The blocks in green, blue and red indicate the temperature at $T_R=25\text{ }^\circ\text{C}$, $T_L=5\text{ }^\circ\text{C}$ and $T_H=60\text{ }^\circ\text{C}$; Bottom: profiles from EDM and EXP. $x_{mod}=0.5$, Henry's constants are from Table 4-7. $V=0.3\text{ ml/min}$, $V_{inj}=400\text{ }\mu\text{L}$ 99

Figure 6-7 Elution profiles for consecutive four injections under isothermal condition and temperature gradient by improved regime. Top: isothermal operation at T_R ; Bottom: gradient operation by improved regime, $T_R=25\text{ }^\circ\text{C}$, $T_L=5\text{ }^\circ\text{C}$ and $T_H=60\text{ }^\circ\text{C}$. The solid line corresponds to chromatogram at left axis. The dashed and dotted lines at right axis correspond to measured temperature T_w and T_{mes} , respectively. The cycle time is the difference between $tinjk = 2$ and $tinjk = 3$. $x_{mod}=0.5$, $V=0.3\text{ ml/min}$, $V_{inj}=400\text{ }\mu\text{L}$ 100

Figure 6-8 Experimental validation of ternary separation under 2-step solvent gradients. Lines in red, green and blue correspond to component C5, C6 and C7, respectively. Elution profiles: EM and EDM; Solvent profiles: ideal step gradients. Coloured solid lines: EM; Coloured dashed lines: EDM; Black solid lines: experiment (EXP). Top: profiles from EM and EDM; Middle: trajectories of chromatograms in the physical plane. The blocks in white and grey indicate the modifier fraction at 0.5 and 0.7; Bottom: profiles from EDM and EXP. No consecutive injections were carried out. $T=25\text{ }^\circ\text{C}$, Henry's constants are from Table 4-7. $V=0.3\text{ ml/min}$, $V_{inj}=400\text{ }\mu\text{L}$ 102

Figure 6-9 Experimental validation of ternary separation under 3-step solvent gradients. Lines in red, green and blue correspond to component C5, C6 and C7, respectively. Elution profiles: EM and EDM; Solvent profiles: ideal step gradients. Coloured solid lines: EM; Coloured dashed lines: EDM; Black solid lines: experiment (EXP). Top: profiles from EM and EDM; Middle: trajectories of chromatograms in the physical plane. The blocks in white, bright grey and dark grey indicate the modifier fraction at 0.5, 0.6 and 0.7; Bottom: profiles from EDM and EXP. No consecutive injections

were carried out. $T=25\text{ }^{\circ}\text{C}$, Henry's constants are from Table 4-7. $V=0.3$ ml/min, $V_{inj}=400\text{ }\mu\text{L}$103

Figure 7-1 Optimal regime of temperature gradients. $T=[5, 60]\text{ }^{\circ}\text{C}$, $x_{mod}=0.5$, $t_i^*=[0, 9, 12, 17.9, 20.8]$ min, $\Delta t_b=[1.4, 3.3, 0, 1.4, 3.3]$ min, $\Delta t_{cyc}=8.9$ min.....107

Figure 7-2 Optimal regime of temperature gradients with modified spatial segmentation. $f_z=0.8$, $T=[5, 60]\text{ }^{\circ}\text{C}$, $x_{mod}=0.5$, $t_i^*=[0, 9, 11.9, 17, 19.9]$ min, $\Delta t_b=[1.4, 2.7, 0, 1.4, 2.7]$ min, $\Delta t_{cyc}=8$ min.....108

Figure 7-3 Modified negative solvent gradients at high temperature. $T=60\text{ }^{\circ}\text{C}$, $x_{mod}=[0.4, 0.5]$, $t_i^*=[10, 12.8, 17.3, 19.1, 21.8, 26.3]$ min, $\Delta t_b=[1.1, 3.1, 0, 1.1, 3.1]$ min, $\Delta t_{cyc}=8.9$ min.109

Figure 7-4 Combined temperature and solvent gradients. $T=[5, 60]\text{ }^{\circ}\text{C}$, $x_{mod}=[0.5, 0.7]$, $t_i^*(T)=[0, 9, 12, 15.9, 18.9]$ min, $t_i^*(x_{mod})=[0, 5.8, 6.8, 12.6, 13.6]$ min, $\Delta t_b=[1.4, 2.1, 0, 1.4, 2.1]$ min, $\Delta t_{cyc}=6.8$ min.....110

List of tables

Table 3-1 Model components and their properties.	44
Table 3-2 Chromatographic system and reference conditions in this study.	45
Table 3-3 Reference conditions and ranges for solvent and temperature gradients used in this study.....	48
Table 4-1 Summary of column and extra-column parameters.....	57
Table 4-2 Selected parameters for detector calibration in Eq. (3-2).	58
Table 4-3 Parameters for calibrating measured temperature in Eq. (3-4) at different flow rate V	58
Table 4-4 Summary of parameters from Van't Hoff model in Eq. (2-7).	60
Table 4-5 Summary of parameters from LSS model in Eq. (2-8).	61
Table 4-6 Isotherm parameters for the combined model in Eq. (2-9).	62
Table 4-7 Specific values of Henry's constants using Eq. (2-9).	63
Table 4-8 Specific values of selectivity, corresponding to Table 4-7.	64
Table 4-9 Parameters of short-cut energy balance as a function of flow rate and thermal operations.....	65
Table 4-10 Physical data to check plausibility of parameter X_1	66
Table 6-1 Performance of temperature and solvent gradients.	105
Table 7-1 Summary of predicted performance of all gradients in EM (parts already in Table 6-1).	112

Nomenclature

Latin symbols

Symbol	Definition	Unit
A_c	Cross-sectional area of the column	cm^2
A^L	Liquid phase heat transfer area	cm^2
A^S	Solid phase heat transfer area	cm^2
C_p^L	Liquid phase heat capacity	$Jg^{-1}K^{-1}$
C_p^S	Solid phase heat capacity	$Jg^{-1}K^{-1}$
c	Mobile phase concentration	g/l
c_{thres}	Threshold concentration	g/l
c_{in}	Concentration at column inlet	g/l
c_{inj}	Injection concentration	g/l
c_{max}	Concentration height after gradients	g/l
D_{app}	Apparent dispersion coefficient	cm^2/min
$D_{c,i}$	Inner diameter of the column	cm
$D_{c,o}$	Outer diameter of the column	cm
d_p	Particle diameter of stationary phase	μm
F	Phase ratio for mass transfer	–
F^T	Phase ratio for heat transfer	–
f_{calb}^λ	Detector calibration factor at wavelength λ	$g/mAU \cdot ml$
f_z	Segmentation factor	–
g_1	Parameter for gradient deviation time in Eq. (2-35)	min^{-1}
g_2	Parameter for gradient deviation time in Eq. (2-35)	min
ΔH_A	Heat of adsorption	kJ/mol
k_H	Henry coefficient	–
Δk_H^{rel}	Relative change of Henry coefficient	–
L_c	Length of the column	cm
N_p	Theoretical plate number	–
Pr	Productivity per column volume, Eq. (2-71)	$g \cdot h^{-1}L^{-1}$
ΔPr^*	Normalised productivity, Eq. (2-75)	$g \cdot h^{-1}L^{-1}$
q	Stationary phase concentration	g/l
R	Ideal gas constant	$kJ \cdot mol^{-1}K^{-1}$
Sig	Detector signal	mAU
T	Temperature	$^\circ C$

T_R	Reference temperature	$^{\circ}\text{C}$
T_L	Lower limit of temperature	$^{\circ}\text{C}$
T_H	Higher limit of temperature	$^{\circ}\text{C}$
T_0	Initial temperature	$^{\circ}\text{C}$
T_w	Water temperature	$^{\circ}\text{C}$
ΔT^{rel}	Relative change of temperature	—
t	Time	<i>min</i>
t_i^*	Switch time	<i>min</i>
Δt_i^*	Relative switch time	<i>min</i>
t_{inj}^{k+}	Start time for next injection	<i>min</i>
Δt_{inj}	Injection period	<i>min</i>
Δt_{cyc}	Cycle time	<i>min</i>
Δt_{extra}	Extra time	<i>min</i>
$\Delta t_b^{(n,n+1)}$	Band break between components	<i>min</i>
Δt_{safe}	Safety time	<i>min</i>
Δt_{tot}	Total production time	
Δt_G	Gradient deviation time	<i>min</i>
t_0	Column dead time	<i>min</i>
t_{plant}	Plant dead time	<i>min</i>
t_{delay}	Delay time	<i>min</i>
t_R	Retention time	<i>min</i>
u	Interstitial velocity	<i>cm/min</i>
u_c	Migration velocity	<i>cm/min</i>
V_c	Column volume	<i>ml</i>
V_{inj}	Injection volume	<i>ml</i>
\dot{V}	Volumetric flow rate	<i>ml/min</i>
V_{plant}	Extra-column volumes of the plant	<i>ml</i>
V_{delay}	Extra-column volumes of the delay	<i>ml</i>
V_{int}	Interstitial volume	<i>ml</i>
V_{ads}	Adsorbent volume	<i>ml</i>
V_{solid}	Solid volume	<i>ml</i>
V_{pore}	Pore volume	<i>ml</i>
w	Bandwidth	<i>min</i>

$w_{0.5}$	Peak width at its half height	<i>min</i>
X_1	Parameter of energy balance in Eq. (2-56)	—
X_2	Parameter of energy balance in Eq. (2-56)	s^{-1}
x	Normalised axial coordinate	—
x_{inj}	Injection volume fraction	—
x_{mod}	Modifier fraction	—
$x_{mod,R}$	Reference modifier fraction	—
$x_{mod,L}$	Lower limit of modifier fraction	—
$x_{mod,H}$	Higher limit of modifier fraction	—
Δx_{mod}^{rel}	Relative change of modifier fraction	—
z	Space coordinate	<i>cm</i>
z^*	Segmented position	<i>cm</i>

Greek Symbols

α_n	Sensitivity constant in LSS model	—
$\alpha^{(n,n+1)}$	Selectivity between neighbouring components	—
β	Steepness of gradient	—
γ	Normalised temperature	—
δ	Heat capacity ratio	—
Δ	Difference between values	—
ε_e	External porosity	—
ε_p	Particle porosity	—
ε_t	Total porosity	—
μ_0	Zeroth moment	$gL^{-1}min$
μ_1	First Moment	<i>min</i>
μ_2	Second Moment	min^2
μ_3	Third Moment	min^3
ρ^L	Liquid phase density	<i>g/ml</i>
ρ^S	Solid phase density	<i>g/ml</i>
λ	Wavelength	<i>nm</i>
λ_{ax}	Axial dispersion coefficient of temperature	cm^2/min
τ	Normalised time	—
σ	Variance	min^2

Subscripts

<i>H</i>	Higher limit
<i>i</i>	<i>i</i> th switch time
<i>j</i>	Discrete point in the physical plane
<i>L</i>	Lower limit
<i>n</i>	<i>n</i> th Component
<i>N</i>	The last component
<i>R</i>	Reference

Superscripts

<i>f</i>	Front band
<i>k</i>	Cycle number
<i>L</i>	Liquid phase
<i>r</i>	Rear band
<i>rel</i>	Relative change to its reference condition
<i>S</i>	Solid phase
*	Switch time
—	Averaged value

Abbreviations

C5	Cyclopentanone
C6	Cyclohexanone
C7	Cycloheptanone
EDM	Equilibrium Dispersion Model
EM	Equilibrium Model
GC	Gas chromatography
H ₂ O	Water
HETP	Height Equivalent to a Theoretical Plate
HPLC	High Performance Liquid Chromatography
LC	Liquid chromatography
LSS	Linear solvent strength
MeOH	Methanol

Chapter 1. Introduction

1.1 Developments in chromatography

Separation is one of most important downstream processes in various manufacturing industries. It is reported that the separation cost possess 40-70% among the total cost [1]. Hence, improvements of separation processes are essential to increase profit. There are many kinds of separation processes according to different separation principles, e.g. distillation, crystallisation, membrane, extraction, filtration, chromatography, etc.

Chromatography is defined in different ways due to interdisciplinary nature [2]. The mechanisms can be sorption, size exclusion, ion exchange, affinity, partition [3], etc. Among them, sorption is the major mechanism. The sorption can be regarded as a formation of binding forces between mobile and stationary phases in a molecular level. The binding forces can be van der Waals forces in a physical phenomenon or valence forces in a chemical phenomenon [4,5].

Depending on purpose, chromatography can be divided into analytical chromatography and preparative chromatography, which differ in the injection amounts. The aim of the former is information acquisition whereas the latter is mass production. The chromatography was first discovered by Tswett [6]. In early time, analytical chromatography for component identification and quantification was mostly used. In preparative separations, complex mixtures with similar physical and chemical properties by other separation technologies were found to be limited. Thus, the preparative chromatography started being exploited and was taken apart from analytical chromatography in late 1940s. The first major projects for preparative chromatography were to purify rare earth elements and isolate hydrocarbons from crude oil [7]. Later it was extended to sugar and pharmaceutical industries. Nowadays chromatography as a common separation technology is widely used in various industries [8].

Chromatography can be classified according to the operating mode. The conventional chromatography using single column for periodic injections and separations is termed as batch chromatography [9]. Besides tubular column, annular chromatography is possible geometry [10–12]. The continuous process by multi-column simulated moving bed (SMB) has demonstrated a great performance improvement in terms of productivity and purity [13–16]. In spite of high performance, application of SMB is still limited to

general two outlets [17,18]. In recent decades, many modified SMB aimed for ternary separation, especially centre-cut separation are being exploited [19–26]. Furthermore, a carousel multi-column setup was proposed as another continuous mode [27].

1.2 Gradient chromatography

Extensive exploitations have been carried out to improve chromatographic performance and cost-effectiveness by introducing new degrees of freedom [28,29]. The SMB is the state of art for preparative chromatography. However, this process accompanies with significant capital and operating costs due to its complexity. On the contrary, repetitive batch processes under periodic modulations provides a simple and versatile alternative. The modulations or gradients vary the interaction strengths between solute and adsorbent. The gradients can be deployed locally and/or temporarily in order to manipulate the migration velocity of each component. The courses of adsorption isotherms are a measure of interaction strengths. They can be influenced by various factors, e.g. adsorbent, pH value, temperature, solvent composition, etc. [30]. Based on these factors, relevant theoretical and experimental investigations have been reported, e.g. stationary phase gradients [31,32], pH gradients [33–35], pressure gradients [36], solvent gradients [37–41] and temperature gradients [37,42,43]. Flow rate gradients are also possible to manipulate migration velocities [44]. Additionally, particle size gradients creating varying column efficiencies were also investigated. They turned out to be less significant with regard to performance [45].

Gradients can be classified by different criteria, as shown in **Figure 1-1**. The criteria can be modulation location, dimension, structure and functional dependence, etc. By modulation location, gradients can be introduced internally at the column inlet via solvent or feed, or externally, e.g. via heat exchange media. By dimension, gradients can be deployed over time and/or space. By structure, gradients can be imposed integrated or segmented. By functional dependence, gradients can be linear, stepwise or of more complex shapes.

In the work described in this thesis, segmented step gradients were applied. The solvent composition was modulated at the column inlet whereas the temperature was altered externally. Thus, both temperature and modifier fraction are a function of time and space.

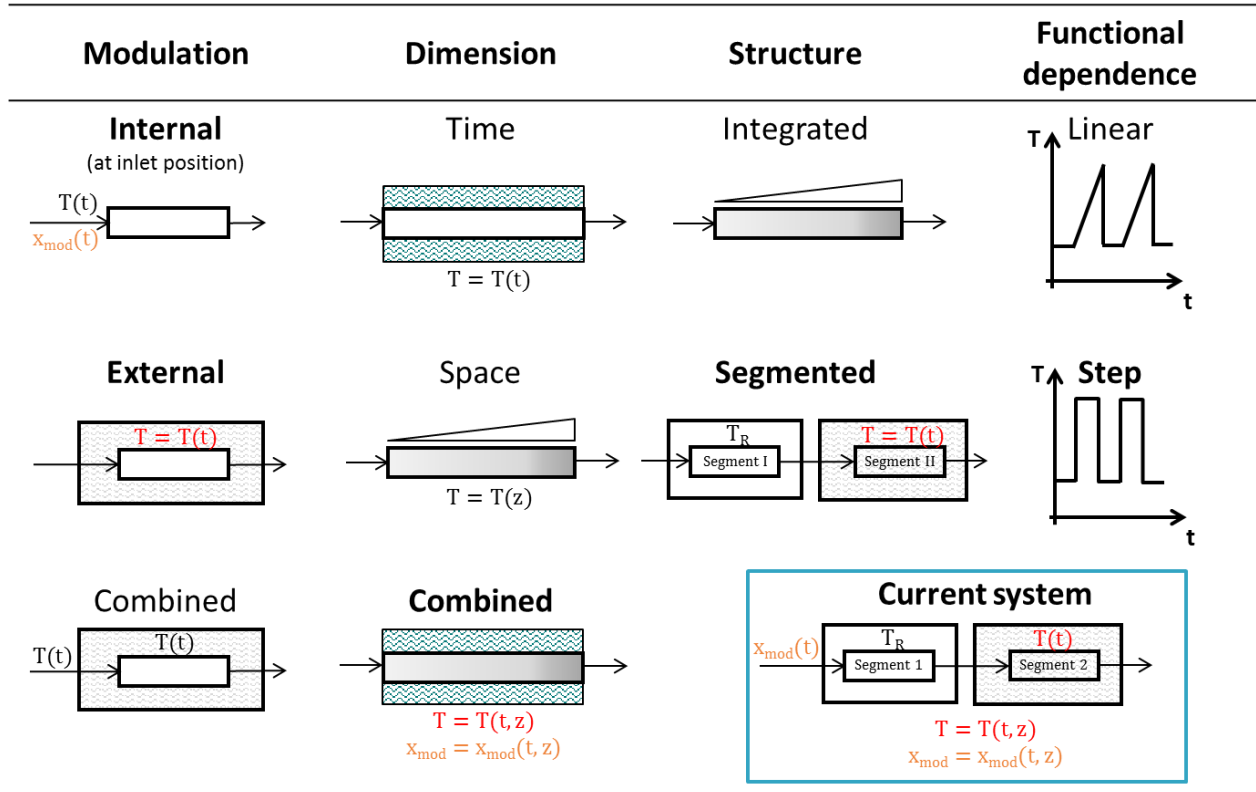


Figure 1-1 Classification of gradients according to different criteria. Bold texts indicate the selected options for the presented system.

Solvent gradients are commonly used in liquid chromatography [37] and they were first introduced by Alm et al [42]. For typical solvent gradients, modifier composition is changed at the column inlet and its change migrates through the column, i.e. the modifier fraction is a function of time and space. They are mostly defined according to functional dependence, as shown in **Figure 1-2**. Depending on separation problems, the functional dependence can be step, linear, or of more complex types. In analytical chromatography, solvent gradients can reduce the analysis time [46], resolve overlapping peaks and improve the peak capacity [47]. In some cases, a “negative gradient” is used to park certain components [48]. In preparative chromatography, solvent gradients can reduce the cycle time, as shown in **Figure 1-3**. In the isocratic operation, the elution strength is typically adjusted to fully separate all components. Consequently, a later eluting component falls behind the others, which leads to long cycle times. By applying a linear gradient, the cycle time can be significantly reduced. For nonlinear gradients, theoretical investigations are reported in [49]. In both scales, the migration speed of the solvent gradient should be considered. Solvent gradients in periodic operation are always followed by a re-equilibration procedure. The solvent migration and re-equilibration are not intuitively reflected in the chromatogram. However, they can be clearly quantified in the physical plane, which will be introduced in section 5.4.

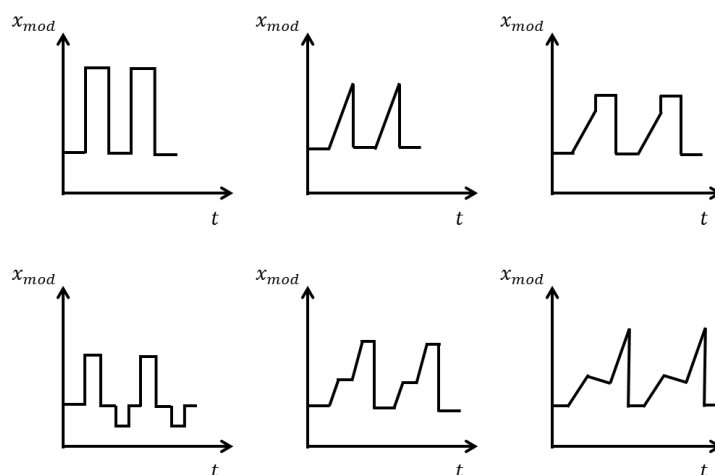


Figure 1-2 Possible functional dependences of solvent gradients expressed via x_{mod} .

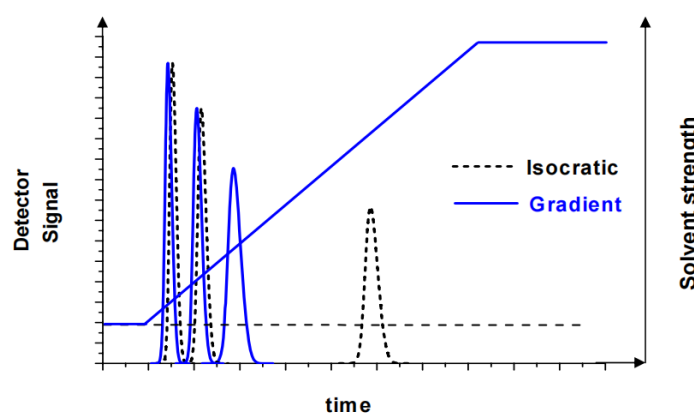


Figure 1-3 Demonstration of the effect of a linear solvent gradient [50].

Temperature gradients are commonly used in gas chromatography, where the temperature is modulated for the entire column, i.e. the temperature is a function of time only. It is well known that temperature gradients can be also used in liquid chromatography. Especially high temperature liquid chromatography was reported to have many advantages, e.g. increased solubility, reduced viscosity connected with allowable higher flow rate and adsorbents in smaller size, replacement of toxic solvent, etc., and thus it is considered as the green chromatography [51–54]. Their limitations can be reduced adsorbent stability, detector capability, heat transfer in scale-up [55]. In recent years, temperature-responsive liquid chromatography [56–61] has become an attractive option in bio-separation and open a door to extensive developments. The temperature effects on chromatographic separations have been reported in single columns [62] and multi-column simulated moving bed processes [63–65].

Temperature gradients can be introduced internally, where the sample and the solvent are introduced at different temperature at the column inlet. This is termed as “hot” or

“cold” injections [66–68]. On the contrary, temperature can be also modulated externally by covering the column with a jacket for complete or segmented heating or cooling via suitable heat exchange media. Water is used as the heat exchange media in common cases. This type of external temperature modulation can be also realised using electrical heating bandages [69,70]. It is reported in a SMB study that the external modulation performed better than internal modulation [71].

According to dimension, temperature gradients can be deployed along either time or space. The former refers to gas chromatography, where the temperature of the entire column changes over time, as described in [72–75]. The latter imposes temperature over the space, as described in [76]. The former is usually termed heating rate operation whereas the latter is thermal gradient [77]. Apparently, the most flexible option is simultaneous temperature modulation over both time and space, which was reported to be attractive to solve various separation problems [78,79].

For theoretical investigation of temperature gradients in liquid chromatography there are some reported models. A simple one-dimensional model neglecting radial dispersion is available [80]. In our work [81], analytical solutions were developed using the classical equilibrium model (EM) [82] by assuming ideal step gradients for the most optimistic scenario. The analytical solutions offer instructive insights into migration behaviour under influence of temperature gradients. Another simple but already more realistic model is the equilibrium dispersion model (EDM). In addition to analytical solutions, numerical solutions using EDM were also developed for comparison [83].

Both solvent and temperature gradients can be clearly used to deal with specific separation problems. A unified approach for jointly applying solvent gradients in LC and temperature gradients in GC was also proposed [84,85]. It is reported that the effect of 1% change in modifier fraction corresponded to 4-5 °C change in temperature [55]. In fact, temperature and solvent gradients are complementary and synergistic. A few researches on combined temperature and solvent gradients have been reported [86–88]. Other gradient combinations are also possible, e.g. temperature gradient with stationary gradient [89], temperature gradient with flow rate gradient [90], etc. In recent decade, artificial intelligence based methods for optimising gradient separations are emerging, e.g. artificial neuron network [39,49,91,92], evolutionary algorithm [93], etc. Retention factors can be predicted by molecular dynamics simulation [94]. These advanced methods are promising for future gradient designs.

1.3 Goal of study and structure of the thesis

As shown in **Figure 1-4**, gradients have two typical applications. One application addresses so-called “partly lagged separations” characterised by a wide retention time spectrum corresponding to either scenario 1 or scenario 2. In this case, a component travels significantly faster or slower than the majority of the other components in the elution train. The main advantage of gradients is to reduce the cycle time compared to “iso” conditions, i.e. isothermal, isocratic, etc. The cycle time covers the entire range from start to end in the elution profile. It is directly related to the productivity. This time difference can be reduced by decelerating fast eluting components or accelerating slowly eluting components using suitable gradients.

The other application of gradients concerns difficult separations or coelutions corresponding to scenario 3. In this case, gradients can be beneficial to improve the resolution and component purities.

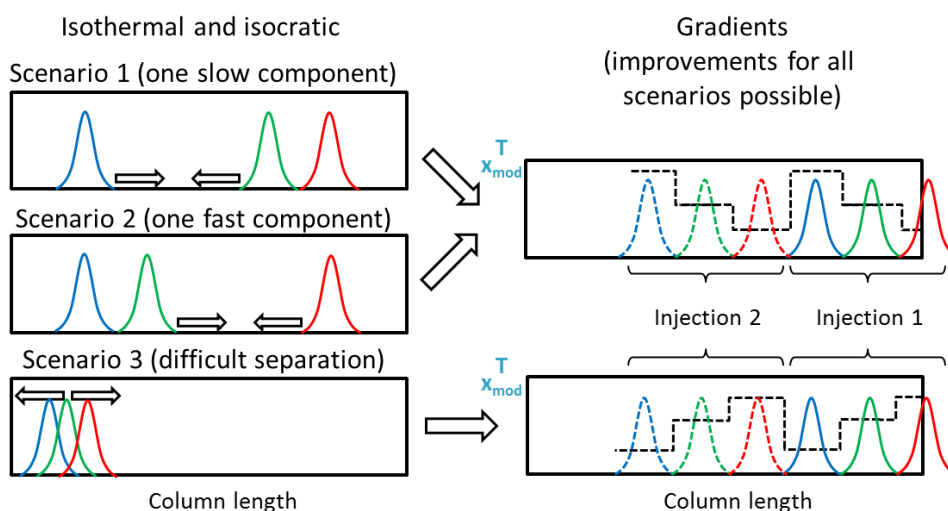


Figure 1-4 General applications of gradients by taking ternary separations as an example. The Scenarios 1 and 2 are termed as partly lagged separations.

In this study, temperature and solvent gradients are analysed. Both theoretical design and experimental validation aiming at reducing the cycle time in partly lagged separations (i.e. scenario 1) are considered. For gradient designs, characteristic switch times are the key parameters depending on how gradients are deployed for specific separations. In a theoretical section, the graphical representation of the chromatographic process in a physical plane will be utilised, where the switch times can be determined. This graphical representation is a versatile tool, which can handle

various separation problems using gradients. In experimental aspect, the gradient concepts and the operating strategies in terms of switch times were validated. Both gradient types were realised experimentally using a lab-scale system. The solvent gradients are commonly used technique in liquid chromatography, which can be easily implemented using modern multi-pump HPLC systems. For temperature gradients, there are many ways for implementation. To decrease the process complexity, in this work just a two-segment step temperature gradients are studied. It could be further improved by more segments, and thus, more complicated gradients. However, such extensions are beyond the scope of this study.

In chapter 2, the theoretical foundation is given. The mathematical models for mass and energy balances are presented. For mass balance, trajectories of chromatograms in the physical plane under equilibrium model characterised by thermodynamics is especially addressed, which is a basis for the entire study. Regarding the energy balance, a short-cut model is introduced to predict temperature profiles. The cycle time and productivity, as the key performance indicators, are explained.

In chapter 3, materials and the experimental system used for the case study are introduced. The temperature gradients are conducted in a segmented system, where only the second segment is externally modulated in a periodic manner. Estimations of parameters for calibration, system, thermodynamics, kinetics, mass and energy balances are described.

In chapter 4, results of parameters in chapter 3 are presented. The thermodynamic parameters are addressed according to temperature and solvent composition, which are the main parameters to design gradients on the physical plane. It is shown that the characteristic switch times and the cycle time are directly related to thermodynamics. The parameters for short-cut energy balance are used to account for nonideality of implementing stepwise temperature gradients.

In chapter 5, the usage of the physical plane for gradient designs and performance prediction is described in detail. Temperature and solvent gradients are individually designed for a ternary separation problem. The physical plane is generated according to certain operating regimes expressed by switch times. The retention times can be identified from the physical plane and the cycle time can be then determined. To get

more realistic predictions, equilibrium dispersion model was used to generate simulated chromatograms.

In chapter 6, the gradient concepts are validated for the ternary separations through experiments according to operating regimes introduced in chapter 5. The performances of both gradient operations by different regimes are summarised and compared.

In the final chapter 7, more advanced gradients designs are discussed using physical planes. The potential of combined gradients of temperature and solvent modulations is suggested. The performance of all aforementioned gradient designs in terms of cycle time and productivity is finally compared. Their merits, drawbacks and future perspective are discussed.

Chapter 2. Theoretical background

In this chapter, theories in chromatography relevant to this work is described, including terminologies, concepts, mathematical models for mass and energy balances, performance indication, etc. Gradients, especially temperature and solvent gradients, as the main focal points are extensively discussed.

2.1 Basic concepts in chromatography and phases involved

Chromatography is a separation technique mainly based on adsorption, as shown in **Figure 2-1**. Each solute from the mixture is carried by the mobile phase (eluent) while interacting with the stationary phase (adsorbent). Each component migrates at different velocity due to difference in adsorption strength. Consequently, the mixture are separated into single components.

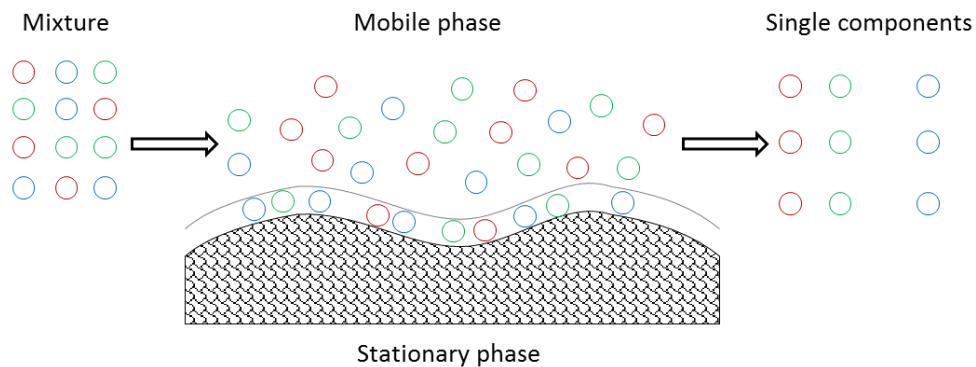


Figure 2-1 Demonstration of the chromatographic process. The three different colours indicate the ternary mixture.

Suitable adsorbents are silica gel, active carbon, zeolites, etc [29]. Among them, the silica gel is commonly used due to cheapness and it is mostly bonded with octadecyl silane (C18) for the reverse phase mode [3]. In terms of structure, adsorbents can be monolithic, porous, core-shell, etc. The internal structure of a packed chromatographic column with porous adsorbents is shown in **Figure 2-2**.

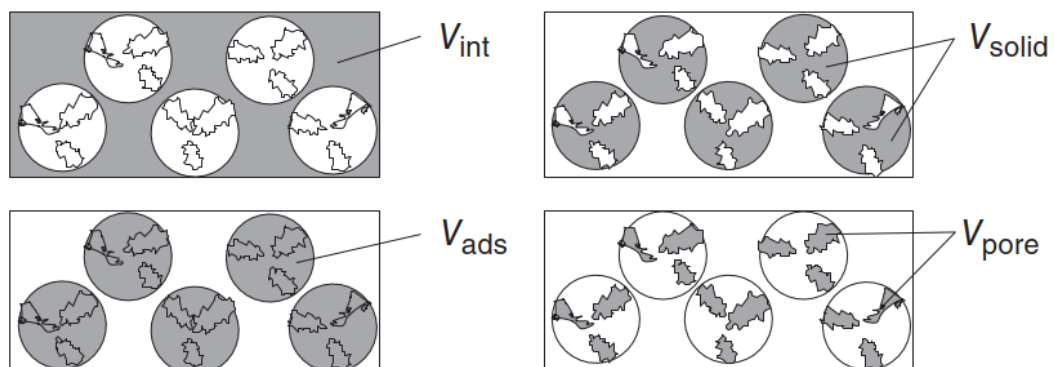


Figure 2-2 Internal structure of in a chromatographic column characterised by various volumes [29].

The volume of the packed column V_c is sum of adsorbent volume V_{ads} and interstitial volume V_{int} as

$$V_c = \frac{\pi D_{c,i}^2 L_c}{4} = V_{ads} + V_{int} \quad (2-1)$$

Where $D_{c,i}$ and L_c refer to inner diameter and length of the column. The adsorbent volume is sum of solid volume V_{solid} and pore volume V_{pore} as

$$V_{ads} = V_{solid} + V_{pore} \quad (2-2)$$

The external porosity is defined by

$$\varepsilon_e = \frac{V_{int}}{V_c} \quad (2-3)$$

The particle porosity is defined by

$$\varepsilon_p = \frac{V_{pore}}{V_{ads}} \quad (2-4)$$

The total porosity ε_t can be expressed by

$$\varepsilon_t = \frac{V_{int} + V_{pore}}{V_c} = \varepsilon_e + (1 - \varepsilon_e)\varepsilon_p \quad (2-5)$$

The recorded detector signal after the column outlet is termed as chromatogram or elution profile. The typical chromatograms are demonstrated in **Figure 2-3**. The detector signal can be converted to concentration of the specific component by calibration, which will be described in section 3.4.1. In ideality, chromatograms have rectangular shapes without any dispersion. In reality, chromatograms of small amount of injections seem like peaks by Gaussian distribution. The first moment of a peak, or the time at peak maxima in a symmetric peak, is recorded. The time for passing through the system without the column is plant dead time t_{plant} . The time of a non-retained component for passing through the column only is column dead time t_0 . The time of retained component for passing through the column only is termed retention time t_R .

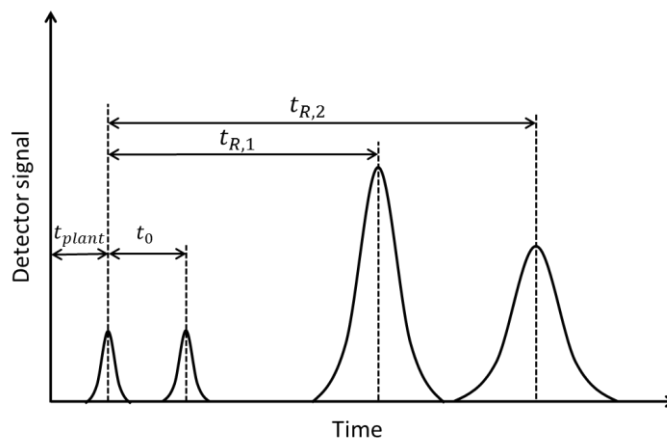


Figure 2-3 Chromatogram characterised by various times connected with system column and component.

2.2 Adsorption isotherm

The relation between mobile phase concentration q and stationary phase concentration c at a constant temperature is termed adsorption isotherm. The most common isotherms are linear, Langmuir and anti-Langmuir. Besides, there are also more complicated isotherms, like BET, bi-Langmuir, etc [29,95,96]. The common isotherms with their featured chromatograms and behaviours of volume overload are demonstrated in **Figure 2-4**. For nonlinear isotherms, i.e. Langmuir and anti-Langmuir, the retention times are shifted by increasing injection volume and the peaks always grow asymmetrically. Similar behaviour can be observed for concentration overload [97].

In this study, the isotherm of a single component was considered to be linear and not affected by the presence of other components. Then holds

$$q(c) = k_H c \quad (2-6)$$

where k_H is Henry's constant. Thus, in this simple isotherm model, the retention time is independent from the concentration. The linearity can be examined by evaluating volume overload experiments. In the linear range, the peak grows symmetrically with the injection volume while maintaining the same retention time, and a forward growing breakthrough plateau is formed when the injection volume reaches to a certain value.

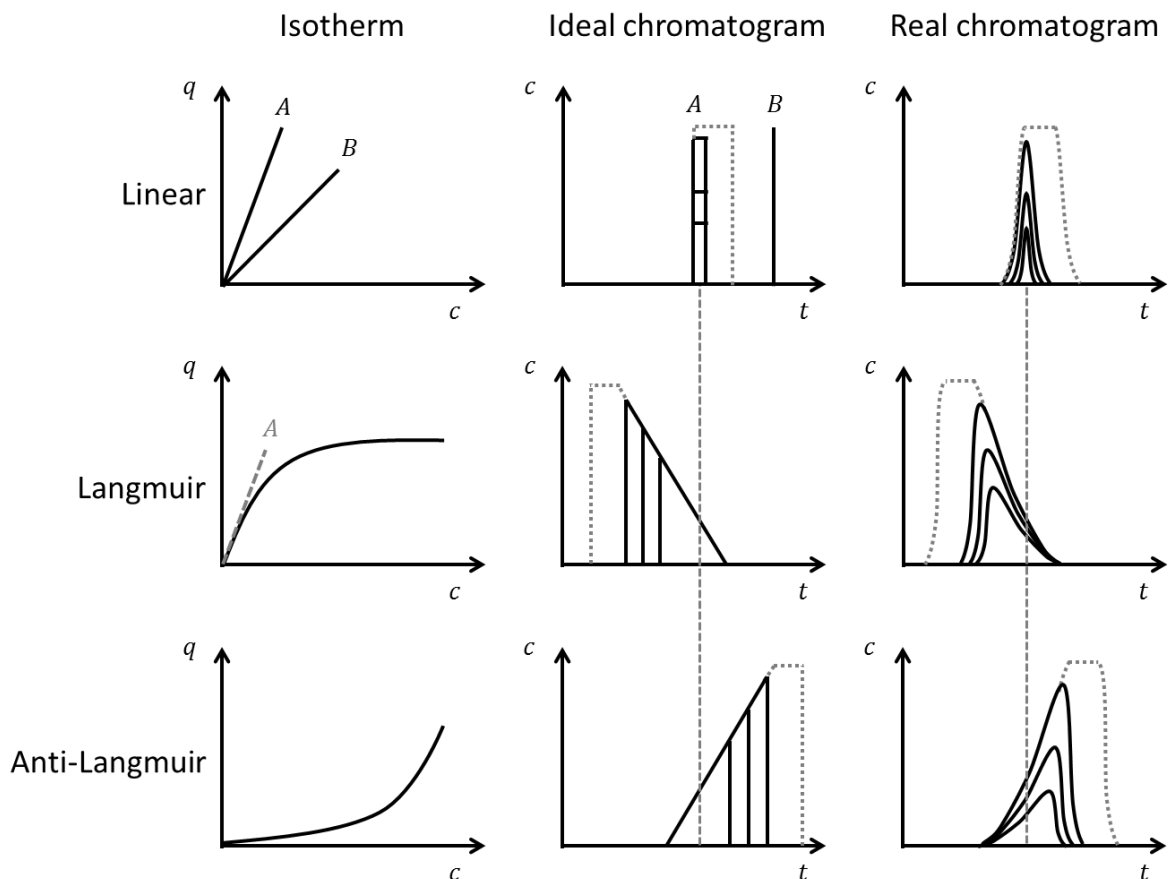


Figure 2-4 Typical isotherms and their elution profiles [29]. Effect of volume overload is also shown.

In this study, temperature T and the solvent composition in terms of modifier fraction x_{mod} were the main controlling variables. The elution strength refers to the ability to decrease Henry's constant. The temperature dependence of Henry's constant can be described by Van't Hoff model [98] as

$$k_H(T) = k_{H,R}(T = T_R)e^{\frac{-\Delta H_A}{R}\left(\frac{1}{T} - \frac{1}{T_R}\right)} \quad (2-7)$$

where $k_{H,R}$ and ΔH_A refer to the Henry's constant at the reference temperature T_R and the heat of adsorption, respectively. For presented model components, $\Delta H_A < 0$, i.e. this adsorption is exothermic process so that the elution strength increases with increasing temperature. This leads to a reduction of loading q . The opposite case of endothermic process is also possible, e.g. polymer components [99]. R is ideal gas constant.

The solvent dependence of Henry's constant can be described by linear solvent strength (LSS) model [37,100,101] as

$$k_H(x_{mod}) = k_{H,0}(x_{mod} = 0)e^{-\alpha x_{mod}} \quad (2-8)$$

where x_{mod} is the fraction of the modifier used in the solvent. $k_{H,0}$ and α refer to the Henry's constant at $x_{mod} = 0$ and sensitivity constant, respectively. The elution strength increases with increasing modifier fraction if $\alpha > 0$ whereas decreases with increasing modifier fraction if $\alpha < 0$. For the model components studied later, $\alpha > 0$. In order to compare performances of the combined gradients, the dependence is expressed empirically by assuming a temperature dependence of each term in Eq. (2-8) in logarithm forms. Then holds

$$\begin{aligned} k_H(T, x_{mod}) &= \exp[\ln k_{H,0}(x_{mod}=0)(T) + \alpha(T)x_{mod}] \\ &= \exp[(a_1 + a_2T) + (a_3 + a_4T)x_{mod}] \end{aligned} \quad (2-9)$$

where a_1 - a_4 are empirical parameters.

2.3 Mass balances of chromatographic columns

There are several models that describe chromatographic processes. The ideal and the simplest model is equilibrium model. It acts as the core model and other models are extended based on it. A practical model to take dispersion effect into account is equilibrium dispersion model.

2.3.1 Equilibrium model

The 1-D equilibrium model was well-established [82], which assumes an equilibrium between mobile and stationary phases without any dispersion. It can be extended to describe ideal step gradients. The mass balance is expressed as

$$\left(1 + F \frac{dq}{dc}\right) \frac{\partial c}{\partial t} + u \frac{\partial c}{\partial z} = 0 \quad (2-10)$$

where q and c refer to stationary and mobile phase concentrations, respectively. t and z indicate time and space coordinate, respectively. u represents interstitial velocity. The phase ratio F is defined by

$$F = \frac{1 - \epsilon_t}{\epsilon_t} \quad (2-11)$$

where ϵ_t is total porosity.

As introduced in **Figure 1-1**, a two-segment system were used in this work. The segmented position z^* where segment I ends can be expressed by

$$z^* = f_z L_c \quad (2-12)$$

where f_z is segmentation ratio. In this study, just $f_z=0.5$ will be used, though other values can be treated analogously. The initial condition is

$$c(t = 0, z) = 0 \quad (2-13)$$

The inlet boundary conditions for the two segments are expressed as

$$c_{segment I}(t, z = 0) = c_{in}(t) = \begin{cases} c_{inj}, & t \in [t_{inj}^k, t_{inj}^k + \Delta t_{inj}] \\ 0, & t \in [t_{inj}^k + \Delta t_{inj}, t_{inj}^{k+1}] \end{cases} \quad k = 1, 2, \dots \quad (2-14)$$

$$c_{segment II}(t, z = z^*) = c_{segment I}(t, z = z^*) \quad (2-15)$$

where c_{inj} is injection concentration. The injections are repeated periodically over an injection period Δt_{inj} . t_{inj}^k represents the start time for k^{th} injection.

The column dead time t_0 , or the retention time for non-retained component can be calculated as

$$t_0 = \frac{L_c}{u} = \frac{\pi L_c D_{c,i}^2 \epsilon_t}{4 \dot{V}} \quad (2-16)$$

Where L_c and $D_{c,i}$ refer to length and inner diameter of the column, respectively. \dot{V} is flow rate. The migration velocity u_c is defined by rearranging Eq. (2-10) for linear isotherm at a certain concentration by method of characteristics [102] as

$$u_c = \left. \frac{\partial z}{\partial t} \right|_c = \frac{u}{1 + F k_H(T, x_{mod})} \quad (2-17)$$

where the dq/dc is equal to Henry's constant k_H according to Eq. (2-6). In this study, Henry's constant is a function of temperature and modifier fraction. The retention time t_R can be calculated as

$$t_R = \frac{L_c}{u_c} = \frac{L_c}{u} [1 + Fk_H(T, x_{mod})] = t_0 [1 + Fk_H(T, x_{mod})] \quad (2-18)$$

It can be seen that $t_R = t_0$ for non-retained component, i.e. $k_H=0$, refer to Figure 2-3.

2.3.2 Trajectories of chromatograms in the physical plane

Chromatographic results can be described in different ways. The chromatogram (c-t plot) is the most common one, which is the detector response in an experiment and the solution of the mass balance at outlet in a simulation. There is also a way of showing concentration relations among components called "hodograph", from which analytical solutions can be derived [103,104].

In current study, a graphical representation by reflecting component migration pathway called "physical plane" [105] was intensively used. An example of a physical plane under isothermal and isocratic condition is shown in **Figure 2-5**. The migration pathways of front and rear bands are projected in a space-time plane (z-t plot), i.e. they are trajectories of chromatograms in the physical plane. They are straight lines without turnings in the linear isotherm range and the slope corresponds to the migration velocity u_c defined in Eq. (2-17). The chromatogram can be obtained at the outlet, which is rectangular in EM. The realistic chromatogram is dispersed due to kinetic effects. The middle point between front and rear bands corresponds to the retention time t_R in Eq. (2-18).

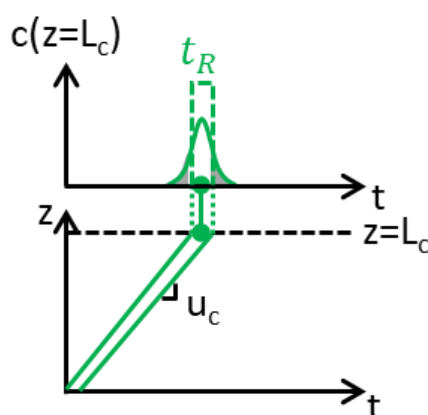


Figure 2-5 Single component behaviour under isothermal and isocratic conditions. Bottom: physical plane, which is the solution of Eq. (2-10); Top: corresponding ideal chromatogram (dashed) and real chromatogram (solid) at column outlet.

The physical planes under gradient conditions are shown in **Figure 2-6**. A positive gradient of temperature (left) and modifier fraction (right) is imposed at switch time t_i^* . Consequently, the migration velocity or the slope is changed upon gradients. The migration pathway turns at the intersection point with the gradient line. The gradient line in temperature gradient is vertical and the other horizontal gradient line exists due to segmentation. In the solvent gradient, the gradient line is inclined with the slope interstitial velocity u , and its horizontal movement within the entire column corresponds to the column dead time t_0 in Eq. (2-16).

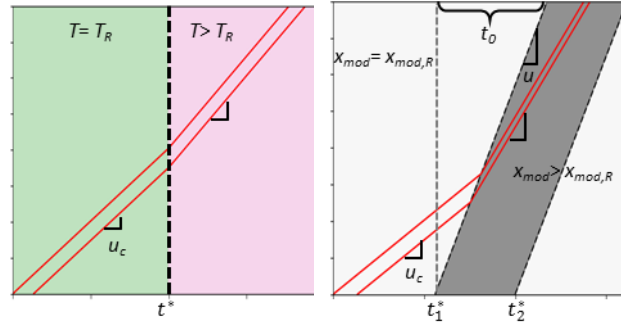


Figure 2-6 Migration behaviour under temperature gradient (left) and solvent gradient (right). Green and red blocks refer to reference temperature at $T_R = 25^\circ\text{C}$ and a higher temperature, respectively. White and grey blocks refer to the reference modifier fraction at $x_{mod,R} = 0.5$ and a higher value, respectively. The black dashed lines indicate the gradient lines at switch time t_i^* .

The temperature and solvent gradients can be deployed individually or simultaneously at single or multiple switch times, i.e.

$$T(t, z \geq f_z L_c) = \begin{cases} T_R, & t \leq t_1^* \\ T_L \text{ or } T_H, & t_1^* < t \leq t_2^* \text{ and/or } x_{mod}(t, z = 0) \\ \dots & \dots \\ T_L \text{ or } T_H, & t_i^* \leq t \end{cases} = \begin{cases} x_{mod,0}, & t \leq t_1^* \\ x_{mod,1}, & t_1^* < t \leq t_2^* \\ \dots & \dots \\ x_{mod,N}, & t_i^* \leq t \end{cases} \quad (2-19)$$

The physical plane can be generated as long as the slopes at all positions are known. The temperature or modifier fraction is constant within the period between switches $[t_i^*, t_{i+1}^*]$

$$\frac{dT}{dt}(t_i^* < t \leq t_{i+1}^*) = 0 \quad (2-20)$$

$$\frac{dx_{mod}}{dt}(t_i^* < t \leq t_{i+1}^*) = 0 \quad (2-21)$$

Hence, the migration velocity is also constant between switches. Due to this feature, characterise times can be calculated via analytic geometry on the physical plane.

2.3.3 Equilibrium dispersion model

More realistic and practical model is equilibrium dispersion model (EDM), where the dispersion or band broadening is taken into consideration. It is extended from EM by introducing a second order axial dispersion term [28,29] as

$$\frac{\partial c}{\partial t} = -\frac{u}{1 + Fk_H} \frac{\partial c}{\partial z} + \frac{D_{app}}{1 + Fk_H} \frac{\partial^2 c}{\partial z^2} \quad (2-22)$$

where D_{app} is apparent dispersion coefficient, which describes the lumped deviations from infinite column efficiency.

To solve Eq. (2-22), the Danckwerts boundary condition [106] is used as

$$c(t, z = 0) = c_{in}(t) + \frac{D_{app}}{u} \left. \frac{dc}{dz} \right|_{z=0} \quad (2-23)$$

and a second boundary condition is also need. The typically used condition is

$$\left. \frac{\partial c}{\partial z} \right|_{z=L_c} = 0 \quad (2-24)$$

The mass balance in Eq. (2-22) is commonly solved by numerical methods [107–112]. Besides physical dispersion, the numerical dispersion should be also considered [113]. The finite volume numerical scheme with upwinding for the advection term was used in previous work [114]. Alternatively, an analytical expression of the chromatogram for EDM with rectangular injections is available for this case of linear isotherm without competition [115]. It can be expressed in term of injection concentration c_{inj} , injection period Δt_{inj} and apparent dispersion coefficient D_{app} as

$$c(t, z = L_c) = \frac{c_{inj}}{2} \left\{ \operatorname{erf} \left[\frac{L_c - u_c(t - \Delta t_{inj}/2)}{\sqrt{4D_{app}u_c(t - \Delta t_{inj}/2)/u}} \right] - \operatorname{erf} \left[\frac{L_c - u_c(t + \Delta t_{inj}/2)}{\sqrt{4D_{app}u_c(t + \Delta t_{inj}/2)/u}} \right] \right\} \quad (2-25)$$

2.3.4 Kinetics: Plate number and efficiency

The dispersion effect by kinetics can be expressed by the well-known Van Deemter equation [116] as

$$\frac{L_c}{N_p} = HETP(u, d_p) = A + \frac{B}{u} + Cu \quad (2-26)$$

where A, B and C are factors contributing band broadening. HETP stands for height equivalent to a theoretical plate and N_p is the theoretical plate number. The column is hypothetically divided into a certain number of plates in Craig's stage model [117]. This

plate number is a measure of column efficiency, i.e. larger plate number, lower HETP, higher efficiency and less dispersion.

The Van Deemter curve according to Eq. (2-26) is plotted in **Figure 2-7**. The HETP according to the interstitial velocity is in a check shape, which is caused by contributions from different factors of band broadening. The A term is contribution of eddy diffusion, which is measure of packing quality of the column. It is a fixed value and independent from the velocity. The B term is contribution of molecular diffusion due to longitudinal natural distribution, which leads HETP to decrease with increasing velocity. The C term is contribution of mass transfer resistance due to adsorbent's geometry, which leads HETP to increase by increasing velocity. The check shape is formed by superimposing these contributions for band broadening. An optimal velocity exists at the minimal HETP, which provides important criteria for determining flow rate. The HETP is also a function of particle diameter d_p , i.e. smaller particle, lower HETP.

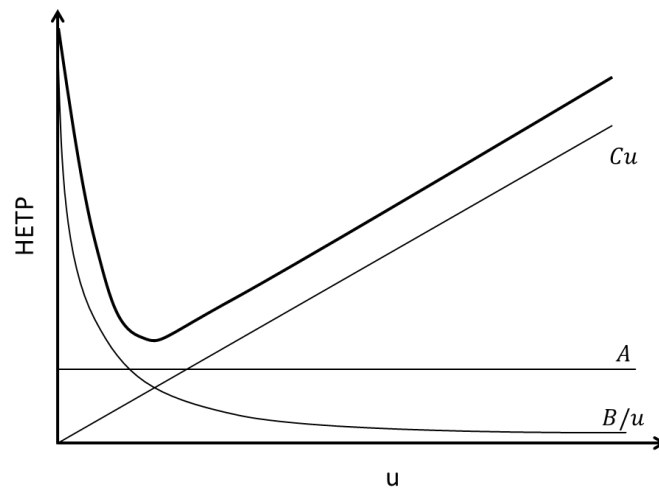


Figure 2-7 Demonstration of the Van Deemter curve [116].

The apparent dispersion coefficient D_{app} in Eq. (2-22) describes the lumped dispersion effect including all factors of band broadening. It can be estimated by the theoretical plate number by using the second moment. The moments from 0th to 3rd are defined as

$$\mu_0 = \int_0^{\infty} c(t) dt \quad (2-27)$$

$$\mu_1 = \frac{\int_0^{\infty} t c(t) dt}{\mu_0} = t_R \quad (2-28)$$

$$\mu_2 = \frac{\int_0^{\infty} (t - \mu_1)^2 c(t) dt}{\mu_0} = \sigma^2 \quad (2-29)$$

$$\mu_3 = \frac{\int_0^{\infty} (t - \mu_1)^3 c(t) dt}{\mu_0} \quad (2-30)$$

From definitions of moments, μ_0 , μ_1 , μ_2 and μ_3 correspond to the area under the chromatogram, retention time, variance and skewness of the chromatogram.

By equating the second moment from EDM and that from the stage model

$$\mu_2^{EDM} = \mu_1^2 \frac{2D_{app}}{uL_c} = \mu_2^{stage} = \frac{\mu_1^2}{N_p} \quad (2-31)$$

The apparent dispersion coefficient can be then expressed as

$$D_{app} = \frac{uL_c}{2N_p} \quad (2-32)$$

Similar approaches by equating the second moments can be used to correlate parameters from different models [118]. The theoretical plate number N_p can be approximated by analysing chromatograms from pulse experiments [28] as

$$N_p = 5.54 \left(\frac{t_R}{w_{0.5}} \right)^2 \quad (2-33)$$

where $w_{0.5}$ is the bandwidth at the half height, as shown in **Figure 2-8**. It is noted that this formula is valid for symmetric Gaussian peaks, i.e. diluted concentration under the linear isotherm. By this formula, the dispersion effect of the injection profiles is also captured on the experimental chromatogram, i.e. the intrinsic plate number would be higher. However, it is helpful and intended since all effects of band broadening should be lumped to the apparent dispersion coefficient.

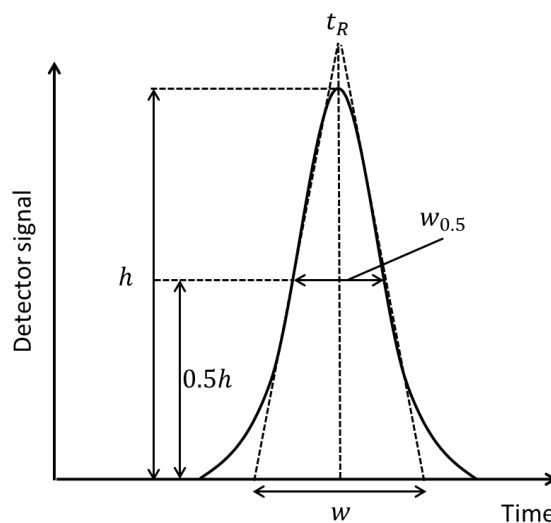


Figure 2-8 Demonstration of an elution profile following Gaussian distribution.

By using Eq. (2-16) and Eq. (2-32), the Eq. (2-25) can be transformed in terms of the retention time and the theoretical plate number N_p as a substitute for D_{app}

$$c(t, z = L_c) = \frac{c_{inj}}{2} \left\{ \operatorname{erf} \left[\frac{1 - (t - \Delta t_{inj}/2)/t_R}{\sqrt{2(t - \Delta t_{inj}/2)/t_R/N_p}} \right] - \operatorname{erf} \left[\frac{1 - (t + \Delta t_{inj}/2)/t_R}{\sqrt{2(t + \Delta t_{inj}/2)/t_R/N_p}} \right] \right\} \quad (2-34)$$

2.3.5 Nonideality of implementing stepwise solvent profiles

In reality, the solvent profile of a solvent step gradient does not behave in an ideal stepwise but rather in an S-shape [119], which can be described by

$$Sig = I_{max} \exp\{-\exp[-g_1(t - g_2)]\} \quad (2-35)$$

where I_{max} is the intensity of reached plateau. g_1 and g_2 are empirical coefficients. The actual solvent profile for step gradient can be fitted by Eq. (2-35), as shown in **Figure 2-9**. It can be performed through a step response experiment. The stepwise change of modifier fraction for a continuous feed via proportioning valve was taken as the input and the step response was recorded.

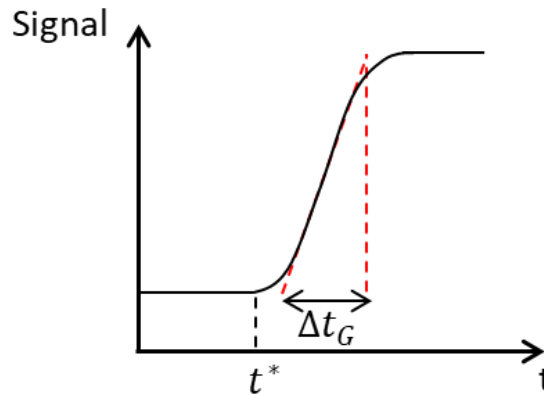


Figure 2-9 Approximation of nonideal stepwise solvent profile.

The response profile can be approximated by a linear gradient [120] as

$$Sig = \frac{I_{max}g_1}{e} (t - g_2) + \frac{I_{max}}{e} \quad (2-36)$$

From this equation, the corresponding slope and dispersion time between two plateaus can be determined. This dispersion time is called here the gradient deviation time Δt_G , which can be solved as

$$\Delta t_G = \left(g_2 + \frac{e - 1}{g_1} \right) - \left(g_2 - \frac{1}{g_1} \right) = \frac{e}{g_1} \quad (2-37)$$

It is the key parameter to account for the actual delay of the step gradient, and used in the linear gradient as

$$x_{mod} = x_{mod}(t = t_i^*) + \frac{\Delta x_{mod}}{\Delta t_G} (t - t_i^*) \quad (2-38)$$

where $\Delta x_{mod}/\Delta t_G$ is gradient steepness.

2.4 Energy balances of chromatographic columns

The energy balance describes the temperature profile influenced by an external source for non-isothermal operation. The complete model has many parameters including the thermal dispersion. To make it simple and realistic, a short-cut model is used by lumping parameters into two and the thermal dispersion is neglected.

2.4.1 Ideal model

For ideal model, the energy balance is not required since the instantaneous full step change of the temperature is assumed, i.e., only the mass balance is required as

$$\left[1 + F \frac{dq}{dc}(T, x_{mod})\right] \frac{\partial c}{\partial t} + u \frac{\partial c}{\partial z} = 0 \quad (2-39)$$

The temperature profile can be expressed by

$$T(t, z \geq f_z L_c) = \begin{cases} T_R, & t \leq t_1^* \\ T_L \text{ or } T_H, & t_1^* < t \leq t_2^* \\ \dots & \dots \\ T_L \text{ or } T_H, & t_i^* \leq t \end{cases} \quad (2-40)$$

where t_i^* is the switch time. T_R , T_L and T_H refer to reference temperature, lower and higher limits of temperature, respectively. This temperature profile can directly input to Eq. (2-17) to calculate the migration velocity and thus generate the trajectories in the physical plane.

2.4.2 Complete energy balance

In this study, the entire column with surrounding water in the water jacket was taken as the system for energy balance. The complete energy balance in one dimension assuming pseudo-homogenous conditions ($T^L = T^S = T$) is expressed as

$$(A^L \rho^L C_p^L + A^S \rho^S C_p^S) \frac{\partial T}{\partial t} + u A^L \rho^L C_p^L \frac{\partial T}{\partial z} = A^T U_o (T_w - T) + \lambda_{ax} \frac{\partial^2 T}{\partial z^2} - \sum_{n=1}^N \Delta H_{A,n} \frac{\partial q}{\partial t} \quad (2-41)$$

where the superscript L and S represent the liquid and solid phase. A , ρ and C_p refer to area, density and specific heat capacity, respectively. T_w is the surrounding water temperature. λ_{ax} axial thermal dispersion coefficient, which is similar to D_{app} the in mass balance. The specific heat transfer area around the column is calculated as

$$A^T = \frac{dA_o}{dV} = \frac{\pi D_{c,o}}{\frac{1}{4} \pi D_{c,o}^2} = \frac{4}{D_{c,o}} \quad (2-42)$$

where $D_{c,o}$ is outer diameter of the column. The overall heat transfer coefficient U_o (based on outer diameter) for the model of double pipe heat exchanger is defined as

$$\frac{1}{U_o} = \frac{D_{c,o}}{D_{c,i}h_i} + \frac{x_w D_{c,o}}{k_w D_L} + \frac{1}{h_o} \quad (2-43)$$

where h_i and h_o refer to individual heat transfer coefficient inside and outside the column, respectively. x_w and k_w are thickness and thermal conductivity of the column wall, respectively. It should be noted that U_o is function of flow rate. The water temperature is defined same as Eq. (2-40) but placed in the source term

$$T_w(t, z \geq f_z L_c) = \begin{cases} T_R, & t \leq t_1^* \\ T_L \text{ or } T_H, & t_1^* < t \leq t_2^* \\ \dots & \dots \\ T_L \text{ or } T_H, & t_i^* \leq t \end{cases} \quad (2-44)$$

In this model, the temperature profile is not ideal step, and it should be solved from Eq. (2-41). The initial and boundary conditions are defined as

$$T(t = 0, z) = T_0 \quad (2-45)$$

$$T(t, z = 0) = T_0 \quad (2-46)$$

$$\frac{dT}{dt}(t, z = 0) = 0 \quad (2-47)$$

For temperature gradients in this study, a two-segment system was used. The temperature of the first segment is kept as T_R whereas that of the second segment is modulated among two levels of T_L and T_H . They are expressed as

$$T_{segment I}(t, 0 < z \leq z^*) = T_R \quad (2-48)$$

$$T_{segment II}(t, z^* < z \leq L_c - z^*) = T(t) \quad (2-49)$$

where $T(t) \in \{T_H, T_L\}$

2.4.3 Short-cut energy balance

To simplify the complete model, terms of thermal dispersion and heat of adsorption are neglected in Eq. (2-41). Heat accumulation in the wall is lumped in a simplifying way using modified solid phase properties (see section 4.5.1). It leads to

$$(A^L \rho^L C_p^L + A^S \rho^S C_p^S) \frac{\partial T}{\partial t} + u A^L \rho^L C_p^L \frac{\partial T}{\partial z} = A^T U_o (T_w - T) \quad (2-50)$$

By defining the parameter X_1 as

$$X_1(F^T, \delta) = \frac{1}{1 + \frac{A^S}{A^L} \cdot \frac{\rho^S C_p^S}{\rho^L C_p^L}} = \frac{1}{1 + F^T \delta} \quad (2-51)$$

where $F^T = A^S/A^L$ is phase ratio for heat transfer, which is similar to F in mass balance. δ is heat capacity ratio of solid to liquid phases. By defining the parameter X_2 as

$$X_2(U_o) = \frac{A^T U_o}{A^L \rho^L C_p^L + A^S \rho^S C_p^S} \quad (2-52)$$

By Eq. (2-51) and Eq. (2-52), the Eq. (2-50) is simplified as

$$\frac{\partial T}{\partial t} = -uX_1 \frac{\partial T}{\partial z} - X_2 T + X_2 T_w \quad (2-53)$$

By normalising time axis with t_0 and space axis with L_c

$$\tau = \frac{t}{t_0} \quad (2-54)$$

$$x = \frac{z}{L_c} \quad (2-55)$$

The Eq. (2-53) finally becomes

$$\frac{\partial T}{\partial \tau} = -X_1 \frac{\partial T}{\partial x} - t_0 X_2 T + t_0 X_2 T_w \quad (2-56)$$

It can be solved analytically by Laplace transform. The derivation procedure is shown in Appendix 3. The analytical solution is expressed as

$$T(\tau, x) = \begin{cases} T_w - (T_w - T_0)e^{-(1-f_z)t_0 X_2 \tau} & \tau \leq \frac{x}{X_1} \\ T_w - (T_w - T_0)e^{-(1-f_z)t_0 \frac{X_2}{X_1} x} & \tau \geq \frac{x}{X_1} \end{cases} \quad (2-57)$$

where t_0 is a function \dot{V} of as defined in Eq. (2-16). It should be re-calculated whenever the flow rate is changed thereafter. Moreover, t_0 should be multiplied by $(1 - f_z)$ due to the fact that the temperature is modulated only on the second segment.

In order to examine how the outlet temperature profile ($x=1$) is influenced by X_1 and X_2 , a parameter study using Eq. (2-57) was performed. A heating process from 5 °C to 60 °C was taken as the example. The effect of X_1 on the temperature profile is illustrated in **Figure 2-10**. As X_1 increases, the final steady state temperature is decreased, i.e. X_1 determines the temperature reachability. The effect of X_2 on the temperature profile is illustrated in **Figure 2-11**. By increasing X_2 , the time to reach steady state is decreased, i.e. X_2 determines the heat transfer efficiency and it acts as the space velocity. The effect of flow rate on the temperature profile is illustrated in **Figure 2-12**. Its trend is similar to that by X_1 but with a reduced extent. It is manifested that effective and efficient heat transfer can be achieved by smaller X_1 , bigger X_2 and lower flow rate.

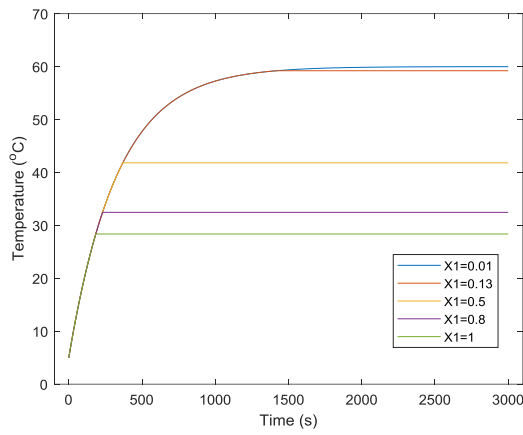


Figure 2-10 Effect of X_1 on the temperature profile at outlet by Eq. (2-57). $\dot{V}=0.3$ ml/min, $X_2=0.003$ s $^{-1}$.

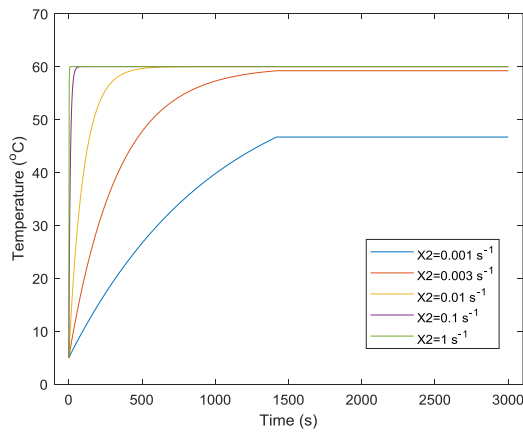


Figure 2-11 Effect of X_2 on the temperature profile at outlet by Eq. (2-57). $\dot{V}=0.3$ ml/min, $X_1=0.13$.

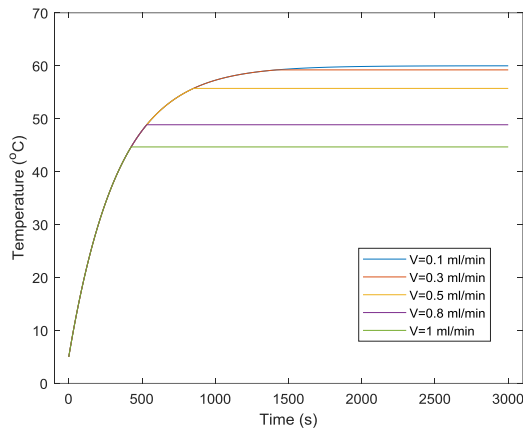


Figure 2-12 Effect of the flow rate \dot{V} on the temperature profile at outlet by Eq. (2-57). $X_1=0.13$, $X_2=0.003$ s $^{-1}$.

For moment calculation, the curve should be in a converged form. Then the analytical solution of temperature profile in Eq. (2-57) is normalised by

$$\gamma = \frac{T(\tau, x) - T_w}{T_0 - T_w} \quad (2-58)$$

Then the analytical solution in terms of γ becomes

$$\gamma(\tau, x) = \begin{cases} e^{-(1-f_z)t_0 X_2 \tau} & \tau \leq \frac{x}{X_1} \\ e^{-(1-f_z)t_0 \frac{X_2}{X_1} x} & \tau \geq \frac{x}{X_1} \end{cases} \quad (2-59)$$

By calculating the first moment of Eq. (2-59):

$$\mu_1 = \frac{\int_0^\infty \tau \gamma(\tau) d\tau}{\int_0^\infty \gamma(\tau) d\tau} = \frac{\frac{-(1-f_z)t_0 X_2 \tau - 1}{[-(1-f_z)t_0 X_2]^2} e^{-(1-f_z)t_0 X_2 \tau} \Big|_0^\infty}{-\frac{1}{(1-f_z)t_0 X_2} e^{-(1-f_z)t_0 X_2 \tau} \Big|_0^\infty} = \frac{1}{(1-f_z)t_0 X_2} \quad (2-60)$$

By substituting μ_1 into γ ,

$$\gamma(\mu_1) = e^{-1} \quad (2-61)$$

Thus, the first moment can be found at where $\gamma(\mu_1) = e^{-1} \approx 0.37$ in the normalised outlet profile. Subsequently, the X_2 can be calculate from Eq. (2-60):

$$X_2 = \frac{1}{(1-f_z)t_0 \mu_1} \quad (2-62)$$

It can be conjectured that the physical meaning of the X_2 is the space velocity and its reciprocal $1/X_2$ is the time to reach gravity centre. The X_1 can be then calculated from Eq. (2-59):

$$X_1 = \frac{-(1-f_z)t_0 X_2}{\ln \gamma^{end}} \quad (2-63)$$

where γ^{end} refers to the final steady state temperature at column outlet.

2.5 Cycle time and productivity

The mass balance in Eq. (2-22) is now indexed by n to describe the mixture of N model components as

$$\left(1 + F \frac{dq_n}{dc_n}\right) \frac{\partial c_n}{\partial t} + u \frac{\partial c_n}{\partial z} = D_{app} \frac{\partial^2 c_n}{\partial z^2} \quad n = 1, N \quad (2-64)$$

If $D_{app}=0$, it becomes EM, whereas if $D_{app}>0$, it is EDM. The corresponding retention times of each component are denoted as $t_{R,n}^f$ and $t_{R,n}^r$ for front and rear bands, respectively.

The selectivity between neighbouring components is defined as

$$\alpha^{(n,n+1)} = \frac{k_{H,n+1}}{k_{H,n}} \quad (2-65)$$

The cycle time is the entire span of effective component bands, as shown in **Figure 2-13**. It is expressed by the retention time difference between rear band of the last eluting component and the front band of the first eluting component as

$$\Delta t_{cyc} = t_{R,end}|_{c_{thres}} - t_{R,start}|_{c_{thres}} \quad (2-66)$$

For EDM, the retention times should be determined at a threshold value c_{thres} . Relevant mathematical procedure are available in [121,122].

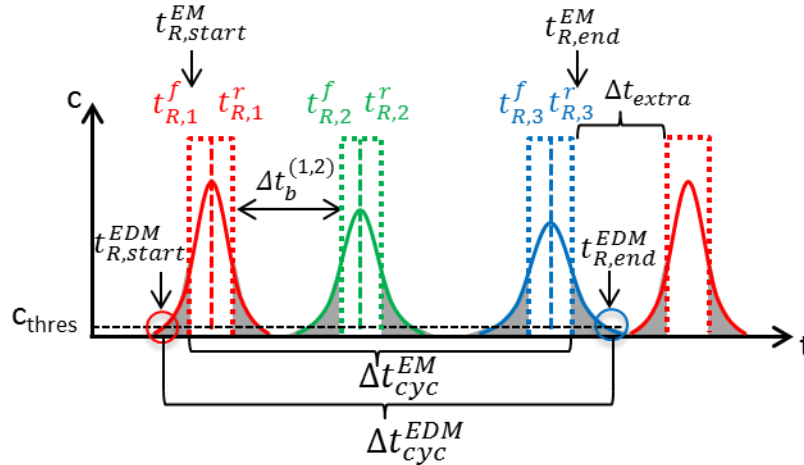


Figure 2-13 Illustration of the cycle time in a ternary mixture.

The cycle time is influenced by the apparent dispersion coefficient or the theoretical plate number N_p , as shown in **Figure 2-14**. It is generated by Eq. (2-34) using different plate numbers. The late eluting component is more dispersed than early eluting component due to longer retention time. The retention times $t_{R,N}^r$ and $t_{R,1}^f$ are changed with the plate number thereby changing the cycle time. If the plate number is high, the chromatograms are very close to that in EM. If the plate number is low, remixing happens.

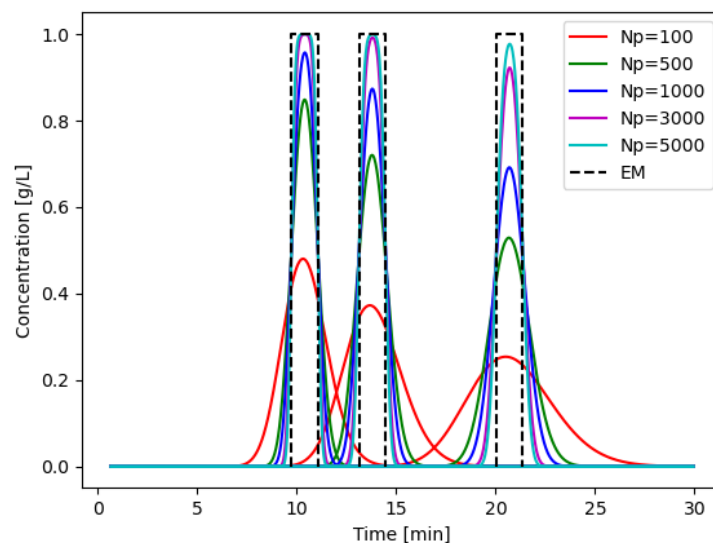


Figure 2-14 Effect of theoretical plate number on the cycle time. The chromatograms are generated by Eq. (2-34).

To account for separation quality, the selectivity $\alpha^{(n,n+1)}$ in Eq. (2-65) is usually used in analytical chromatography. However, in preparative chromatography the band break between neighbouring components $\Delta t_b^{(n,n+1)}$ is more indicative and practical, which is defined as

$$\Delta t_b^{(n,n+1)} = t_{R,n+1}^f - t_{R,n}^r \quad (2-67)$$

The band break between the last component and the first component in the next cycle $\Delta t_b^{(N,1)}$ is related to the extra time Δt_{extra} in Figure 2-13. To avoid remixing in the actual process, the band break between the last component and the first component in the next cycle $\Delta t_b^{(N,1)}$ as a safety margin can also be actively adjusted. In some gradient operations, an unavoidable safety time Δt_{safe} is passively generated, which will be mentioned in section 5.3.1 and section 5.4. Hence, the extra time is the bigger value between them as

$$\Delta t_{extra} = \max \{ \Delta t_b^{(N,1)}, \Delta t_{safe} \} \quad (2-68)$$

Regardless of gradients, there are four possible chromatograms in terms of selectivity and cycle time, as shown in **Figure 2-15**. If the selectivity is low and remixing happens, the method is not applicable in spite of a short cycle time. If the selectivity is high but with a long cycle time, further improvements can be done using gradients to reach optimal selectivity and the cycle time.

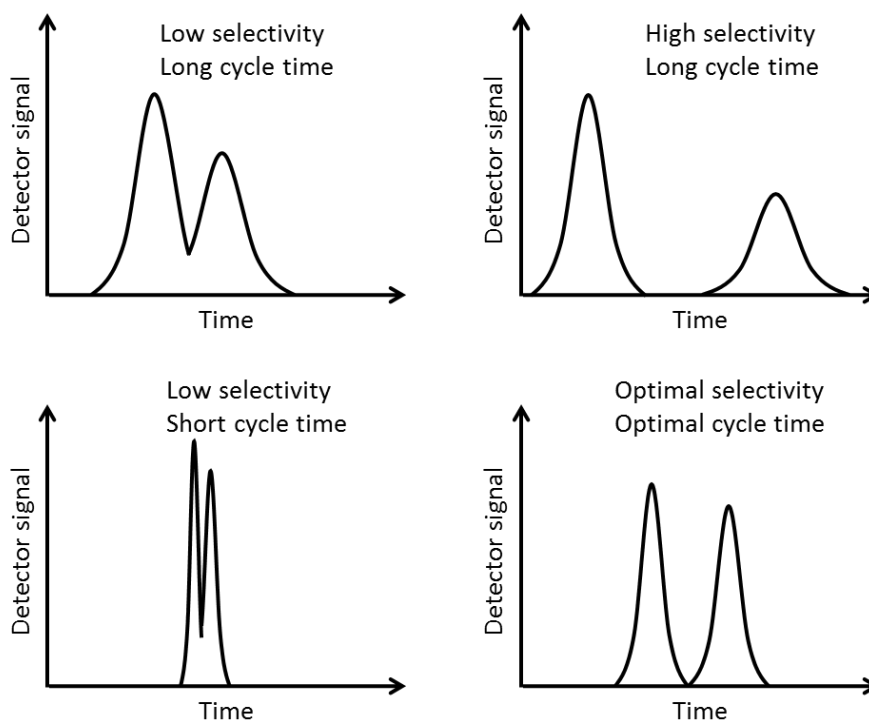


Figure 2-15 Demonstration of various separation scenarios.

In preparative chromatography, the performances are usually indicated by productivity, purity and yield. The purity is defined as

$$Pu_n = \frac{m_{o,n}}{\sum_{j=1}^N m_{o,n}} \quad (2-69)$$

The yield is defined as

$$Y_n = \frac{m_{o,n}}{m_{f,n}} \quad (2-70)$$

where $m_{o,n}$ refers to the injection mass.

The productivity is taken as the main performance indicator in this study, which is defined as

$$Pr_n = \frac{m_{o,n}}{V_c \Delta t_{tot}} = \frac{m_{o,n}}{V_c (\Delta t_{cyc} + \Delta t_{extra})} \quad (2-71)$$

where $m_{o,n}$ refers to the mass collected at the outlet. V_c is column volume as the scale relevant quantity. Δt_{tot} is the total production time defined as

$$\Delta t_{tot} = \Delta t_{cyc} + \Delta t_{extra} \quad (2-72)$$

The extra time typically exist in gradient operations.

To compare the performance for different gradients or their combinations, the input of additional energy and material should be taken into account. Since the temperature and modifier fraction have different metrics, they are converted to relative changes to their reference of temperature ΔT^{rel} and modifier fraction Δx_{mod}^{rel} , as defined in Eq. (2-73) and Eq. (2-74).

$$\Delta T^{rel} = |T - T_R|/T_R \quad (2-73)$$

$$\Delta x_{mod}^{rel} = \frac{|x_{mod} - x_{mod,R}|}{x_{mod,R}} \quad (2-74)$$

For actual performance comparison, the normalised productivity ΔPr^* is evaluated by their weighted sum as

$$\Delta Pr_n^* = \frac{Pr - Pr(Ref)}{w_1 \Delta T^{rel} + w_2 \Delta x_{mod}^{rel}} \quad (2-75)$$

where $w_1 = w_2 = 1$ was set for simplicity in this study. In practice, the weights should be determined based on careful consideration.

In summary, the two types of mass balances in Eq. (2-10), Eq. (2-22) and the short-cut energy balance in Eq. (2-53) are ingredients of the models used in the following parts. They will be used in chapter 5 and 6.

Chapter 3. Case study and experimental system

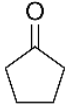
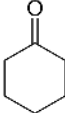
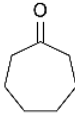
In this chapter, materials used for chromatographic systems including solutes, mobile and stationary phases are introduced. Then the experimental system is illustrated and measurements of extra-column effects are described. Parameter determination methods for thermodynamic and kinetic effects are discussed. The determination of the parameters for the short-cut energy balance is also addressed.

3.1 Model components and adsorption system

In this study, a series of cycloketone, namely Cyclopentanone (C5), Cyclohexanone (C6) and Cycloheptanone (C7) from Alfa Aesar were chosen as the model components due to its simplicity, cheapness and available data [123]. They are widely used for researches in chromatographic processes [22,39,124–128]. Their chemical structures and physical properties are summarised in **Table 3-1**. A C18 column (Agilent Zorbax Eclipse XDB, $D_c=4.6$ mm, $L_c=100$ mm, $d_p=5$ μ m) was used as the stationary phase. The adsorbent is usually packed by dynamic axial compression method [129]. Methanol (Sigma-Aldrich) as modifier and distilled water filtrated with filter paper (Sartorius Stedim Biotech GmbH, 0.45 μ m) were used as the mobile phase. This combination for eluent is widely used in reverse phase chromatography [28,29]. The well-acknowledged modifiers are methanol and acetonitrile. Normal selection criteria are high solute solubility, low corrosivity, UV absorbance, viscosity, flammability and toxicity [130]. Acetonitrile has lower UV cutoff and viscosity, whereas methanol has lower price and toxicity. The mobile phase may contain other species, e.g. buffer for modulation [131].

The modifier fractions in this work were set at a reference $x_{mod,R}=0.5$. A lower limit $x_{mod,L}=0.3$ and a higher limit $x_{mod,H}=0.7$ was selected. In this range, significant changes in retention times were expected. Due to the reverse phase feature, the components are eluted in the order C5, C6 and C7. It will be shown later that the chromatograms of their mixtures under isothermal and isocratic conditions form a typical partly lagged problem, as described in section 1.3.

Table 3-1 Model components and their properties.

Component name	Cyclopentanone	Cyclohexanone	Cycloheptanone
Formula	C_5H_8O	$C_6H_{10}O$	$C_7H_{12}O$
Abbreviation	C5	C6	C7
Structure			
Form	Liquid	Liquid	Liquid
Molecular weight [g/mol]	84.12	98.15	112.17
Density [g/ml]	0.949	0.948	0.956
Boiling point [°C]	130.6	155.7	179.0
Melting point [°C]	-58.2	-47.0	-21

The injection concentrations $c_{inj,n}$ were prepared in volume fraction $x_{inj}=0.1$ vol% in the reference mobile phase ($x_{mod}=0.5$), corresponding to concentrations of 0.949 g/L, 0.948 g/L and 0.956 g/L, respectively. In preliminary tests, it was found out that under this condition the linear range of the isotherms are valid. The flow rate \dot{V} was fixed at 0.3 ml/min in this study. The relatively lower flow rate was selected to allow sufficient heat exchange, as described in section 2.4.3. The injection volumes V_{inj} used in this study were 50 μ L, 400 μ L, 1500 μ L (via pump) for determination of kinetic and thermodynamic parameters (section 4.3 and section 4.4), mixture separation (section 6.3.2 and section 6.4) and validation of temperature gradients (section 6.3.1), respectively. Corresponding injection periods $\Delta t_{inj}(=V_{inj}/\dot{V})$ at fixed flow rate were 0.17 min, 1.33 min and 5 min, respectively. The reason why these injection volumes were chosen are explained in section 6.3. As shown in **Figure 3-1**, the retention times in chromatograms do not change with the injection volumes used in the entire study. The largest injection volume of C7 in the same concentration was injected by pump and the resulting chromatogram was corrected by the delay time. This is in accordance with the behaviour described in **Figure 2-4**.

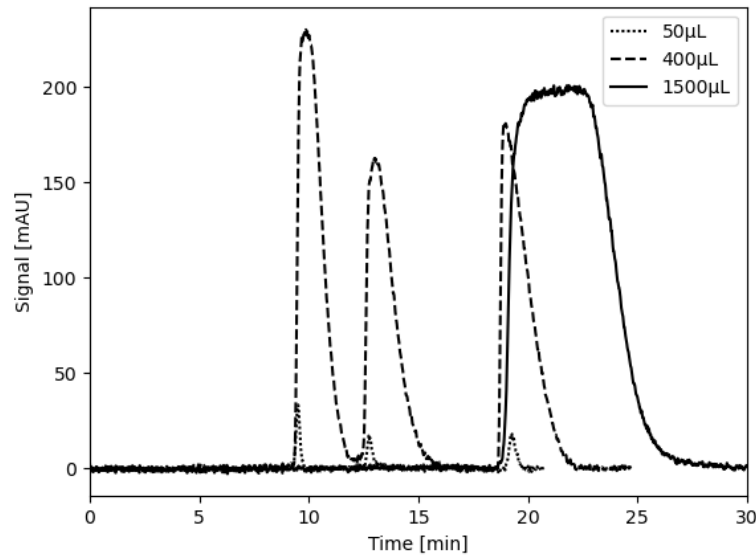


Figure 3-1 Results of volume overload experiments for checking linearity of isotherm. $c_{inj,n}=[0.949, 0.948, 0.956]$ g/L, $V_{inj}=50, 400$ μ L. An injection volume $V_{inj}=1500$ μ L of C7 was injected as single solute (solid line). $\dot{V}=0.3$ ml/min.

The all applied chromatographic conditions are summarised in **Table 3-2**.

Table 3-2 Chromatographic system and reference conditions in this study.

Symbol	Name	Value
L_c	Column length	2×100 mm
$D_{c,i}$	Column diameter	4.6 mm
d_p	Adsorbent diameter	5 μ m
x_{inj}	Injection volume fraction	0.1 vol%
$c_{inj,n}$	Injection concentration, n=C5,C6,C7	[0.949, 0.948, 0.956] g/L
\dot{V}	Volumetric flow rate	0.3 ml/min
V_{inj}	Injection volume	50 μ L (section 4.3 + section 4.4)
		400 μ L (section 6.3.2 + section 6.4)
		1500 μ L (section 6.3.1)
Δt_{inj}	Injection period ($= V_{inj}/\dot{V}$)	0.17 min (section 4.3 + section 4.4)
		1.33 min (section 6.3.2 + section 6.4)
		5 min (section 6.3.1)

3.2 Experimental setup for implementing gradients

The schematic diagram of experimental set-up for solvent and segmented temperature gradients is illustrated in **Figure 3-2** whereas the real experimental set-up is shown in **Figure 3-3**.

The solvent gradient in terms of modifier fraction x_{mod} is modulated by a proportioning valve built in a HPLC under the low pressure mixing. The range of modifier fraction applied was between 0.3 and 0.7. The fraction is changed by proportional flow time from each channel, which was confirmed to provide reproducible results compared to a premixed single solvent channel.

The temperature gradient is realised by extending a typical HPLC set (Hewlett Packard 1100) with a temperature modulation unit in a segmented way. The segmented system is formed by connecting two identical columns in series via a short and thin capillary, which can be allowed to consider them as a single column. One column is placed in the HPLC oven and the other one in a cylindrical water jacket.

The temperature of the first segment of whole column is kept at reference temperature ($T_{segment I} = T_R = 25^\circ\text{C}$) whereas that of the second column is controlled by the circulating water from two thermostats to water jacket. The mobile phase inside the column and the water in water jacket flow in a counter-current manner. One thermostat is circulating hot water while the other one is circulating cold water. The water from each thermostat can be circulated internally or externally via 3-way switch valves. Between each switch, one thermostat is circulating internally while the other one externally. Upon switch, the circulating combination becomes opposite and the water in the water jacket is replaced by that from the other thermostat at different temperature. Hence, the temperature of the second column can be modulated stepwise by switch valves between low temperature T_L and high temperature T_H , i.e. $T_{segment II} = T \in \{T_L, T_H\}^\circ\text{C}$. By considering the safety range of the column, the temperature of lower limit T_L and higher limit T_H were set as 5°C and 60°C , respectively.

Ideally, the adsorption temperature refers to the interface between mobile and stationary phases. However, the exact temperature inside a lab-scale column or capillary line (0.17mm in inner diameter) at outlet cannot be measured due to technical difficulty in matching sizes between the outlet line and the probe of thermocouple, whereas it can be measurable in a preparative column. Hence, the temperatures were measured at two feasible positions by thermocouples: one inside the water jacket inlet T_w , and the other on the outer surface of the column outlet line T_{mes} . Both temperatures were measured and recorded in real time. As mentioned in section 2.3.2, the temperature

during each period between two switch times are constant, and thus this period can be considered under isothermal condition. In ideal model for energy balance, equilibria between column interior, column wall and surrounding water were assumed so that the adsorption temperature is equal to the water temperature, i.e. $T = T_w$. The real adsorption temperature can be approximated by an additional calibration, which will be discussed in the section 3.4.2.

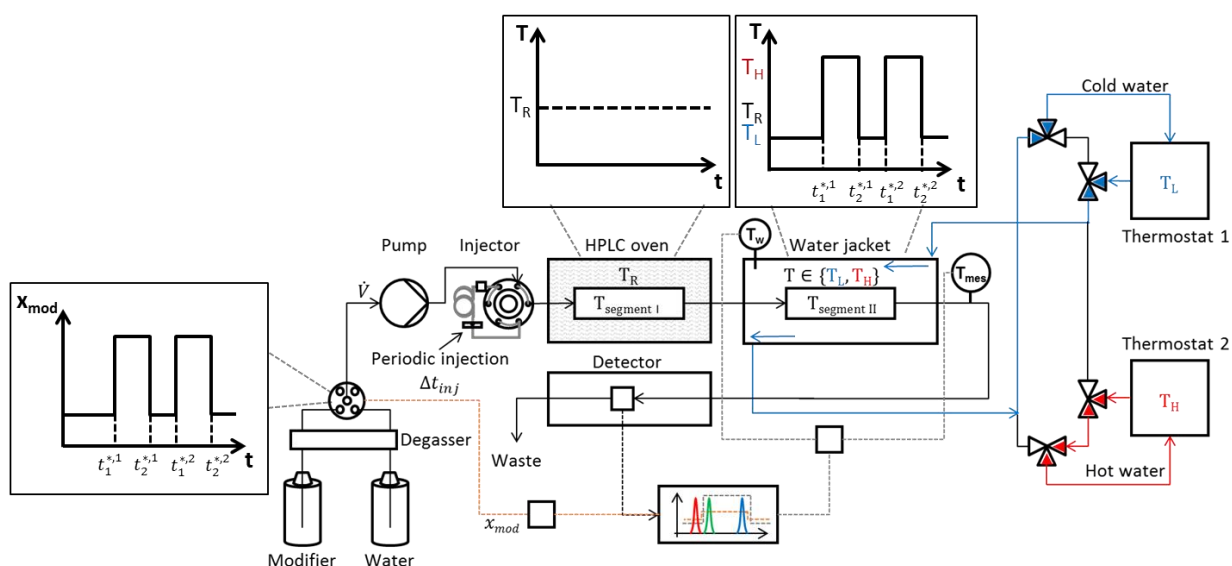


Figure 3-2 Schematic diagram of experimental set-up for solvent and segmented temperature gradients. It is an extension of a typical HPLC with an external temperature modulation unit consisting of water jacket and thermostats. The modifier fraction x_{mod} is modulated by a proportioning valve built in the HPLC. The temperature is modulated at the second segment in the water jacket to low or high temperatures, $T_{segment II} = T \in \{T_L, T_H\}^{\circ}\text{C}$. The temperatures are measured in real time at a position inside the water jacket inlet T_w , and at the other position on the outer surface of the column outlet line T_{mes} . Both modulations are characterised by switch times $t_i^{*,k}$. As already mentioned above, the flow rates provided by the pump was fixed at $\dot{V}=0.3$ ml/min.

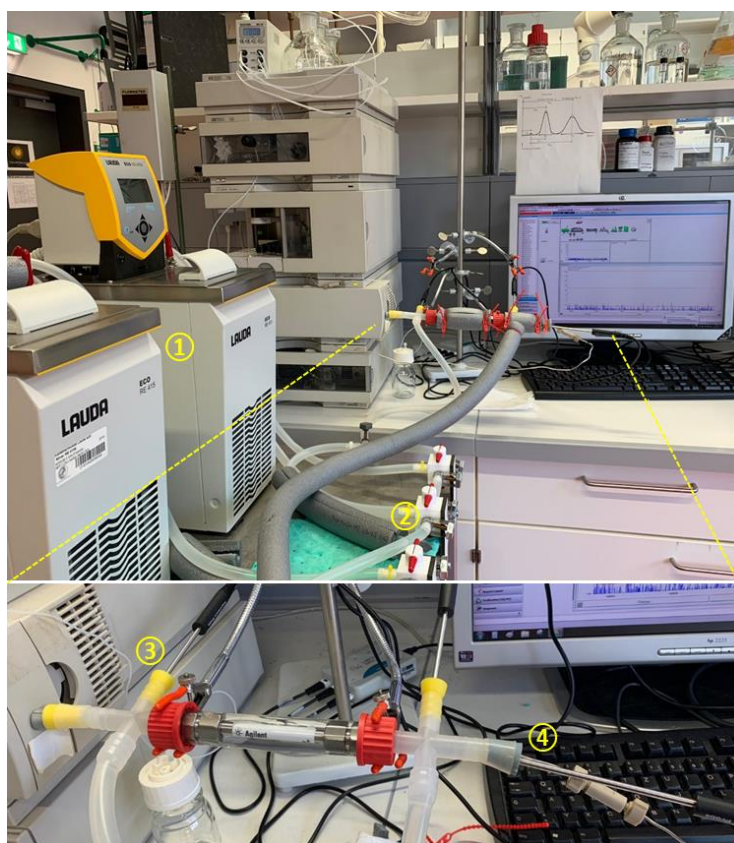


Figure 3-3 Real experimental set-up for solvent and segmented temperature gradients. 1- Thermostats; 2-Switching valves; 3- T_w ; 4- T_{mes}

The conditions of temperature and solvent gradients are summarised in **Table 3-3**. The modifier fraction was used in the whole range for determination of thermodynamic parameters (section 4.4) whereas only the range between $x_{mod,R}$ and $x_{mod,H}$ during mixture separation (section 5.4 and section 6.4) was used.

Table 3-3 Reference conditions and ranges for solvent and temperature gradients used in this study.

Symbol	Name	Value
<i>Solvent gradients</i>		
$x_{mod,R}$	Reference modifier fraction	0.5
$x_{mod,L}$	Lower limit of modifier fraction	0.3
$x_{mod,H}$	Higher limit of modifier fraction	0.7
<i>Temperature gradients</i>		
T_R	Reference temperature	25 °C (298 K)
T_L	Lower limit of temperature	5 °C (278 K)
T_H	Higher limit of temperature	60 °C (333 K)

3.3 Measurement of extra-column parameters

The times of extra-column should be always determined prior to experiments planned. They are plant dead time t_{plant} , column dead time t_0 and delay time t_{delay} . These times are illustrated in **Figure 3-4**. It should be noted that these times are dependent of flow rate and thus corresponding volumes are preferably reported.

The time t_{plant} refers to the time needed to transport the fluid from the injection valve to the detector flow cell without the columns, which can be measured by a small amount of tracer dissolved in the mobile phase in a marker experiment. Thiourea from Merck was used as the tracer in this study. The time t_0 refers to the time that the mobile phase passes through the column, which can be measured by a non-retained component. The same tracer was used as the non-retained component in this study. It should be noticed that the plant dead time should be subtracted from the observed column dead time to get the correct value. Once the plant dead time and the column dead time are known, the total porosity of the column can be calculated by rearranging Eq. (2-18) as:

$$\epsilon_t = \frac{4\dot{V}t_0}{\pi L_c D_{c,i}^2} \quad (3-1)$$

where L_c and $D_{c,i}$ are the length and inner diameter of the column, respectively.

Under solvent gradient operations, an additional delay time t_{delay} from the confluence point of mixer to the injection valve should be considered since it is related to the switch times. In actual operations, the delay time should be always subtracted from the calculated switch times.

In the case that the gradient is designed to start with the eluting components at the column inlet at the same time, the injection valve should be programmed to wait for a delay time long for the first injection. It is relatively easy to be programmed in the preparative scale using a pump for injection. However, it is complicated in the analytical scale using an auto-sampler for larger volume injection, since the entire time for injection is varied with injection volume and vial position. The standard action of an injection with an auto-sampler includes initial ejection, arm movement, vial transportation, feed loading (load position) and elution start (inject position). This entire action time should be considered for programming a regime which performs consecutive injections.

The delay time can be determined by subtracting the plant dead time from the total plant dead time without columns. Ideally, a pulse experiment is desired to measure the retention time. However, it led to a flat or undetectable signal due to the severe dispersion as the inner diameter of the line between mixer and pump is much larger than capillary line in the rest parts. Hence, a step response experiment is instead conducted. The step response can be generated from a step input via the proportional valve of the mixer. Theoretically, the retention time is the inflection point in a non-ideal step response. However, it is difficult to be determined without smoothening since the signal contains oscillation in the actual case. Therefore, the time at half height is considered as the retention time in practice.

The injection valve position has a direct influence on the delay time. For the standard injection by HPLC, the valve is initially set at the mainpass (inject) position. Upon loading, the valve is switching to the bypass (load) position for feed loading followed by returning to the mainpass position for injection. In the case of preparative scale, it has no issue since a sample loop with a certain volume is used. However, in the analytical scale, a suction pump with a volume controller is built in a fixed sample loop in order to tackle with various injection volumes. If the injection volume is much smaller than the sample loop volume, it leads to unnecessary longer delay time. In this study, the injection volume and sample loop volume are 400 μL and 900 μL , respectively. Ideally, the delay time should be kept as short as possible to deploy solvent gradients promptly. In order to shorten the delay time, the injection valve is programmed to switch to the bypass position after a feeding time, which is the period for the loaded feed in the sample loop fully leaves from the injection valve. This feeding time corresponds to the wait time in the injector programme, which depends on the flow rate, injection volume and injector dead volume including the seat volume. It can be empirically determined by finding out the minimal wait time that generates the same chromatogram without feed loss as that in a non-switched injection. If the feeding time is longer than the delay time, the earliest start time of the gradient is their difference.

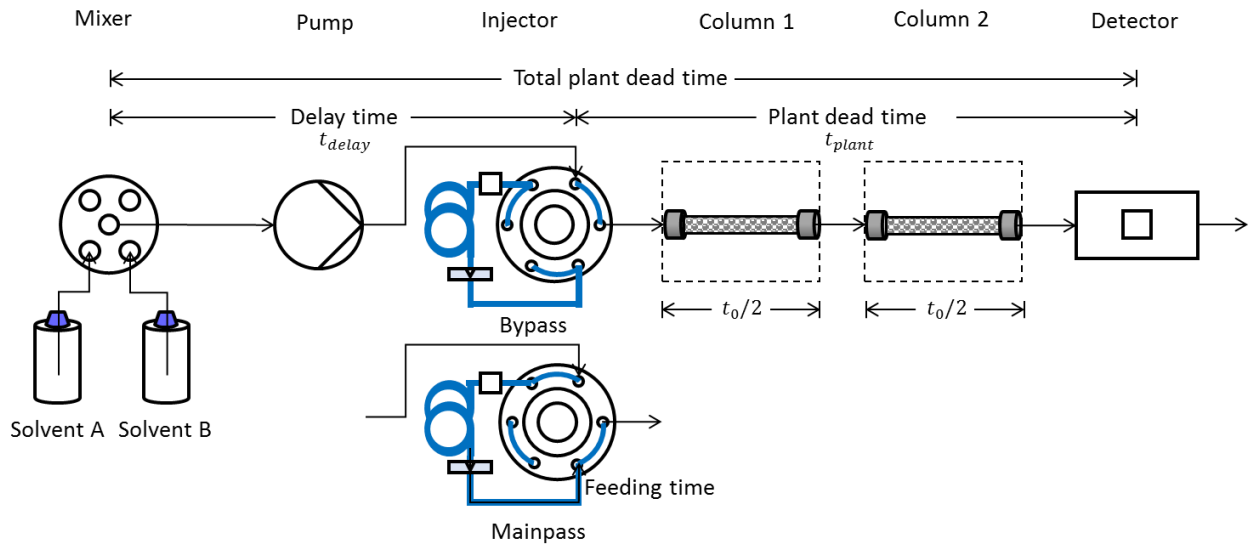


Figure 3-4 Schematic diagram for various times of extra-column. The entire path includes from the confluence point of mixer to the detector flow cell.

3.4 Calibrating sensors

On one hand, detector should be calibrated in terms of calibration factor $f_{calb,n}^\lambda$ for each component to convert signals to concentration profiles before processing chromatograms. On the other hand, the measured temperature should be calibrated before determining parameters for energy balance.

3.4.1 UV Detector calibration

Each component has a unique spectrum of UV light absorbance according to the wavelength λ , which can be measured by a UV spectroscopy. The proper wavelength should be chosen by comparing spectra to make sure all components as well as disturbing impurities detectable. The function of diode array detection can be used beforehand to detect impurities in entire range of wavelength. Depending on the separation problem, multiple wavelengths can also be used. In analytical scale under the dilute condition, the wavelength is usually chosen around the local maximum in the spectrum to get recognisable peaks with less deviation. In preparative scale under the overload condition, the wavelength is preferably chosen at lower intensity range in order to avoid detector overload. In most diluted conditions, the detector response is linear, i.e. the signal is linearly dependent with solute concentration. From a certain high concentration, this relationship might become nonlinear or even overloaded, as shown in **Figure 3-5**. Therefore, the linearity of detector response should always be check before calibration. There are two popular calibration methods, namely area method and plateau method [132].

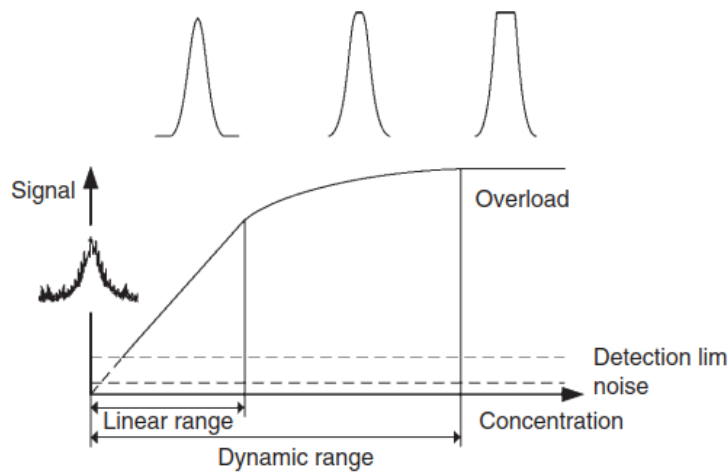


Figure 3-5 Demonstration of different ranges of detector response [29].

The area method is limited to the linear response range of the detector. The detector signal $Sig(t)$ and concentration profile $c(t)$ at wavelength λ are linearly correlated by the detector calibration factor $f_{calb,n}^\lambda$ as:

$$c(t) = f_{calb,n}^\lambda Sig^\lambda(t) \quad (3-2)$$

By multiplying the flow rate \dot{V} and integrating both sides, the injection mass m_{inj} can be obtained as:

$$m_{inj} = \dot{V} \int_0^\infty c(t) = \dot{V} f_{calb,n}^\lambda \int_0^\infty Sig^\lambda(t) = \dot{V} f_{calb,n}^\lambda A_{peak}^\lambda \quad (3-3)$$

where the injection mass m_{inj} and peak area A_{peak} are linearly correlated by the detector calibration factor at the fixed flow rate. Hence, the wavelength dependent detector calibration factor can be extracted from the slope of a m_{inj} - A_{peak} plot in a loading increment experiment.

The plateau method is more intuitive and not limited to the linear response range. In this method, solutions of each component in mobile phase with known concentrations are continuously fed to the system without columns and the detector generates the response in a plateau form. Thus, the responded signal intensities are directly correlated with known concentrations, e.g. a constant $f_{calb,n}^\lambda$ in Eq. (3-2) under the linear response range. As the signal intensities without columns are much higher than those with columns, lower concentrations are usually applied. In order to generate feeds with different concentrations and different modifier fractions in a simple way, the staircase formulation like in frontal analysis can be utilised. It can be implemented by mixing concentrated mother solution and mobile phase via mixer. The concentration of mother solution should be high enough to cover the intended concentration and modifier fraction

ranges. Additionally, higher flow rate can be used in this calibration procedure in order to save time.

3.4.2 Calibrating measured temperature

For energy balance under non-isothermal condition, equilibria between column wall, mobile and stationary phase and were assumed. As mentioned in section 3.2, the temperature inside a lab-scale column is not measurable due to technical difficulty and thus the water temperature T_w and outlet temperature T_{mes} (in **Figure 3-2** and **Figure 3-3**) were instead measured. However, the T_{mes} cannot necessarily represent the adsorption temperature inside the column and leads to irrational values. This issue was identified by an experiment for flow rate effect. As described in **Figure 2-11**, the final steady state temperature decrease with the increasing flow rate. However, the preliminary measurement results showed the opposite trend due to unavoidable heat exchange with ambience. In case of heating, the measured outlet temperature is lower than the true temperature inside the column, as shown in **Figure 3-6**.

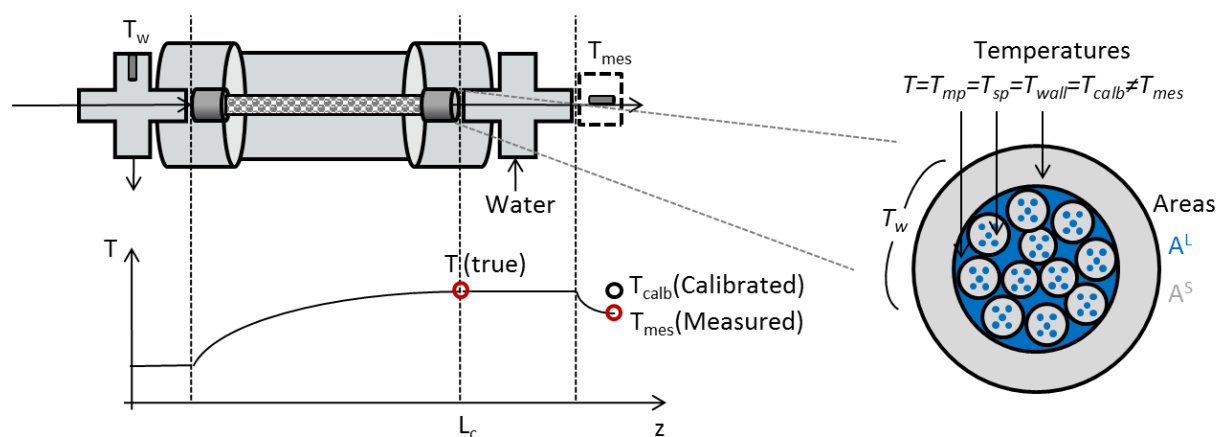


Figure 3-6 Schematic temperature profile along the column in case of heating. The measured outlet temperature is not equal the true temperature so that a calibration procedure is required.

To approximate the real adsorption temperature, an additional calibration procedure is required. The column inside the water jacket was replaced by a long steel tube with a bigger inner diameter (0.75 mm), as shown in **Figure 3-7**. The eluent passes through the tube line at the same flow rate. Once a temperature was set, this system was stayed untouched for half an hour in order to reach equilibrium among all elements in the water jacket. Then the temperature T_1 and T_2 corresponding to T_w and T_{mes} in the normal setup were recorded. By repeating this procedure for different temperatures, a calibration formula correlating T_1 and T_2 can be obtained. It was also repeated for different flow rates. Thus, the real adsorption temperature can be approximated by correcting T_{mes} using the calibration formula as follows

$$T = T_1 = p_1 T_2 + p_2 = p_1 T_{mes} + p_2 \quad (3-4)$$

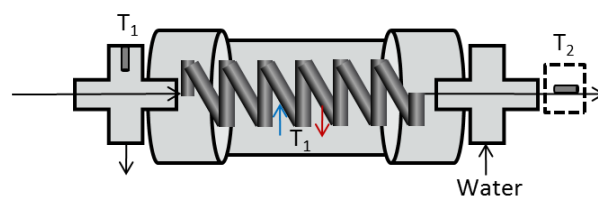


Figure 3-7 Experimental set-up for calibrating measured temperature.

3.5 Estimation of kinetic effect in column

As aforementioned, the theoretical plate number N_p can be used to estimate apparent dispersion coefficient D_{app} by Eq. (2-32). In this study, symmetric Gaussian peak is assumed due to linear isotherm. The N_p can be then approximated by Eq. (2-33). The chromatograms from pulse experiments can be used to calculate N_p . Theoretically the N_p is function of temperature and modifier fraction, and it will be examined by experimental data.

3.6 Estimation of Henry's constants

Once the plant dead time, the column dead time and porosity are known, Henry's constant k_{H_n} as the thermodynamic parameter under the linear isotherm can be determined by a pulse experiment. It can be implemented by injecting small amount of solute dissolved in the mobile phase and recording the retention time. The same chromatograms for estimation of the theoretical plate number were used. As the main thermodynamic factors in this study, pulse experiments under different temperatures and modifier fractions were carried out. The Henry's constant can be calculated by rearranging Eq. (2-18) as:

$$k_{H_n}(T, x_{mod}) = F \left[\frac{t_{R,n}(T, x_{mod}) - t_{plant}}{t_0} - 1 \right] \quad n = 1, N \quad (3-5)$$

where $t_{R,n}$ is the retention time of each component. Together with Henry's constant it is a function of temperature and modifier fraction.

As mentioned in section 2.2, the dependence in temperature and modifier fraction of Henry's constant can be described by Van't Hoff relation and linear solvent strength model, respectively. The experimental data can be used to validate them.

Chapter 4. Determined parameters for the case study

In this chapter, results of various parameters for system, thermodynamic and kinetic effects described from the previous chapter are given. The obtained parameters for system energy balance are also discussed. Some example chromatograms under “iso” conditions and gradient conditions are shown.

4.1 Extra-column parameters of the chromatographic system

All extra-column parameters were determined according to the description in section 3.3 and summarised at the end.

First, the plant dead time t_{plant} and column dead time t_0 were measured by marker experiments using Thiourea as the tracer, as shown in **Figure 4-1**. As a result, t_{plant} and t_0 were determined to be 0.25 min and 6.2 min, respectively. The plant dead volumes V_{plant} at $\dot{V}=0.3$ ml/min was calculated to be 0.075 ml. The total porosity of the column ε_t was calculated using Eq. (3-1) to be 0.555. The corresponding phase ratio F was then calculated to be 0.802.

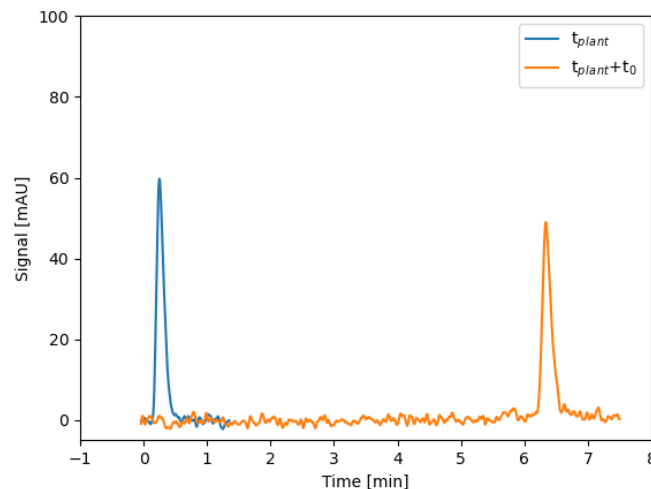


Figure 4-1 Marker experiments to determine t_{plant} , t_0 and ε_t at $\dot{V}=0.3$ ml/min. $V_{inj}=50$ μ L.

Next, the delay time t_{delay} was measured by a step response experiment, as shown in **Figure 4-2**. The step input was generated by switching the proportional valve from the pure mobile phase to the tracer solution at $t=0$ min. From the resulting step response, the time at half height was taken as the delay time. The responses for different injection valve positions were recorded. Consequently, the t_{delay} at bypass and mainpass positions were determined to be 2.6 min and 8.4 min. Their difference is due to the large sample loop volume and the lower flow rate. As aforementioned, the valve is switched

to the bypass position after a feeding time. The feeding time was determined to be 2.3 min for the injection period $\Delta t_{inj}=1.3$ min ($V_{inj}=400$ μ L, $\dot{V}=0.3$ ml/min). Thus the injector dead time was then determined to be 1 min corresponding to the injector dead volume of 0.3 ml.

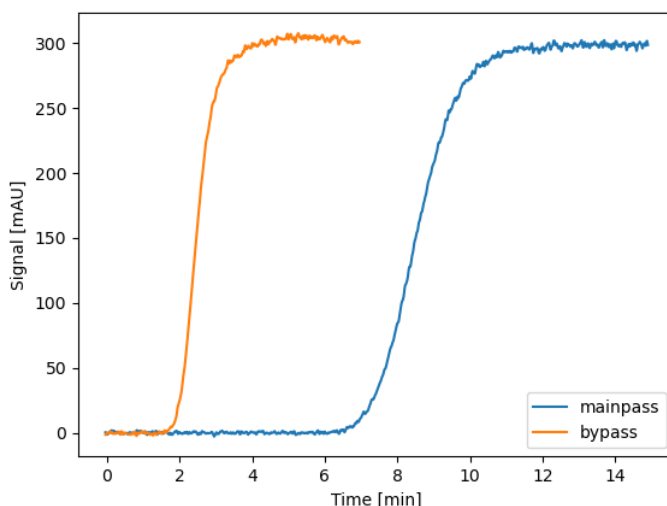


Figure 4-2 Step response experiment to determine t_{delay} . The responses at injection valve positions of mainpass and bypass are compared. The flow rate was fixed at $\dot{V}=0.3$ ml/min.

Additionally, the gradient deviation time Δt_G described in section 2.3.5 was determined. The fitted signal of step response using Eq. (2-35) is illustrated in **Figure 4-3**. By using Eq. (2-37), the gradient deviation time Δt_G was determined to be 1 min.

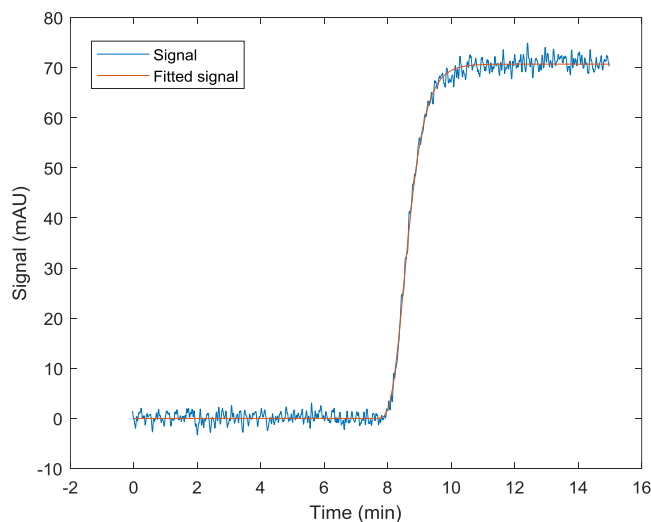


Figure 4-3 Illustration of solvent profile after step changes and fitted curve by Eq. (2-35) for determining gradient deviation time Δt_G in Figure 2-9.

The determined extra-column parameters are summaries in **Table 4-1**.

Table 4-1 Summary of column and extra-column parameters.

Symbol	Name	Value
ϵ_t	Column total porosity	0.555
F	Phase ratio for mass transfer	0.802
t_0	Column dead time at $\dot{V}=0.3$ ml/min	6.2 min
t_{plant}	Plant dead time	0.25 min
V_{plant}	Plant dead volume	0.075 ml
t_{delay}	Delay time (Bypass position)	2.6 min
V_{delay}	Delay volume	0.78 ml

4.2 Calibration parameters

Calibration parameters mentioned in section 3.4 are determined. For detector calibration, the plateau method was used in this study. The plateaus were formulated in a staircase manner in order to deal with different feed concentrations and modifier fractions, as shown in **Figure 4-4**. Five wavelengths, namely 240, 260, 280, 300, 320 nm were recorded, and $\lambda=280$ nm was finally adopted due to high sensitivity. The concentrations were set between 0.1 and 0.5 vol% as the calibration data and their corresponding intensities were recorded. The detector responded linearly in this concentration range. This procedure was repeated within the range of modifier fraction x_{mod} between 0.3 and 0.7. The mother solution was prepared in 0.84 vol% in the reference mobile phase $x_{mod,R}=0.5$, and the mixing proportion from each channel of mother solution and modifier can be calculated from material balance. The flow rate was set as $\dot{V}=1$ ml/min and each plateau concentration including the final reset was maintained for 5 min. As a result, the modifier fractions had little influence on the calibration factor and thus their average values were used for simplicity. The averaged calibration factors of C5, C6 and C7 were determined to be 0.004, 0.005 and 0.005 $\text{gL}^{-1}\text{mAU}^{-1}$, respectively. For temperature calibration, the method mentioned in section 3.4.2 was used. The determined parameters for detector and temperature are summarised in **Table 4-2** and **Table 4-3**.

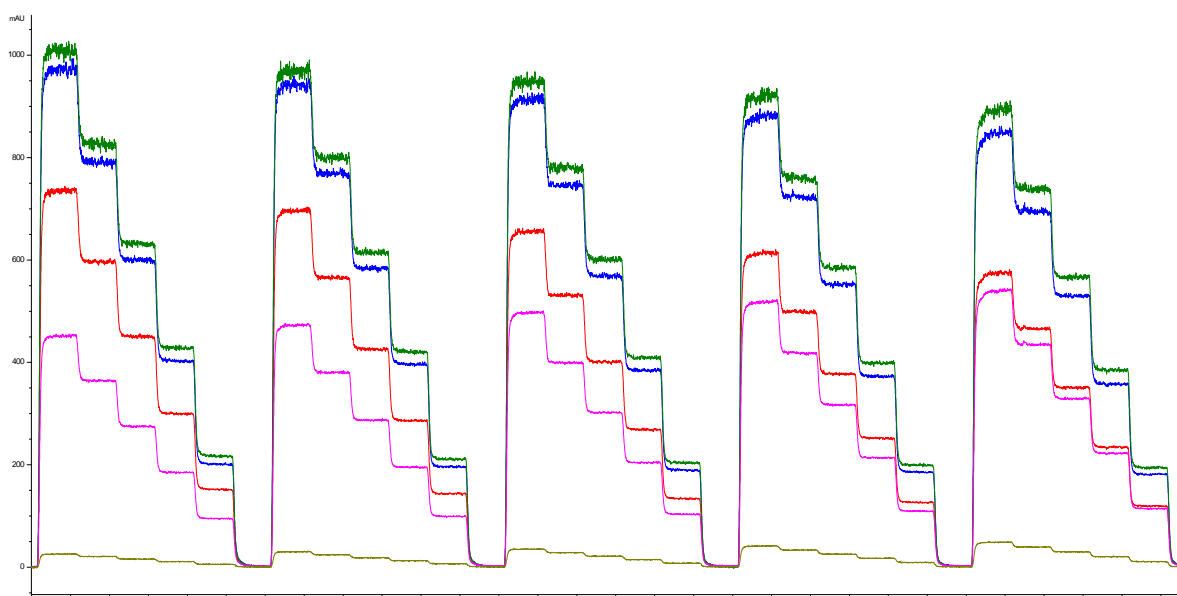


Figure 4-4 Detector calibration using a staircase plateau method for C7 as an example. Blue, red, green, purple and yellow correspond to the wavelength 240, 260, 280, 300, 320 nm, respectively.

Table 4-2 Selected parameters for detector calibration in Eq. (3-2).

Symbol	Name	Value
$f_{calb,C5}^{\lambda=280\text{ nm}}$	Detector calibration factor of C5 at $\lambda = 280\text{ nm}$	$0.004\text{ gL}^{-1}\text{ mAU}^{-1}$
$f_{calb,C6}^{\lambda=280\text{ nm}}$	Detector calibration factor of C6 at $\lambda = 280\text{ nm}$	$0.005\text{ gL}^{-1}\text{ mAU}^{-1}$
$f_{calb,C7}^{\lambda=280\text{ nm}}$	Detector calibration factor of C7 at $\lambda = 280\text{ nm}$	$0.005\text{ gL}^{-1}\text{ mAU}^{-1}$

Table 4-3 Parameters for calibrating measured temperature in Eq. (3-4) at different flow rate \dot{V} .

\dot{V} (ml/min)	ρ_1 (-)	ρ_2 (°C)
0.2	1.8135	-19.813
0.3	1.6297	-15.298
0.4	1.5403	-13.240
0.5	1.4882	-12.009
0.6	1.4521	-11.166

4.3 Kinetic parameters of column

As aforementioned, the dispersion is described by the kinetic parameter in terms of theoretical plate number N_p in EDM. It can be measured from the elution profiles from pulse experiments by Eq. (2-33). Its dependences of temperature and modifier fraction are shown in **Figure 4-5**. Consequently, N_p had no clear dependence of temperature whereas it was linearly dependent with modifier fraction. On one hand, the mass transfer could be fast enough so that the temperature has no obvious influence on dispersion. On the other hand, the retention time are greatly changed by the modifier so that the dispersion is strongly affected. Given that the deviation of N_p is in a relatively narrow

range, the average value of all component in the applied ranges of temperature and modifier fraction was used for simplicity. The averaged theoretical plate number $\overline{N_p}$ was determined to be 2871 for a single column, and the corresponding averaged apparent dispersion coefficient was then calculated to be $\overline{D_{app}} = 0.0057 \text{ cm}^2/\text{min}$.

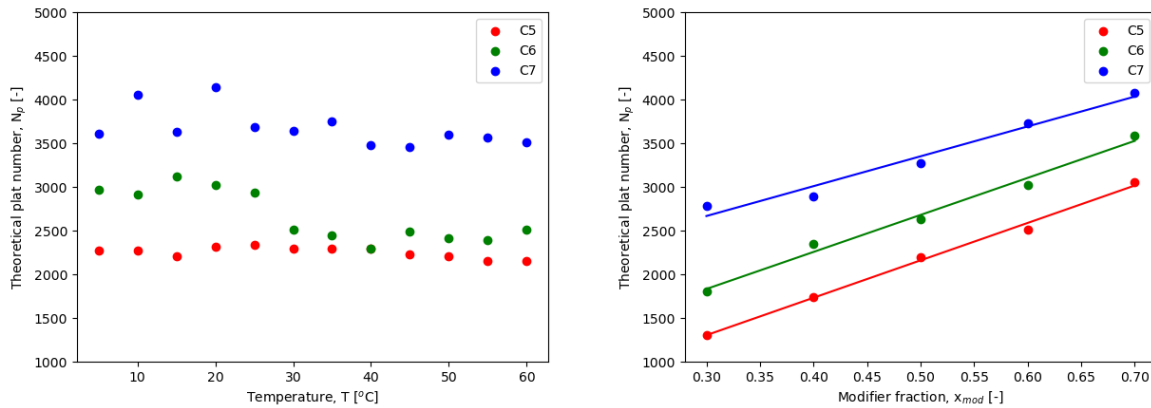


Figure 4-5 Theoretical plate number N_p according to temperature at $x_{mod,R}=0.5$ (left) and modifier fraction at $T_R=298 \text{ K}$ (right) using Eq. (2-33).

4.4 Thermodynamic parameters

Thermodynamics or adsorption isotherms can be influenced by many factors. In this study, temperature and modifier fraction act as the main factors within the linear isotherm range. Their dependence can be determined in either individual or combined way. As described in section 3.6, Henry's constant k_{H_n} can be determined by Eq. (3-5) in pulse experiments. The injection volume $V_{inj} = 50 \mu\text{L}$ is used for pulse experiments to ensure the retention times can be clearly identified in the chromatogram. The complete data for the entire range is placed in Appendix 2.

4.4.1 Effect of temperature on Henry's constant

As described in section 2.2, the temperature dependence of Henry's constant under the isocratic condition is normally described by the Van't Hoff relation. By logarithmically linearising and rearranging Eq. (2-7), a linear relationship between the logarithm of relative Henry's constant to a reference Henry's constant at this temperature $\ln(k_H/k_{H,R})$ and the reciprocal of temperature $1/T$ for each component can be found. The Henry's constant of each component was measured within a broader temperature range and fitted to a line, as shown in **Figure 4-6**. The heat of adsorption ΔH_A can be determined from the slope of this line. As a result, the correlation between $\ln(k_H/k_{H,R})$ and $1/T$ was not perfectly linear, which indicates a more complicated thermodynamics. The heat of adsorption of C5, C6 and C7 were determined as -5.481 kJ/mol , -6.674 kJ/mol and -8.180 kJ/mol , respectively. They are also shown in **Table 4-4**.

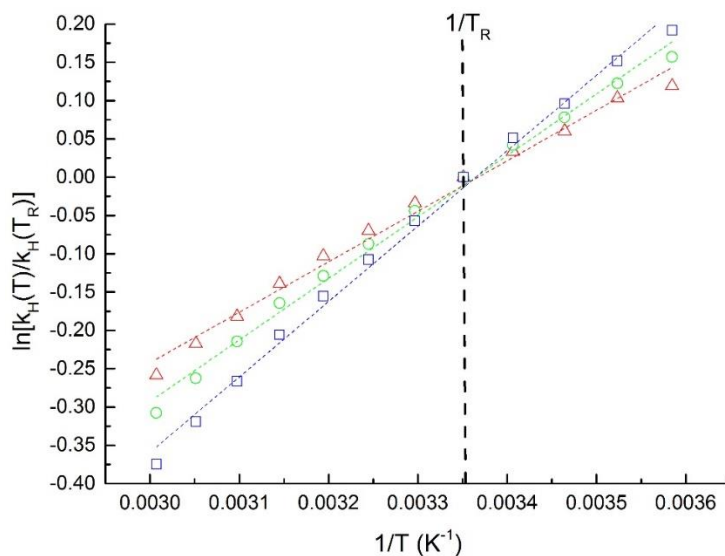


Figure 4-6 Van't Hoff plot, $\ln(k_H/k_{H,R})$ vs $1/T$, for C5 (triangle), C6 (circle) and C7 (square). $\dot{V}=0.3$ ml/min, $V_{inj}=50$ μ L, $x_{inj}=0.1$ vol%, $x_{mod}=0.5$.

Table 4-4 Summary of parameters from Van't Hoff model in Eq. (2-7).

Component	$k_{H,R}$ (-)	ΔH_A (kJ/mol)
C5	0.692	-5.481
C6	1.347	-6.674
C7	2.634	-8.180

4.4.2 Effect of modifier fraction on Henry's constant

As described in section 2.2, the modifier fraction dependence of Henry's constant under the isothermal condition is normally described by the LSS model. By taking logarithm of Eq. (2-8), a linear relationship between the logarithm of Henry's constant $\ln(k_H)$ and the modifier fraction x_{mod} for each component can be found. The Henry's constant of each component was measured within the certain modifier fraction range and fitted to a line, as shown in **Figure 4-7**. They were fitted very well by straight lines. The slope and intercept correspond to the parameters α and $\ln(k_{H0})$ in Eq. (2-8), respectively. The determined parameters of each component are summarised in **Table 4-5**.

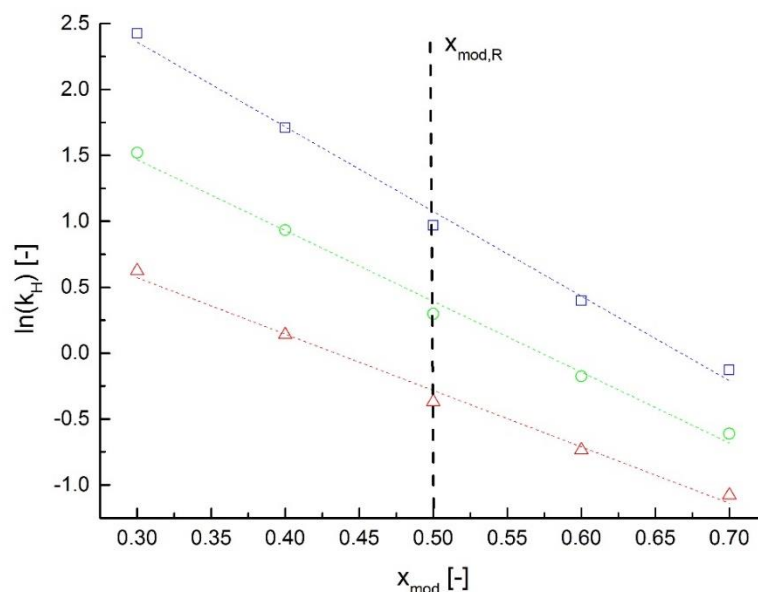


Figure 4-7 LSS plot, $\ln(k_H)$ vs x_{mod} , for C5 (triangle), C6 (circle) and C7 (square). $\dot{V}=0.3$ ml/min, $V_{inj}=50$ μ L, $x_{inj}=0.1$ vol%, $T=298$ K.

Table 4-5 Summary of parameters from LSS model in Eq. (2-8).

Component	k_{H0} (-)	α (-)
C5	6.4	4.3
C6	21.7	5.4
C7	72.5	6.4

4.4.3 Combined effect of temperature and modifier fraction

The dependences of temperature and modifier fraction of Henry's constant were described before by individual models. However, it is quite limited under combined gradients and deviations always exist between models for the same condition. In order to unify the dependence of temperature and modifier fraction for simulations, the combined model was applied. A two-dimensional fitting of Henry's constant in terms of temperature and modifier fraction for Eq. (2-9) was performed using `nlinfit` function in Matlab. The determined parameters are summarised in Table 4-6. The fitted plots are illustrated in **Figure 4-8**, **Figure 4-9** and **Figure 4-10**.

It can be seen from the results that the solvent gradients have a stronger elution strength than temperature gradients since the slopes for solvent gradients are steeper than temperature gradients. For the current model components, the temperature appeared to be more sensitive within the lower modifier fraction range, which has a potential of saving more solvent. The temperature has little influence where the modifier fraction larger than 0.7. The combined dependence is useful to identify the sensitive range and

find the appropriate gradient combinations, though fewer data points might be required in practice.

Table 4-6 Isotherm parameters for the combined model in Eq. (2-9).

	C5	C6	C7
a_1	4.5994	7.3245	9.5832
a_2	-0.0087	-0.0137	-0.0172
a_3	-5.6582	-8.8906	-10.9581
a_4	0.0035	0.0104	0.0137

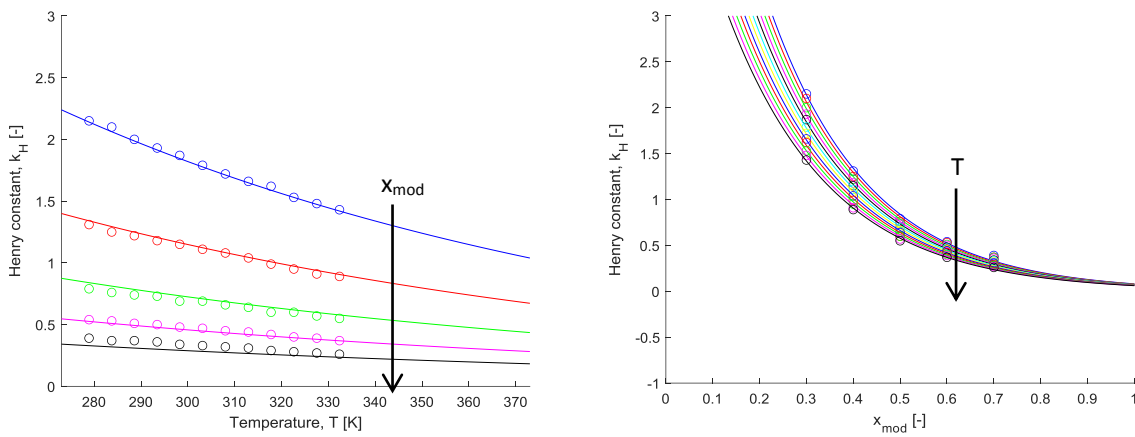


Figure 4-8 Combined dependence of temperature and modifier fraction by Eq. (2-9) for C5. Left: function of temperature; Right: function of modifier fraction. The temperature range from 278 K to 333 K whereas the modifier fraction from 0.3 to 0.5. The arrow indicates the increasing direction.

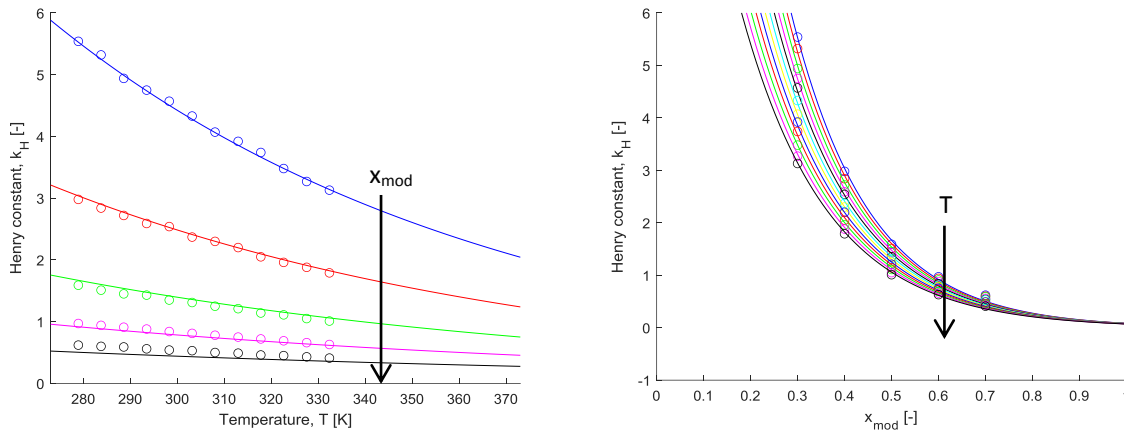


Figure 4-9 Combined dependence of temperature and modifier fraction by Eq. (2-9) for C6. Left: function of temperature; Right: function of modifier fraction. Applied ranges are same as in Figure 4-8.

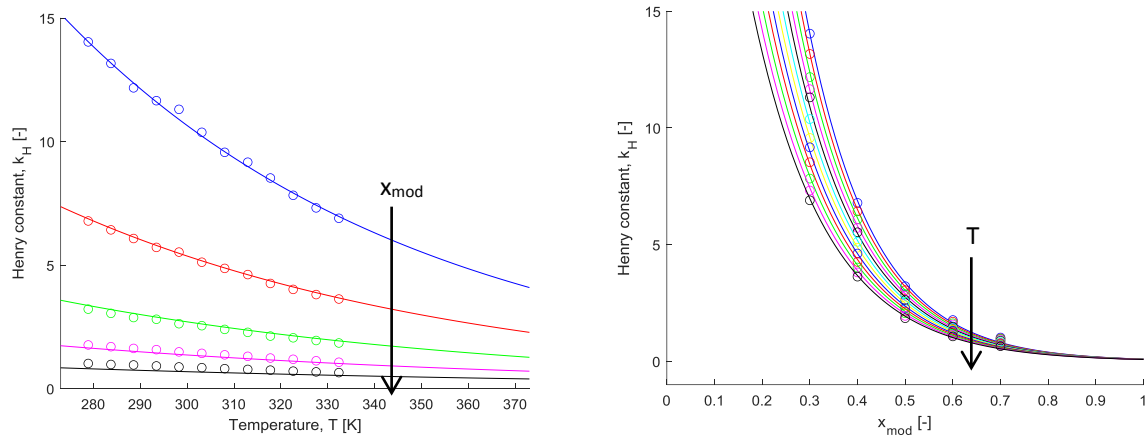


Figure 4-10 Combined dependence of temperature and modifier fraction by Eq. (2-9) for C7. Left: function of temperature; Right: function of modifier fraction. Applied ranges are same as in Figure 4-8.

In order to get first insights for the applicability of gradients, the boundary was identified beforehand. Henry's constants at higher and lower limits for temperature and modifier fraction of each component were calculated using Eq. (2-9) with determined parameters from Table 4-6. The boundary values are summarised in **Table 4-7**. The Henry's constant of C7 has much higher value than other two components in the entire range, which manifests the typical partly lagged separation problem. Their selectivities by Eq. (2-65) are summarised in **Table 4-8**. The selectivity is decreased by increasing temperature or modifier fraction. While deploying gradients in the mixture separation to reduce the cycle time, selectivities should be also considered to avoid remixing.

Table 4-7 Specific values of Henry's constants using Eq. (2-9).

$k_{H,C5}$		T_L	T_R	T_H
		278 K	298 K	333 K
$x_{mod,L}$	0.3	2.171	1.863	1.425
$x_{mod,R}$	0.5	0.851	0.740	0.580
$x_{mod,H}$	0.7	0.333	0.294	0.236
$k_{H,C6}$		T_L	T_R	T_H
		278 K	298 K	333 K
$x_{mod,L}$	0.3	5.563	4.502	3.109
$x_{mod,R}$	0.5	1.676	1.414	1.050
$x_{mod,H}$	0.7	0.505	0.444	0.355
$k_{H,C7}$		T_L	T_R	T_H
		278 K	298 K	333 K
$x_{mod,L}$	0.3	14.250	10.968	6.937
$x_{mod,R}$	0.5	3.410	2.773	1.930
$x_{mod,H}$	0.7	0.816	0.701	0.537

Table 4-8 Specific values of selectivity, corresponding to Table 4-7.

$\alpha^{(C5,C6)}$		T_L	T_R	T_H
		278 K	298 K	333 K
$x_{mod,L}$	0.3	2.56	2.42	2.18
$x_{mod,R}$	0.5	1.97	1.91	1.81
$x_{mod,H}$	0.7	1.52	1.51	1.50

$\alpha^{(C6,C7)}$		T_L	T_R	T_H
		278 K	298 K	333 K
$x_{mod,L}$	0.3	2.56	2.44	2.23
$x_{mod,R}$	0.5	2.03	1.96	1.84
$x_{mod,H}$	0.7	1.62	1.58	1.51

4.5 Parameters of short-cut model in energy balance

The parameters X_1 and X_2 in energy balance were determined using Eq. (2-61), (2-62) and (2-63). The operating conditions and determined parameters are summarised in **Table 4-9**. In principle, the X_1 should be a constant since it contains only density and specific heat capacity as constants by definition in Eq. (2-51). Therefore, the averaged value of X_1 was used. The average X_1 was determined to be 0.13 and the corresponding heat capacity ratio δ was then calculated to be 2.0. The X_2 is in principle flow rate dependent since it contains the heat transfer coefficient in Eq. (2-52). Although it can be empirically correlated with the flow rate by fitting data, the precision is still limited since this parameter is quite sensitive. Besides, the profiles of heating and cooling were not symmetrical due to uncertainties of thermostats. Hence, the averaged \bar{X}_2 of heating and cooling at the specific flow rate was instead used in this study. At the reference flow rate $\dot{V}=0.3$ ml/min, \bar{X}_2 was determined to be 0.003 s⁻¹. It means the time to reach gravity centre is ca. 5.5 min. It can be expected that the thermal conductive adsorbent can have bigger X_2 value and thus shorter equilibration time.

Table 4-9 Parameters of short-cut energy balance as a function of flow rate and thermal operations.

\dot{V} (ml/min)	T_o (°C)	T_w (°C)	X_1 (-)	X_2 (s ⁻¹)
0.2	5	60	0.207	0.0027
0.2	60	5	0.160	0.0021
0.3	5	60	0.163	0.0032
0.3	60	5	0.128	0.0025
0.4	5	60	0.144	0.0036
0.4	60	5	0.095	0.0028
0.5	5	60	0.134	0.0040
0.5	60	5	0.093	0.0031
0.6	5	60	0.123	0.0043
0.6	60	5	0.076	0.0032

The comparison of temperature profiles for heating and cooling at the reference flow rate $\dot{V}=0.3$ ml/min are shown in **Figure 4-11**. Upon a stepwise change, the water temperature T_w responded not in a perfect stepwise manner and there was a buffering zone due to uncertainty from the thermostats. This buffering zone was more obvious in the cooling operation since cooling is always slower than heating at thermostats. The measured temperature T_{mes} before calibration apparently reached a reduced level of steady state temperature. After calibration, the calibrated temperature profile T_{calb} became reasonable. By substituting prior determined X_1 and X_2 parameters into the analytical solution in Eq. (2-53), the analytical temperature profile T_{ana} can be plotted. The analytical temperature profile was in a good agreement with the calibrated temperature profile in the heating profile. Although there was a deviation in the cooling profile, the analytical solution can still capture the major trend. Hence, the analytical solution was successfully validated.

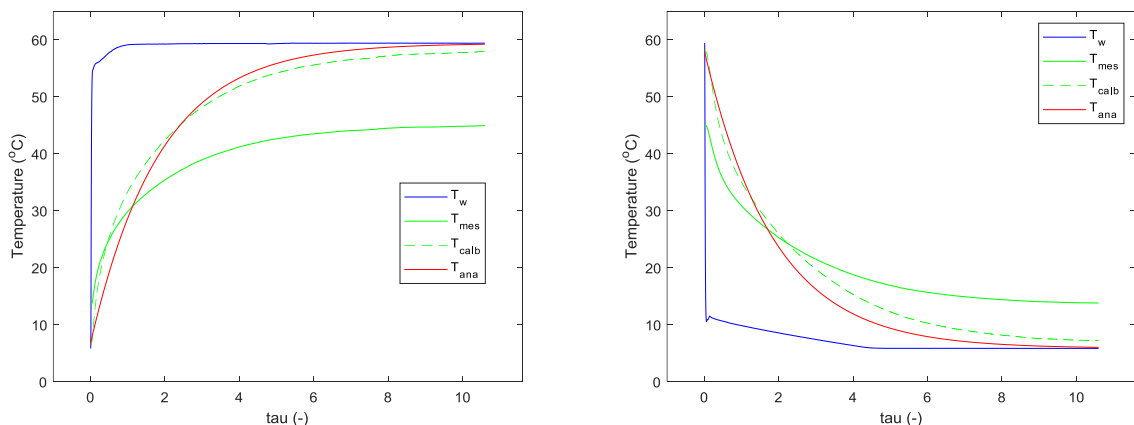


Figure 4-11 Comparison of temperature profiles before and after calibration, heating (left) and cooling (right) between 278 K and 333 K. The normalised time τ is defined in Eq. (2-54). The profile by analytical solution using Eq. (2-57) with $X_1=0.5$, $X_2=0.003$ s⁻¹ was also plotted.

4.5.1 Plausibility test for X_1

In fact, the parameter X_1 can be validated from the physical data. These data were obtained from manufacturer and literatures, as summarised in **Table 4-10**. The methanol mixed with water was taken as the liquid phase. The adsorbent together with column wall was taken as the solid phase since they together were consider as the system. The column wall is made from stainless steel. The adsorbent was assumed as pure silica by neglecting the content of ODS due to quantification difficulty. The mixed properties were calculated based on fractions. The volume fraction was used for mixed density whereas the mass fraction for specific heat capacity. The heat transfer area was calculated from the column geometry.

Table 4-10 Physical data to check plausibility of parameter X_1 .

Symbol	Property	Values*
$D_{c,i}$	Column inner diameter	0.46 cm
$D_{c,o}$	Column outer diameter	0.64 cm
ρ_{mod}	Density of modifier (methanol)	0.79 g/cm ³
ρ_{aq}	Density of aqueous solvent (water)	0.997 g/cm ³
ρ_{ads}	Density of silica (skeleton of adsorbent)	2.65 g/cm ³
ρ_{cw}	Density of column wall (stainless steel)	7.5 g/cm ³
$C_{p,mod}$	Heat capacity of modifier (methanol)	2.53 J/g.K
$C_{p,aq}$	Heat capacity of aqueous solvent (water)	4.184 J/g.K
$C_{p,ads}$	Heat capacity of silica (skeleton of adsorbent)	0.703 J/g.K
$C_{p,cw}$	Heat capacity of column wall (stainless steel)	0.468 J/g.K

* Obtained from manufacturer information and Engineering ToolBox (www.engineeringtoolbox.com).

The liquid phase mixed density is calculated by

$$\rho^L = x_{mod}\rho_{mod} + (1 - x_{mod})\rho_{aq} \quad (4-1)$$

The liquid phase mixed specific heat capacity is calculated by

$$C_p^L = \phi_m C_{p,mod} + (1 - \phi_m)C_{p,aq} \quad (4-2)$$

where the modifier mass fraction is defined as

$$\phi_m = \frac{\rho_{mod}}{\rho_{mod} + \rho_{aq}} \quad (4-3)$$

The cross-sectional areas of liquid eluent and solid adsorbent can be calculated from the total porosity ϵ_t as

$$A^L = (1 - \epsilon_t)A_i \quad (4-4)$$

$$A_{ads} = \epsilon_t A_i \quad (4-5)$$

where A_i refers to complete inner cross-sectional area of the column. In addition to solid adsorbent, energy accumulation also occurs in the column wall. A differential annular volume of the column wall can be calculated by

$$dV_{cw} = (A_o - A_i)dz = \frac{\pi}{4}(D_{c,0}^2 - D_{c,i}^2)dz \quad (4-6)$$

Then the total differential volume of solid adsorbent and wall is

$$dV^S = dV_{ads} + dV_{cw} \quad (4-7)$$

The adsorbent volume fraction is

$$\theta_V = \frac{dV_{ads}}{dV^S} \quad (4-8)$$

The corresponding adsorbent mass fraction is

$$\theta_m = \frac{\rho_{ads}dV_{ads}}{\rho_{ads}dV_{ads} + \rho_{cw}dV_{cw}} \quad (4-9)$$

For rough estimation, the overall solid phase density and heat capacity can be estimated as

$$\rho^S = \theta_V \rho_{ads} + (1 - \theta_V) \rho_{cw} \quad (4-10)$$

$$C_p^S = \theta_m C_{p,ads} + (1 - \theta_m) C_{p,cw} \quad (4-11)$$

By using all of these property data, the X_1 was theoretically calculated to be 0.24 and the corresponding heat capacity ratio δ was 1.0. They were in the same order of magnitude as the experimentally determined values, which is in the range as expected.

In order to examine the influence of flow rate on the temperature profile for given X_1 value, the analytical temperature profiles are generated in **Figure 4-12**. The flow rate has very limited influence for the experimentally determined value $X_1=0.13$ (left) whereas a relatively small influence for the predicted value $X_1=0.24$ (right). Increment of X_1 leads to the increase in the gaps between final steady state temperatures.

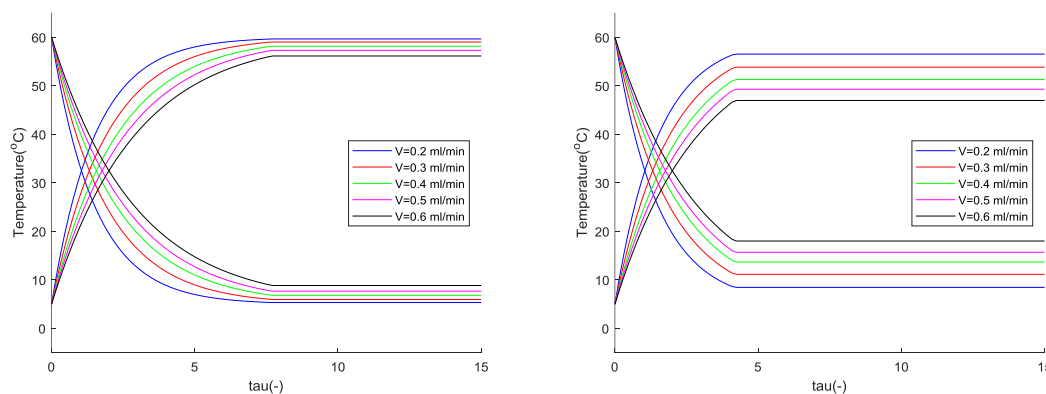


Figure 4-12 Influence of flow rate \dot{V} on the temperature profile. Left: $X_1=0.13$ from experiments; Right: $X_1=0.24$ from physical data. The profile is generated by Eq. (2-57) with $X_2=0.003 \text{ s}^{-1}$.

To examine the effect of X_1 on the final steady state temperature γ^{end} for different flow rates, the Eq. (2-63) is rearranged as

$$\gamma^{end} = e^{-(1-f_z)t_0 \frac{X_2}{X_1}} \tag{4-12}$$

and plotted in **Figure 4-13**. The final steady state temperature is less influenced by the flow rate since X_1 placed in the lower range in the current system. It means smaller X_1 is desirable for effective heat transfer, which provide a practical insight for material selection of chromatographic system, i.e., larger heat capacity ratio δ and phase ratio for heat transfer F^T .

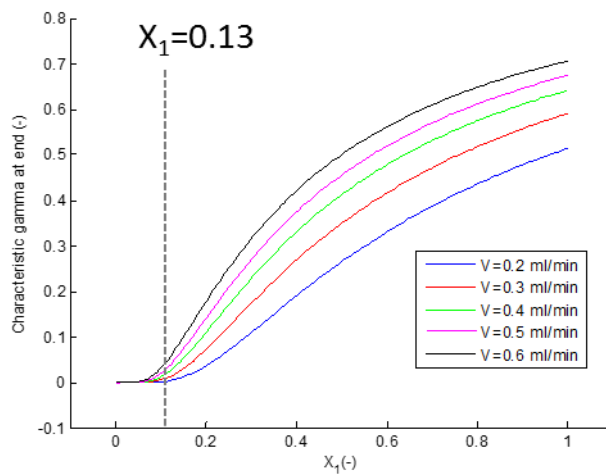


Figure 4-13 Effect of X_1 and \dot{V} on γ^{end} in Eq. (4-12).

Chapter 5. Quantitative description of chromatograms under gradient conditions

In this chapter, predictions of chromatograms based on trajectories of chromatograms in the physical plane are described. Gradients are designed based on the courses in the physical plane under equilibrium conditions and for ideal step profiles. A programme tool was developed and applied, where switch times can be either calculated for certain operating regimes or defined by user. Then the retention times can be determined at the outlet boundary. Once retention times are known, the important cycle time Δt_{cyc} and the corresponding productivity Pr_n can be determined using Eqs. (2-66) and (2-71). To check and evaluate the prediction, the more realistic equilibrium dispersion model can be used to account for band broadening by inputting kinetic parameter. For further improved predictions, nonidealities of step gradients can be corrected by using nonideality parameters.

5.1 Isothermal and isocratic operations of ternary mixture

As described in **Figure 2-5**, the migration paths of a component on physical planes are uniform without any turnings under isothermal and isocratic conditions. Migration paths of ternary mixture at $T_R=25$ °C, $x_{mod,R}=0.5$ are shown in **Figure 5-1**. The injection start time for next injection t_{inj}^{k+} is the essential characteristic time to determine. To maximise the ideal productivity, the rear band of the last eluting component and the front band of the first eluting component from the next injection should be just in touch. In such a case, the start time for a next injection, which equals to the cycle time, can be calculated as

$$t_{inj}^{k+} = \Delta t_{cyc} = t_{R,3}^r - t_{R,1}^f = \Delta t_{inj} + t_0 F [k_{H_3}(T_R) - k_{H_1}(T_R)] \quad (5-1)$$

The maximal productivity can be obtained by consecutive injections applying this injection pattern.

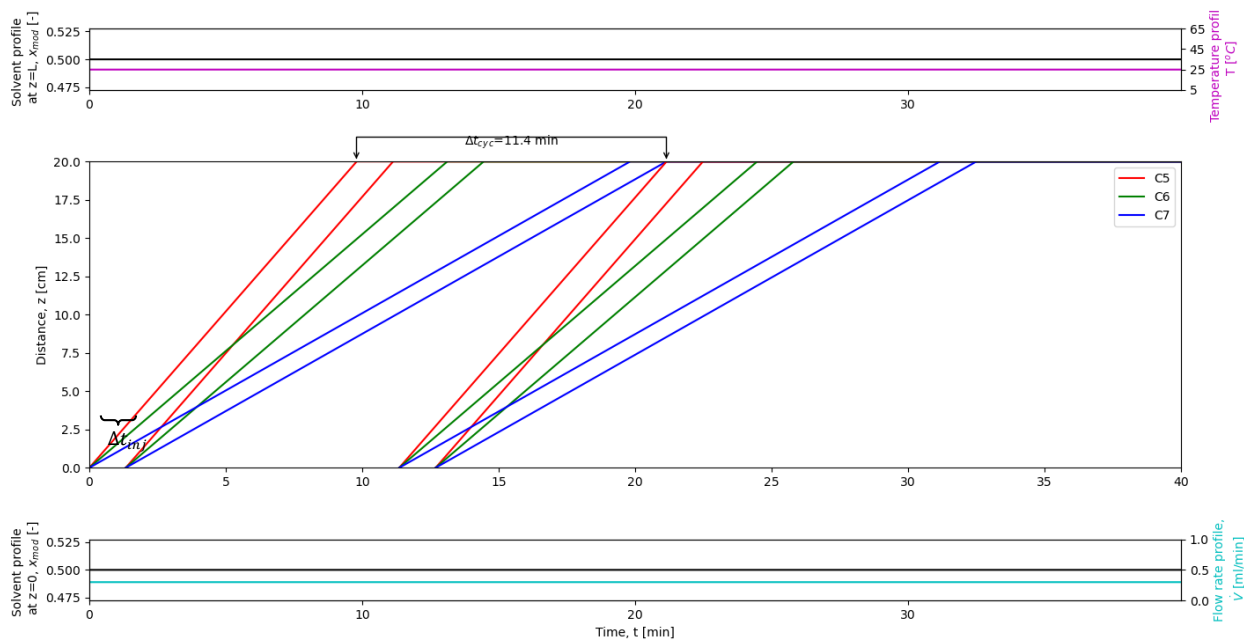


Figure 5-1 Trajectories of chromatograms in the physical plane for ternary separation under isothermal and isocratic operation with two consecutive injections. Middle: Physical plane. Red, green and blue pathways correspond to component C5, C6 and C7, respectively. Each component has two pathways for front and rear bands, and their difference is injection period Δt_{inj} . The cycle time is denoted above. The left axis at top and bottom subplots correspond to solvent profile (black line) at column inlet and outlet, respectively. The right axis at top subplot is temperature profile (purple line). The right axis at bottom is flow rate profile (cyan line). $T=25$ °C, $x_{mod}=0.5$. Henry's constants are from Table 4-7. $\dot{V}=0.3$ ml/min, $V_{inj}=400$ μ L. $\Delta t_b=[2.0, 5.4, 0, 2.0, 5.4]$ min, $\Delta t_{cyc}=11.4$ min.

Similarly, the chromatograms in the physical plane under isothermal and isocratic operation at higher temperature $T_H=60$ °C is shown in **Figure 5-2**. Although the cycle time is reduced significantly at higher temperature, the band break between first two components become very small. It leads to remixing in the actual experiment, which will be described in Figure 6-1.

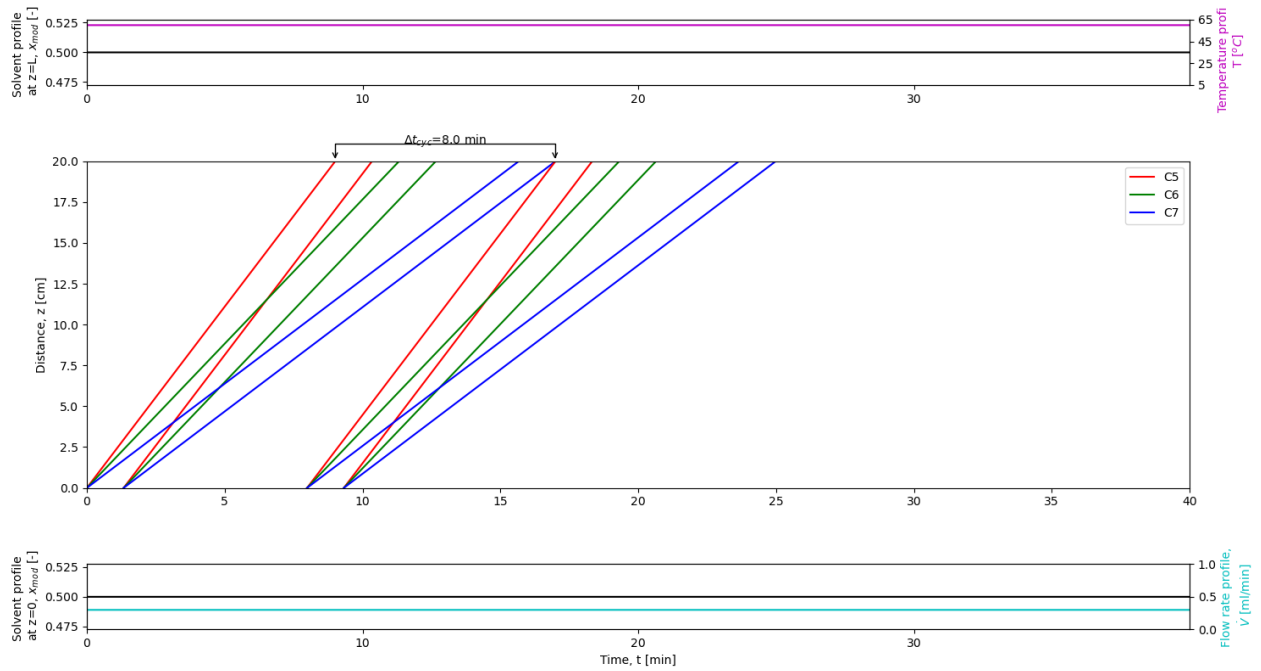


Figure 5-2 Trajectories of chromatograms in the physical plane for ternary separation under isothermal and isocratic operation at $T_H=60$ °C, $X_{mod,R}=0.5$ with two consecutive injections. $\dot{V}=0.3$ ml/min, $V_{inj}=400$ μ L. $\Delta t_b=[1.0, 3.0, 0, 1.0, 3.0]$ min, $\Delta t_{cyc}=8$ min.

5.2 Repetitive chromatography under gradient operations

As mentioned in section 2.3.2, trajectories of chromatograms in the physical plane depict the migration path of each component under influence of gradients, where some characteristic times including switch times and start time for next injection can be determined. In real cases, these times should be extended by adding a safety margin to avoid remixing.

These characteristic switch times in k^{th} cycle, indicated by $t_i^{*,k}$, are the key information and they are applied repetitively over the same interval in each cycle. To express it in a repetitive manner, relative switch times Δt_i^* are defined relative to the start time for k^{th} injection as

$$\Delta t_i^* = t_i^{*,k} - t_{inj}^k \quad (5-2)$$

where $t_i^{*,k=1} = \Delta t_i^*$ if $t_{inj}^{k=1} = 0$. If the total production time Δt_{tot} in Eq. (2-71) is determined, the start time of next injection can be calculate as

$$t_{inj}^{k+} = k\Delta t_{tot} = k(\Delta t_{cyc} + \Delta t_{extra}) \quad k = 1, 2 \dots \quad (5-3)$$

In order to see to which extent the component retentions can be influenced by gradients, the courses of chromatograms in the physical plane using boundary values from **Table 4-7** are depicted in **Figure 5-3**. The switch times were chosen arbitrary. The first eluting component C5 was influenced to a very little extent by both gradient scenarios

introduced since it is much less adsorbed. The retention time is altered aggressively by the solvent gradient since it has a stronger elution strength than that by temperature gradient, especially for C7. In practice, the modifier fraction should be carefully selected to make the retention neither too long nor too short. Due to inclined nature of the solvent gradient line, the components are influenced by solvent from the intersection point in a reverse order of elution. On the contrary, the impact of temperature gradients is milder but instantaneous due to the vertical gradient line. For both gradients, finding suitable switch times to reduce the cycle time without rendering separation quality is the main challenge.

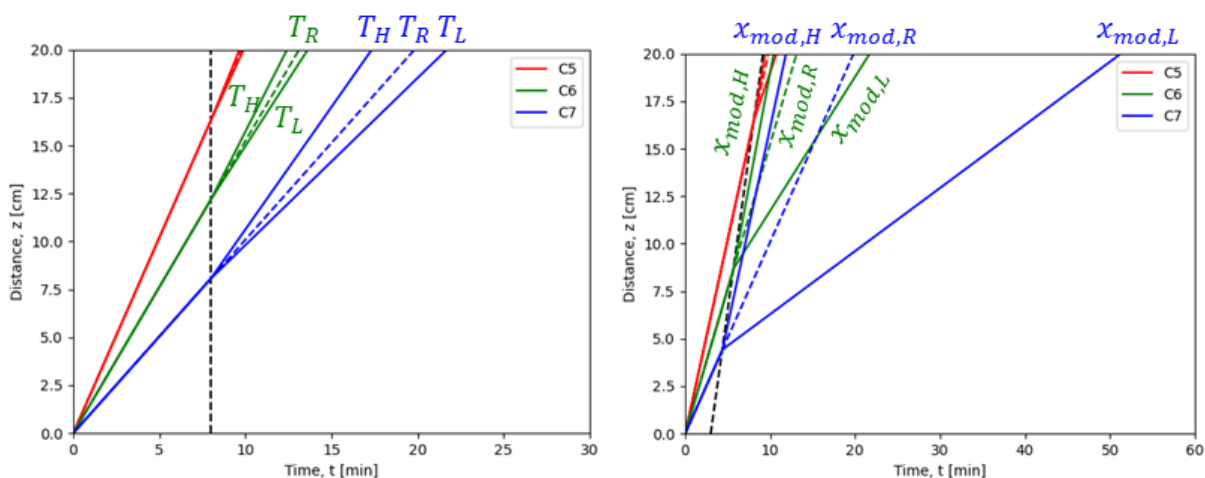


Figure 5-3 Illustration of chromatograms in the physical plane according to the boundary of Henry's constants. Left: temperature gradients at $x_{mod,R}=0.5$; Right: solvent gradients at $T_R=298$ K.

5.3 Temperature gradient

In this study, the temperature gradients were implemented in a segmented modulation system characterised by the segmentation ratio f_z . Due to the segmented nature, this system cannot deploy heating and cooling simultaneously. Having this fact in mind, different operating regimes, i.e. conservative and improved regimes were exploited. The gradient lines are horizontal or vertical in temperature gradients. The characteristic times to determine are switch times t_i^* and the start time for next injection t_{inj}^{k+} , which can be calculated from intersections and boundaries by analytical geometry. The nonideal stepwise temperature profile can be expressed by the analytical solution in Eq. (2-57).

5.3.1 Ternary separation by certain operating regimes

Below two operating regimes are introduced, namely the conservative regime and the improved regime.

(a) Conservative regime

To minimise the cycle time, gradients should be deployed according to the principal strategy that deceleration for fast components by cooling and acceleration for slow components by heating. However, they cannot be done simultaneously due to the segmented modulation. With a rather conservative operating strategy, it is assured that the fast component is cooled and the slow components are heated within their entire migration as shown in **Figure 5-4**, which is called here “conservative regime”. The blocks in blue and red (segment II) and green (segment I) correspond to the temperature T_L , T_H and T_R , respectively. The segment II is initially under the cooling status to decelerate the first eluting component, and then it switches to the heating status to accelerate the intermediate and the last eluting components when the first eluting component completely leaves the column. At the same time, the first eluting component should just reach the segment II to make sure it is cooled during the upcoming cycle. By this constraint, the start time for next injection can be calculated. Under this kind of operating regime, a gap between consecutive injections in the chromatogram is unavoidably formed. This gap can be called safety time Δt_{safe} .

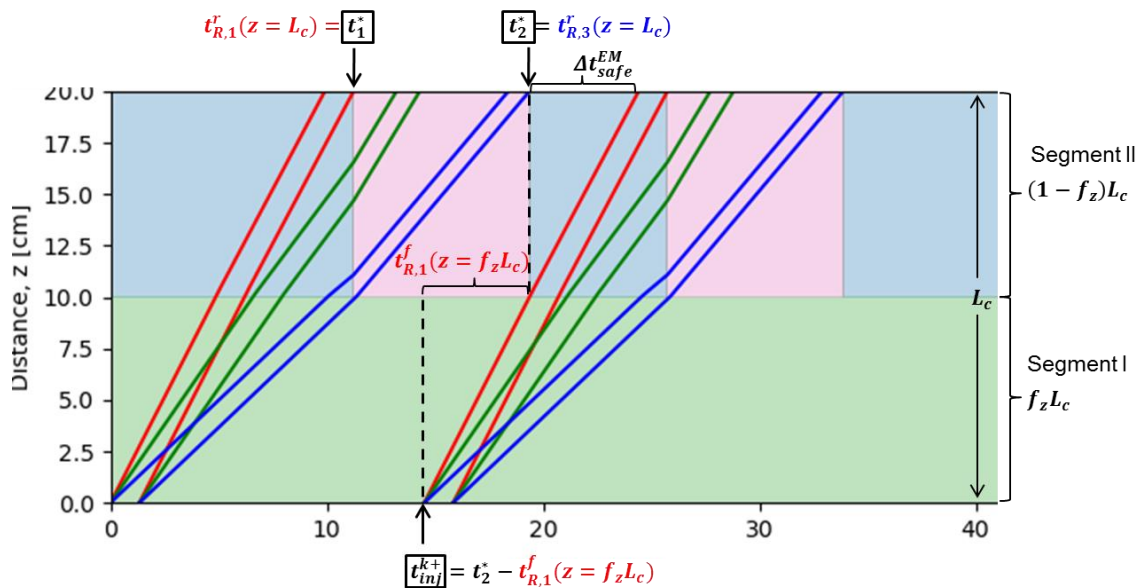


Figure 5-4 Temperature gradients by conservative regime. The green, blue and red blocks indicate modulated temperature at T_R , T_L and T_H , respectively.

The first switch time is rear band retention time of the first eluting component, it can be calculated as

$$\begin{aligned}
 t_1^* &= \Delta t_{inj} + t_0 f_z [1 + F k_{H_1}(T_R)] + t_0 (1 - f_z) [1 + F k_{H_1}(T_L)] \\
 &= \Delta t_{inj} + t_0 + t_0 F [f_z k_{H_1}(T_R) + k_{H_1}(T_L) - f_z k_{H_1}(T_L)]
 \end{aligned}
 \tag{5-4}$$

The second switch time is the rear band retention time of the last eluting component. Depending on Henry's constant, the last eluting component has two possible migration paths, as shown in **Figure 5-5**. One is travelling through both the cooling and heating zones, whereas other one is only through the heating zone. Hence, the second switch time should be calculated according to different possibilities. It can be judge by the chronological sequence between the first switch time and the retention time until the interface between two segments, i.e. $t_{R,3}^r(z = f_z L_c) = t_0 f_z [1 + F k_{H_3}(T_R)] + \Delta t_{inj}$.

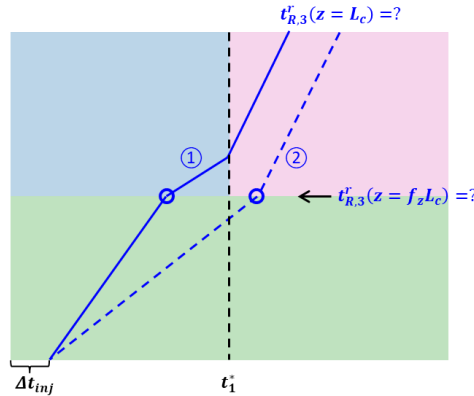


Figure 5-5 Possible routes of the last eluting component in conservative regime for temperature gradients.

In case $t_{R,3}^r(z = f_z L_c) < t_1^*$:

$$\begin{aligned}
 t_2^* &= t_1^* + \frac{L_c(1 - f_z) - \left[t_1^* - \frac{L f_z}{u_{c,3}(T_R)} - \Delta t_{inj} \right] u_{c,3}(T_L)}{u_{c,3}(T_H)} \\
 &= t_1^* + \left[t_0(1 - f_z) - \frac{t_1^* - \Delta t_{inj}}{1 + F k_{H_3}(T_L)} + \frac{1 + F k_{H_3}(T_R)}{1 + F k_{H_3}(T_L)} t_0 f_z \right] [1 + F k_{H_3}(T_H)]
 \end{aligned} \tag{5-5}$$

In case $t_{R,3}^r(z = f_z L_c) \geq t_1^*$:

$$\begin{aligned}
 t_2^* &= \Delta t_{inj} + t_0 f_z [1 + F k_{H_3}(T_R)] + t_0(1 - f_z) [1 + F k_{H_3}(T_H)] \\
 &= \Delta t_{inj} + t_0 + t_0 F [f_z k_{H_3}(T_R) + k_{H_3}(T_H) - f_z k_{H_3}(T_H)]
 \end{aligned} \tag{5-6}$$

The start time for the next injection can be calculated as:

$$t_{inj}^{k+} = t_2^* - t_0 f_z [1 + F k_{H_1}(T_R)] = \Delta t_{tot} \tag{5-7}$$

Thus, the cycle time by this regime for the model component can be expressed as

$$\begin{aligned}\Delta t_{cyc} &= t_2^* - t_{R,1}^f \\ &= \Delta t_{inj} + t_0 F [f_z k_{H_3}(T_R) + k_{H_3}(T_H) - f_z k_{H_3}(T_H) - f_z k_{H_1}(T_R) \\ &\quad - k_{H_1}(T_L) + f_z k_{H_1}(T_L)]\end{aligned}\quad (5-8)$$

The safety time can be expressed as

$$\begin{aligned}\Delta t_{safe} &= \Delta t_{tot} - \Delta t_{cyc} \\ &= t_0 + t_0 F [f_z k_{H_1}(T_R) + k_{H_1}(T_L) - f_z k_{H_1}(T_L)] - t_0 f_z [1 + F k_{H_1}(T_R)]\end{aligned}\quad (5-9)$$

By this operating regime, the cycle time is indeed reduced as compared to isothermal operation. However, the total production time is even longer than that of isothermal operation due to this safety time leading to a lower productivity, which is not a desirable improvement. The safety time should be reduced or fully eliminated.

(b) Improved regime

To eliminate the safety time thus to improve productivity, the cooling zone is confined, as shown in **Figure 5-6**, which is called here “improved regime”. In this regime, there is no gap between cycles since the cooling period starts from the front band retention time of the first eluting component $t_{R,1}^f$. The first eluting component is not limited to pure cooling, as its rear band undergoes a hybrid course of heating followed by cooling. This partial cooling cannot contribute to reduction of the cycle time but can improve the resolution. Without this cooling zone, there is a remixing between the first and intermediate eluting components at high temperature in actual experiments. The cooling zone ends up when the rear band of the first eluting component leaves the column. However, it can be expanded up to the front band retention time of the intermediate eluting component $t_{R,2}^f$, where the cycle time is not obviously influenced.

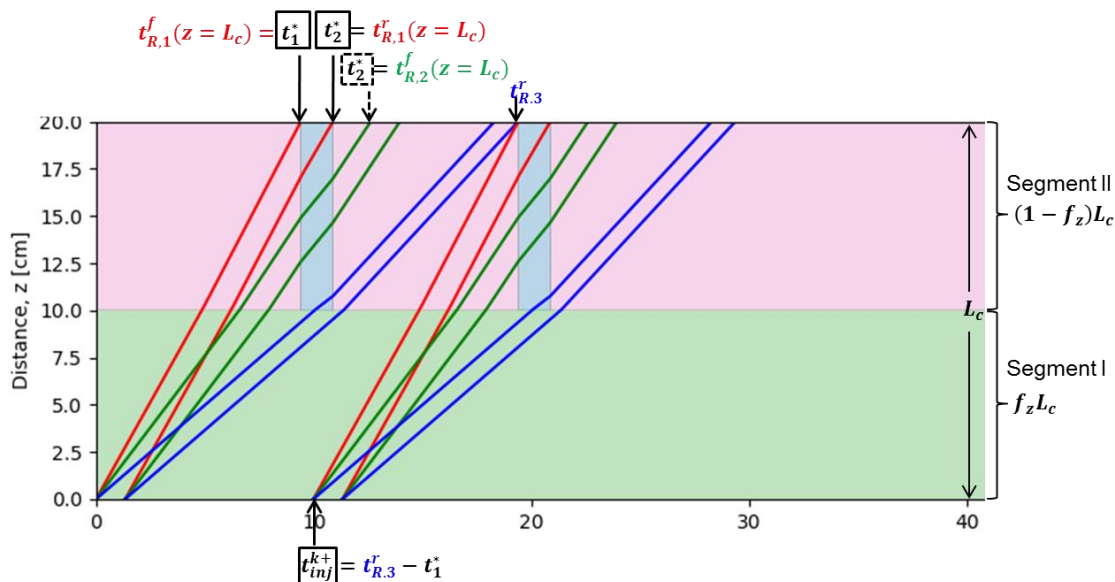


Figure 5-6 Temperature gradients by improved regime. The green, blue and red blocks indicate modulated temperature at T_R , T_L and T_H , respectively.

The first switch time is front band retention time of the first eluting component, it can be calculated as

$$t_1^* = t_0 f_z [1 + Fk_{H_1}(T_R)] + t_0(1 - f_z)[1 + Fk_{H_1}(T_H)] \quad (5-10)$$

Similarly, possible migration paths of its rear band should be discussed separately, as shown in **Figure 5-7**. It can be judge by the chronological sequence between the first switch time and the retention time until the interface between two segments, i.e.

$$t_{R,1}^r(z = f_z L_c) = t_0 f_z [1 + Fk_{H_1}(T_R)] + \Delta t_{inj}.$$

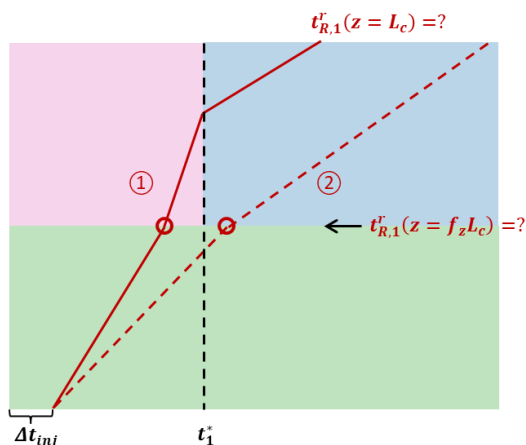


Figure 5-7 Possible routes of the first eluting component in improved regime for temperature gradients.

In case $t_{R,1}^r(z = f_z L_c) \leq t_1^*$:

$$\begin{aligned}
 t_2^* &= t_1^* + \frac{L_c(1 - f_z) - \left[t_1^* - \frac{L f_z}{u_{c,1}(T_R)} - \Delta t_{inj} \right] u_{c,1}(T_H)}{u_{c,1}(T_L)} \\
 &= t_1^* + \left[t_0(1 - f_z) - \frac{t_1^* - \Delta t_{inj}}{1 + Fk_{H_1}(T_H)} + \frac{1 + Fk_{H_1}(T_R)}{1 + Fk_{H_1}(T_H)} t_0 f_z \right] [1 + Fk_{H_1}(T_L)]
 \end{aligned} \tag{5-11}$$

In case $t_{R,1}^r(z = f_z L_c) > t_1^*$:

$$t_2^* = t_0 f_z [1 + Fk_{H_1}(T_R)] + t_0(1 - f_z) [1 + Fk_{H_1}(T_L)] \tag{5-12}$$

As aforementioned, the cooling zone is used to improve resolution and it can be expanded up to the front band retention time of the intermediate eluting component $t_{R,2}^f = t_0 f_z [1 + Fk_{H_2}(T_R)]$. Then the calculation of the second switch time is changed accordingly.

In case $t_{R,2}^f \leq t_1^*$:

$$\begin{aligned}
 t_2^* &= t_1^* + \frac{L_c(1 - f_z) - \left[t_1^* - \frac{L f_z}{u_{c,2}(T_R)} \right] u_{c,2}(T_H)}{u_{c,2}(T_L)} \\
 &= t_1^* + \left[t_0(1 - f_z) - \frac{t_1^*}{1 + Fk_{H_2}(T_H)} + \frac{1 + Fk_{H_2}(T_R)}{1 + Fk_{H_2}(T_H)} t_0 f_z \right] [1 + Fk_{H_2}(T_L)]
 \end{aligned} \tag{5-13}$$

In case $t_{R,2}^f > t_1^*$:

$$t_2^* = t_0 f_z [1 + Fk_{H_2}(T_R)] + t_0(1 - f_z) [1 + Fk_{H_2}(T_L)] \tag{5-14}$$

When it comes to the start time of next injection, the rear band retention time of the last eluting component is concerned. It has four possible migration paths, as shown **Figure 5-8**. It can be judge by the chronological sequence among the first and second switch times and the retention time until the interface between two segments, i.e. $t_{R,3}^r(z = f_z L_c) = t_0 f_z [1 + Fk_{H_3}(T_R)] + \Delta t_{inj}$.

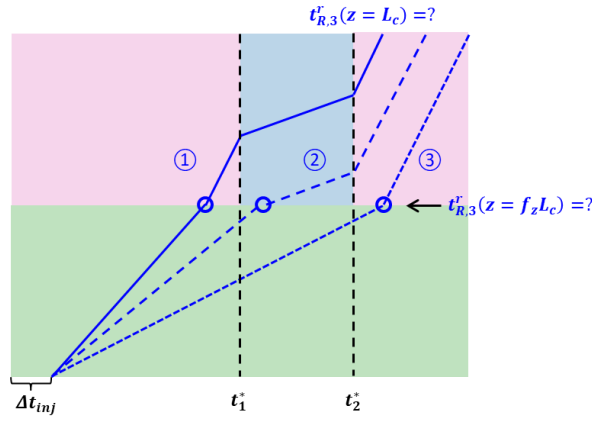


Figure 5-8 Possible routes of the last eluting component in improved regime for temperature gradients.

In case $t_{R,3}^r(z = f_z L_c) \leq t_1^*$:

$$\begin{aligned}
 t_{R,3}^r &= t_2^* + \\
 &\frac{L_c(1 - f_z) - \{t_1^* - t_0 f_z [1 + Fk_{H_3}(T_R)] - \Delta t_{inj}\} u_{c,3}(T_H) - (t_2^* - t_1^*) u_{c,3}(T_L)}{u_{c,3}(T_H)} \\
 &= t_2^* + \\
 &\left\{ t_0(1 - f_z) - \frac{t_1^* - t_0 f_z [1 + Fk_{H_3}(T_R)] - \Delta t_{inj}}{1 + Fk_{H_3}(T_H)} - \frac{t_2^* - t_1^*}{1 + Fk_{H_3}(T_L)} \right\} [1 + Fk_{H_3}(T_H)]
 \end{aligned} \quad (5-15)$$

In case $t_1^* < t_{R,3}^r(z = f_z L_c) \leq t_2^*$:

$$\begin{aligned}
 t_{R,3}^r &= t_2^* + \frac{L_c(1 - f_z) - \left[t_2^* - \frac{L f_z}{u_{c,3}(T_R)} - \Delta t_{inj} \right] u_{c,3}(T_L)}{u_{c,3}(T_H)} \\
 &= t_2^* + \left[t_0(1 - f_z) - \frac{t_2^* - \Delta t_{inj}}{1 + Fk_{H_3}(T_L)} + \frac{1 + Fk_{H_3}(T_R)}{1 + Fk_{H_3}(T_L)} t_0 f_z \right] [1 + Fk_{H_3}(T_H)]
 \end{aligned} \quad (5-16)$$

In case $t_{R,3}^r(z = f_z L_c) > t_2^*$:

$$t_{R,3}^r = \Delta t_{inj} + t_0 f_z [1 + Fk_{H_3}(T_R)] + t_0(1 - f_z) [1 + Fk_{H_3}(T_H)] \quad (5-17)$$

Finally, the start time of the next injection can be calculated as

$$t_{inj}^{k+} = t_{R,3}^r - t_1^* = \Delta t_{tot} \quad (5-18)$$

Thus, the cycle time by this regime for the model component can be expressed as

$$\begin{aligned}
 \Delta t_{cyc} &= \Delta t_{tot} \\
 &= \Delta t_{inj} + t_0 F f_z [k_{H_3}(T_R) - k_{H_1}(T_R)] + t_0 F (1 - f_z) [k_{H_3}(T_H) - k_{H_1}(T_H)]
 \end{aligned} \quad (5-19)$$

By the improved regime, there is no safety time, i.e. $\Delta t_{safe} = 0$. Hence, the total production time Δt_{tot} ($=\Delta t_{cyc}$) is shorter than that under isothermal operation leading to a higher productivity, which is attributed to acceleration of the slow eluting components. The productivity can be calculated by Eq. (2-71). The calculated performance will be compared in section 6.5. Nonetheless, this regime is still not the optimal and further improvements are discussed in section 7.1.

5.3.2 Nonideality of implementing stepwise temperature profiles

The more realistic temperature profile is calculated using Eq. (2-57) with determined parameters $X_1=0.13$ and $X_2=0.003 \text{ s}^{-1}$ (section 4.5). The chromatograms in the physical plane for ternary separation under the temperature gradient by conservative regime using this profile is generated, as shown in **Figure 5-9**. The nonideal temperature distribution along time and space can be observed. According to the profile, temperature switches before it reaches to the final steady state, and the actually reached value was used as the initial temperature for the next switch. The resulting temperature profile at outlet in purple is a curve in a periodic concave-convex shape. Due to this behaviour, the modulation zone of the first cycle seem a bit different from that of the second cycle. The slopes of component migration paths are gradually changed. Due to the nonideal temperature profile, the cycle time got longer to a small extent since the elution strength of temperature is not so strong. The applicability of this more realistic temperature profile depends on accuracy requirements. It should be carefully designed especially for the temperature sensitive components.

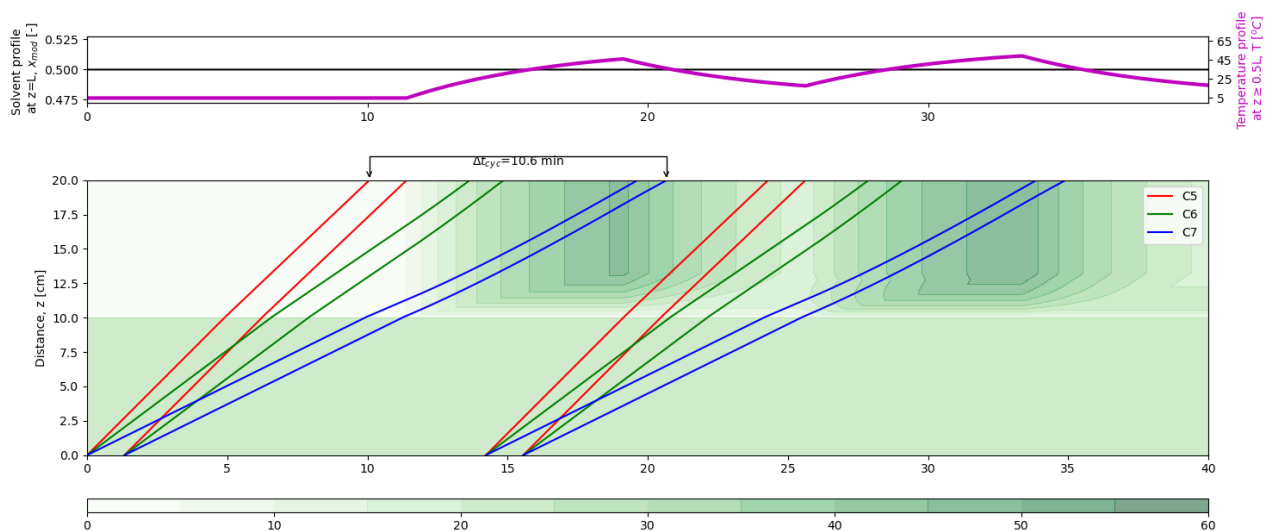


Figure 5-9 Temperature gradients by conservative regime using nonideal temperature profile. The nonideal temperature profile at outlet (purple line) is shown at the top. Henry's constants are calculated by Eq. (2-9). Temperature profile is generated by Eq. (2-57).

5.4 Solvent gradient

Solvent gradients can be classified into step, linear and nonlinear according to the functional dependence. As a more common technique, the linear gradient is first illustrated in the physical plane. The step gradients are then presented. The gradient lines are inclined with the slope value of the interstitial velocity u and the space side value of the column dead time t_0 . The operating regime in solvent gradients is relatively simple. The elution strength in terms of modifier fraction increase in a monotonic way followed by a regeneration step to the initial status. The safety time always exists due to the regeneration step.

5.4.1 Linear solvent gradients

Linear gradients are widely used for solvent gradients in both analytical and preparative chromatography. An exemplar physical plane for a linear gradient is shown in **Figure 5-10**. Unlike step gradients, the migration paths of components are rather smooth due to gradually increasing elution strength. There are two switch times for start and end, and they are repeated in the following cycles. Compared to step gradients, linear gradients have reduced elution strength and thus a bit longer cycle time. Its major merit is the focusing effect, i.e. minimisation of dispersion. By this effect, the peaks appear to be sharper. According to our preliminary study, the second moment of a linear gradient is smaller than that of isocratic elution at high modifier fraction. This focusing effect is caused from the feature that the rear band meets the inclined gradient line earlier than the front band and leads to peak contraction. This behaviour is more obvious in linear gradients than step gradients. Hence, linear gradients are especially useful for delicate separations where concentrated bands are required.

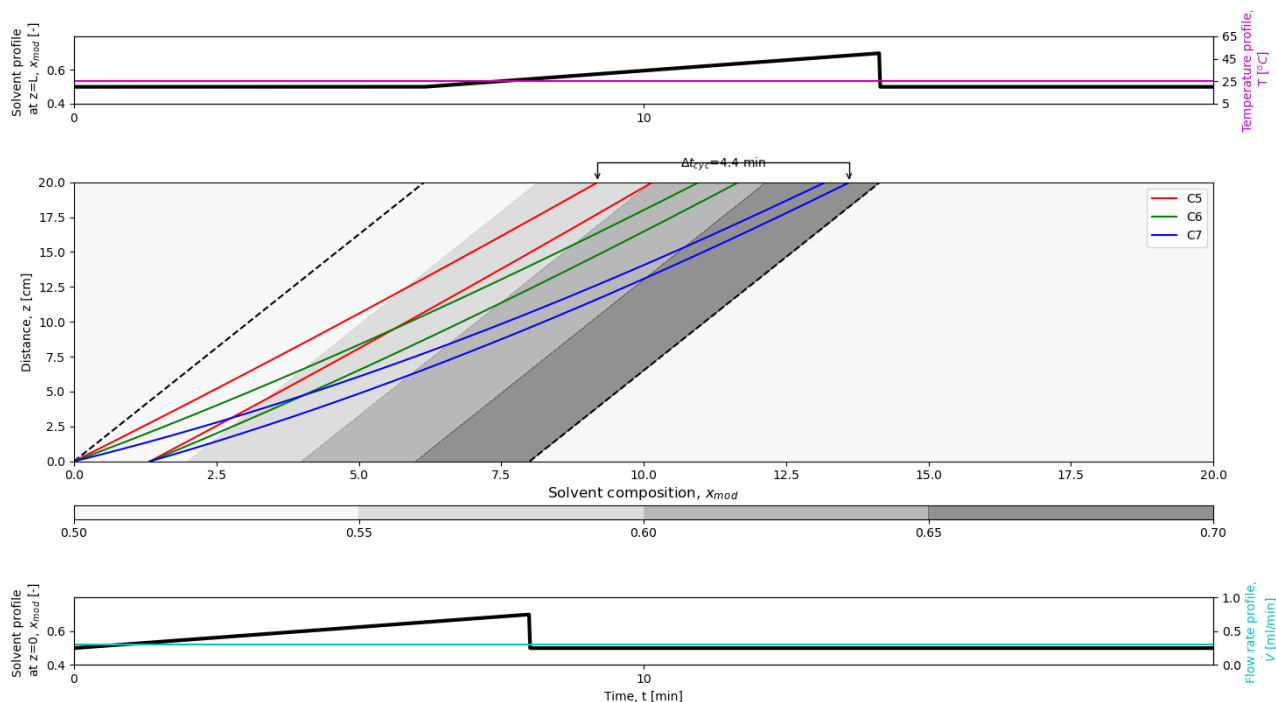


Figure 5-10 Example of linear solvent gradient. The solvent profiles at inlet and outlet are shown at bottom and top, respectively. $T=25$ °C, $x_{mod}=[0.5, 0.7]$. Henry's constants are calculated by Eq. (2-9). $\dot{V}=0.3$ ml/min, $V_{inj}=400$ μ L. $t_i^*=[0, 8]$ min, $\Delta t_b=[0.8, 1.5]$ min, $\Delta t_{cyc}=4.4$ min.

5.4.2 Stepwise solvent gradients

For step gradients, each switch time is the rear band retention time of specific components by subtracting t_0 . The last switch time is the regeneration step, which is also the earliest start time of the next injection meanwhile equals to the total production time, i.e. $t_{i=l}^* = t_{inj}^{k+} = \Delta t_{tot}$. Similar to temperature gradients, switch times t_i^* and the start time for next injection t_{inj}^{k+} can be calculated from intersections and boundaries. Below 2-step and 3-step solvent gradients are introduced.

(a) 2-step solvent gradients

In case of the 2-step solvent gradient, two switch times are connected to the retention times of the first and last eluting components, as shown in **Figure 5-11**. The higher elution strength is actually deployed from the second (instead of third) eluting component due to safety for remixing, which will be shown in section 6.1. The intersection point at coordinate (t', z') is used for calculation. The modifier fractions are in the ascending level of $[x_{mod,1}, x_{mod,2}]$, where $x_{mod,1}=x_{mod,R}$ and $x_{mod,2}=x_{mod,H}$ in this study.

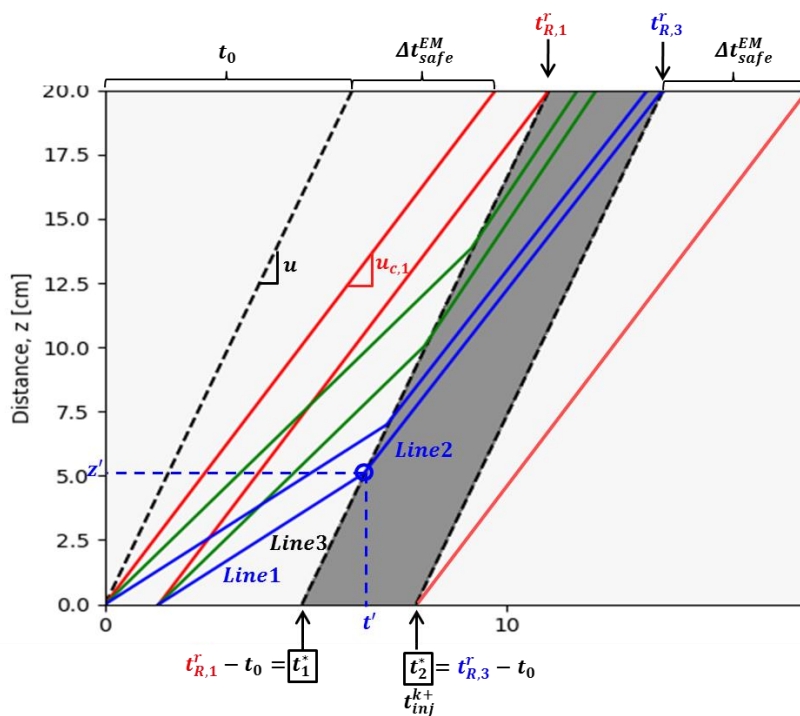


Figure 5-11 2-step solvent gradient. The white and grey blocks indicate modulated modifier fraction at $x_{mod,1}$ and $x_{mod,2}$ respectively.

The first eluting component is under the initial $x_{mod,1}$, and the first switch time can be calculated as

$$t_1^* = t_{R,1}^r - t_0 = t_0 [1 + Fk_{H_1}(x_{mod,1})] + \Delta t_{inj} - t_0 \quad (5-20)$$

The rear band line of last eluting component (line 1) meets the gradient line for the first switch time (Line 3) at intersection point (t', z') . At the intersection point,

$$z' = z_1(t = t') = z_3(t = t') \quad (5-21)$$

or

$$u_{c,3}(x_{mod,1})(t' - \Delta t_{inj}) = L_c/t_0(t' - t_1^*) \quad (5-22)$$

This point (t', z') can be solved as:

$$\begin{aligned} t' &= \frac{u_{c,3}(x_{mod,1})\Delta t_{inj} - \frac{L_c}{t_0}t_1^*}{u_{c,3}(x_{mod,1}) - \frac{L_c}{t_0}} = \frac{\frac{L_c}{t_0} \Delta t_{inj} - \frac{L}{t_0}t_1^*}{\frac{L_c}{t_0} - \frac{L}{t_0}} \\ &= \frac{\Delta t_{inj} - t_1^*[1 + Fk_{H_3}(x_{mod,1})]}{-Fk_{H_3}(x_{mod,1})} \end{aligned} \quad (5-23)$$

and

$$z' = L_c/t_0(t' - t_1^*) = \frac{L_c}{t_0} \left\{ \frac{\Delta t_{inj} - t_1^*[1 + Fk_{H_3}(x_{mod,1})]}{-Fk_{H_3}(x_{mod,1})} - t_1^* \right\} \quad (5-24)$$

Then the second switch time can be calculated via this intersection point.

$$\begin{aligned} t_2^* &= t_{R,3}^r - t_0 = t' + \frac{L_c - z'}{u_{c,3}(x_{mod,2})} - t_0 \\ &= \frac{\Delta t_{inj} - t_1^*[1 + Fk_{H_3}(x_{mod,1})]}{-Fk_{H_3}(x_{mod,1})} + \frac{L_c - \frac{L_c}{t_0} \left\{ \frac{\Delta t_{inj} - t_1^*[1 + Fk_{H_3}(x_{mod,1})]}{-Fk_{H_3}(x_{mod,1})} - t_1^* \right\}}{\frac{L_c/t_0}{1 + Fk_{H_3}(x_{mod,2})}} - t_0 \\ &= \frac{\Delta t_{inj} - t_1^*[1 + Fk_{H_3}(x_{mod,1})]}{-Fk_{H_3}(x_{mod,1})} \\ &\quad + [1 + Fk_{H_3}(x_{mod,2})] \left\{ t_0 - \frac{\Delta t_{inj} - t_1^*[1 + Fk_{H_3}(x_{mod,1})]}{-Fk_{H_3}(x_{mod,1})} - t_1^* \right\} - t_0 \end{aligned} \quad (5-25)$$

As aforementioned, the last switch time is the earliest start time of next injection meanwhile the total production time, i.e.

$$t_2^* = t_{inj}^{k+} = \Delta t_{tot} \quad (5-26)$$

If a re-equilibrium time t_{eq} between the cycles are considered, then the total production time becomes:

$$\Delta t_{tot} = t_2^* + t_{eq} \quad (5-27)$$

Thus, the cycle time can be expressed as

$$\begin{aligned} \Delta t_{cyc} &= t_2^* + t_0 - t_{R,1}^f \\ &= \frac{\Delta t_{inj} - t_1^*[1 + Fk_{H_3}(x_{mod,1})]}{-Fk_{H_3}(x_{mod,1})} \\ &\quad + [1 + Fk_{H_3}(x_{mod,2})] \left\{ t_0 - \frac{\Delta t_{inj} - t_1^*[1 + Fk_{H_3}(x_{mod,1})]}{-Fk_{H_3}(x_{mod,1})} - t_1^* \right\} \\ &\quad - t_0[1 + k_{H_1}(x_{mod,1})] \end{aligned} \quad (5-28)$$

The safety time can be expressed as

$$\Delta t_{safe} = \Delta t_{tot} - \Delta t_{cyc} = t_{R,1}^f - t_0 = t_0 f_Z [1 + Fk_{H_1}(T_R)] - t_0 \quad (5-29)$$

(b) 3-step solvent gradients

In case of the 3-step solvent gradients, three switch times are connected to the retention times of all three components, as shown in **Figure 5-12**. The calculation procedure of

switch times is similar as two-step gradients, but there are three intersection points need to be calculated. The modifier fractions are in the ascending level of $[x_{mod,1}, x_{mod,2}, x_{mod,3}]$, where $x_{mod,1}=x_{mod,R}$ and $x_{mod,3}=x_{mod,H}$ in this study.

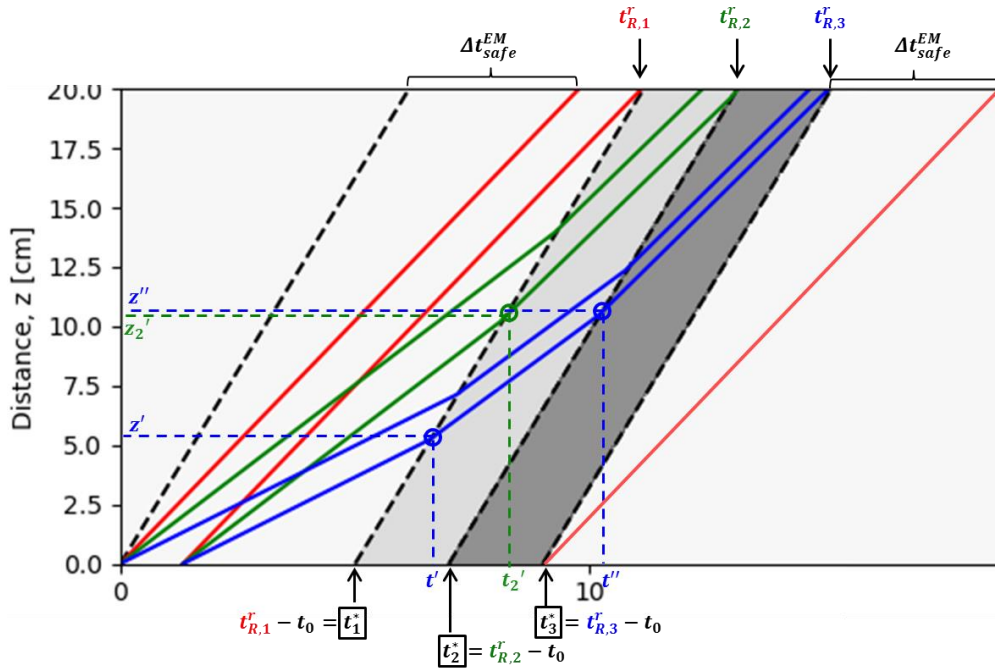


Figure 5-12 3-step solvent gradient. The white and darkening grey blocks indicate modulated modifier fraction at $x_{mod,1}$, $x_{mod,2}$ and $x_{mod,3}$ respectively.

The first switch time is same as that in two-step gradient as

$$t_1^* = t_{R,1}^r - t_0 = t_0 [1 + Fk_{H_1}(x_{mod,1})] + \Delta t_{inj} - t_0 \quad (5-30)$$

The rear band line of the intermediate eluting component and the gradient line for the first switch time are intersected at point (t_2', z_2') as

$$u_{c,2}(x_{mod,1})(t_2' - \Delta t_{inj}) = L/t_0(t_2' - t_1^*) \quad (5-31)$$

This point can be solved as

$$\begin{aligned} t_2' &= \frac{u_{c,2}(x_{mod,1})\Delta t_{inj} - \frac{L_c}{t_0}t_1^*}{u_{c,2}(x_{mod,1}) - \frac{L_c}{t_0}} = \frac{\frac{\frac{L_c}{t_0}}{1 + Fk_{H_2}(x_{mod,1})}\Delta t_{inj} - \frac{L_c}{t_0}t_1^*}{\frac{\frac{L_c}{t_0}}{1 + Fk_{H_2}(x_{mod,1})} - \frac{L_c}{t_0}} \\ &= \frac{\Delta t_{inj} - t_1^*[1 + Fk_{H_2}(x_{mod,1})]}{-Fk_{H_2}(x_{mod,1})} \end{aligned} \quad (5-32)$$

and

$$z_2' = L_c/t_0(t_2' - t_1^*) = \frac{L_c}{t_0} \left\{ \frac{\Delta t_{inj} - t_1^*[1 + Fk_{H_2}(x_{mod,1})]}{-Fk_{H_2}(x_{mod,1})} - t_1^* \right\} \quad (5-33)$$

The second switch time can be calculated based on the point (t_2', z_2') as

$$\begin{aligned}
 t_2^* &= t_{R,2}^r - t_0 = t_2' + \frac{L_c - z_2'}{u_{c,2}(x_{mod,2})} - t_0 \\
 &= \frac{\Delta t_{inj} - t_1^*[1 + Fk_{H_2}(x_{mod,1})]}{-Fk_{H_2}(x_{mod,1})} + \frac{L_c - \frac{L_c}{t_0} \left\{ \frac{\Delta t_{inj} - t_1^*[1 + Fk_{H_2}(x_{mod,1})]}{-Fk_{H_2}(x_{mod,1})} - t_1^* \right\}}{\frac{L/t_0}{1 + Fk_{H_2}(x_{mod,2})}} - t_0 \\
 &= \frac{\Delta t_{inj} - t_1^*[1 + Fk_{H_2}(x_{mod,1})]}{-Fk_{H_2}(x_{mod,1})} \\
 &\quad + [1 + Fk_{H_2}(x_{mod,2})] \left\{ t_0 - \frac{\Delta t_{inj} - t_1^*[1 + Fk_{H_2}(x_{mod,1})]}{-Fk_{H_2}(x_{mod,1})} - t_1^* \right\} - t_0
 \end{aligned} \tag{5-34}$$

The rear band line of the last eluting component and the gradient line for the first switch time are intersected at point (t', z') and they can be solved as

$$t' = \frac{\Delta t_{inj} - t_1^*[1 + Fk_{H_3}(x_{mod,1})]}{-Fk_{H_3}(x_{mod,1})} \tag{5-35}$$

and

$$z' = \frac{L}{t_0} \left\{ \frac{\Delta t_{inj} - t_1^*[1 + Fk_{H_3}(x_{mod,1})]}{-Fk_{H_3}(x_{mod,1})} - t_1^* \right\} \tag{5-36}$$

The rear band line of the last eluting component and the gradient line for the second switch time are intersected at point (t'', z'') as

$$u_{c,3}(x_{mod,2})(t'' - t') + z' = L/t_0(t'' - t_2^*) \tag{5-37}$$

This point can be solved as

$$\begin{aligned}
 t'' &= \frac{t' - [1 + Fk_{H_3}(x_{mod,2})](t_2^* + z't_0/L)}{-Fk_{H_3}(x_{mod,2})} \\
 &= \frac{\frac{\Delta t_{inj} - t_1^*[1 + Fk_{H_3}(x_{mod,1})]}{-Fk_{H_3}(x_{mod,1})} - [1 + Fk_{H_3}(x_{mod,2})] \left\{ t_2^* + \frac{\Delta t_{inj} - t_1^*[1 + Fk_{H_3}(x_{mod,1})]}{-Fk_{H_3}(x_{mod,1})} - t_1^* \right\}}{-Fk_{H_3}(x_{mod,2})} \\
 &= \frac{\Delta t_{inj} - t_1^*[1 + Fk_{H_3}(x_{mod,1})]}{F^2k_{H_3}(x_{mod,1})k_{H_3}(x_{mod,2})} + \frac{1 + Fk_{H_3}(x_{mod,2})}{Fk_{H_3}(x_{mod,2})} \left\{ t_2^* + \frac{\Delta t_{inj} - t_1^*[1 + Fk_{H_3}(x_{mod,1})]}{-Fk_{H_3}(x_{mod,1})} - t_1^* \right\}
 \end{aligned} \tag{5-38}$$

and

$$z'' = \frac{L}{t_0}(t'' - t_2^*) \tag{5-39}$$

The third switch time can be calculated based on the point (t'', z'') as

$$t_3^* = t_{R,3}^r - t_0 = t'' + \frac{L_c - z''}{u_{c,3}(x_{mod,3})} - t_0 = t'' + \frac{t_0[1 + Fk_{H_3}(x_{mod,3})](L_c - z'')}{L_c} - t_0 \tag{5-40}$$

Again, the last switch time equals to the earliest start time of next injection and the total production time as

$$t_3^* = t_{inj}^{k+} = \Delta t_{tot} \quad (5-41)$$

Thus, the cycle time can be expressed as

$$\begin{aligned} \Delta t_{cyc} &= t_3^* + t_0 - t_{R,1}^f \\ &= t'' + \frac{t_0[1 + Fk_{H_3}(x_{mod,3})] \left[L_c - \frac{L}{t_0}(t'' - t_2^*) \right]}{L_c} - t_0[1 + k_{H_1}(x_{mod,1})] \end{aligned} \quad (5-42)$$

The safety time is the same as that in 2-step as

$$\Delta t_{safe} = \Delta t_{tot} - \Delta t_{cyc} = t_{R,1}^f - t_0 = t_0 f_z [1 + Fk_{H_1}(T_R)] - t_0 \quad (5-43)$$

Consequently, the 2-step gradient has a shorter cycle time and total production time than 3-step gradient leading to a higher productivity, since the highest elution strength is imposed from the second eluting component. The productivity can be calculated by Eq. (2-71). The calculated performance will be compared in section 6.5.

5.5 Protocol to predict chromatograms using EM and EDM

To calculate the ideal cycle time and productivity, only retention times are enough. However, chromatograms are better representation, especially when comparing with experimental profiles.

To generate a chromatogram in EM, retention times of front and rear bands for each component and their bandwidths and band heights are required. The retention times and bandwidths can be directly obtained from the physical plane, so the heights are the only concern. In case of the isocratic and isothermal condition, the bandwidth is not changed and it equals to the injection period. However, the bandwidths are changed in gradient operations, and thus the band heights are changed accordingly. The maximal height c_{max} can be calculated according to the mass balance as follows

$$m_{inj} = c_{inj}V_{inj} = c_{inj}\Delta t_{inj}\dot{V} = c_{max}w\dot{V} \quad (5-44)$$

where w refers to the bandwidth. It should be noted that this formula is in principle valid for the cases where the migrations pathways of front and rear bands are identical. They are identical in most cases of solvent gradients, but not same in a few cases of temperature gradients. If the front and rear bands of a component travel with different

courses of gradients, the profile exhibit a splitting behaviour, which influences the precision of bandwidths. Given that the elution strength of temperature gradients is not strong, this factor can be neglected and the formula can be still used for rough calculation.

The simulated chromatograms in EDM is normally obtained by solving the mass balance differential equations in Eq. (2-64) with a numerical method, which consumes much time and computation power. Alternatively, it can be done in an easier way. By using Eq. (5-44), the Eq. (2-34) can be further transformed in terms of bandwidth as

$$c(t, z = L_c) = \frac{m_{inj}}{2\dot{V}w} \left\{ erf \left[\frac{1 - (t - w/2)/t_R}{\sqrt{2}(t - w/2)/t_R/N_p} \right] - erf \left[\frac{1 - (t + w/2)/t_R}{\sqrt{2}(t + w/2)/t_R/N_p} \right] \right\} \quad (5-45)$$

Hence, the chromatograms can be generated by inputting retention times, bandwidths and theoretical plate number.

To calculate the cycle time in EDM, the front band retention time of the first eluting component $t_{R,1}^f$ and the rear band retention time of the last eluting component $t_{R,N}^r$ at the threshold concentration c_{thres} are required. They can be determined by finding the root of the following equation

$$f(t) = c_{thres} - c(t, z = L_c) = 0 \quad (5-46)$$

In this study, the threshold was set as 2×10^{-5} g/L in simulations whereas in experiments as 5 mAU. The bisection method was used to find roots.

5.6 Summary of procedure for predicting chromatograms

The overall procedure for gradient design is demonstrated in **Figure 5-13**. The gradient conditions can be defined by the certain operating regimes, where switch times are connected to retention times of certain components.

For simple cases, i.e., single gradient and fewer components, switch times can be easily expressed in an explicit way in terms of isotherm parameters through analytic geometry. Meanwhile, the retention times are also analytically expressed, which directly leads to the performances to predict, i.e. the cycle time and productivity. In fact, these explicit expressions are the function of Henry's constant.

For complicated cases, derivation of analytical expressions requires a huge effort. In such cases, a numerical calculation procedure is desirable. By inputting calculated

isotherm data, gradients fields covering the entire physical plane are generated. The migration velocity at each point can be calculated with Henry's constant and additional column data and flow condition. Each migrating point is calculated with the migration velocity at the corresponding space and time using the first order Euler method. By iteration until the outlet boundary, the migration path of each component is drawn and the retention times then come out. Subsequently, the cycle time as well as productivity can be calculated. In this numerical scheme, switch times can be defined by user with the full freedom, which is more flexible for designing combined gradients. In this study, the calculation is based on EM. However, it can be extended to EDM by using a zone spreading rate parameter connected with the apparent dispersion coefficient [133].

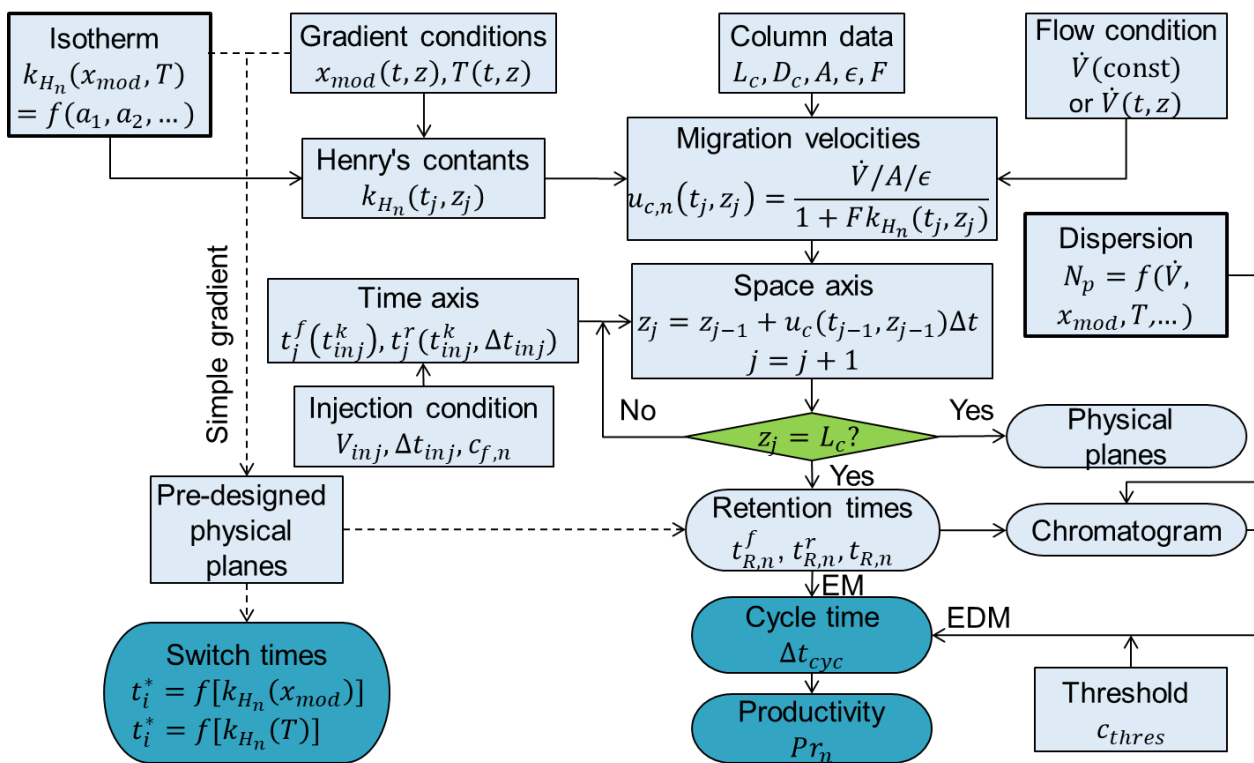


Figure 5-13 Summary of tasks to predict chromatograms and performance for gradient and isocratic/isothermal conditions.

Chapter 6. Experimental demonstration and model validation

In this chapter, both temperature and solvent gradients are demonstrated experimentally. Chromatograms under isothermal and isocratic conditions are shown. Then the concepts of temperature gradients were theoretically demonstrated followed by the experimental validation. The previously designed operating regimes for both gradients (section 5.3 and 5.4) were applied in actual experiments. The switch times and cycle times were determined in actual experiments. Finally, their performances were summarised and compared.

6.1 Illustration of selected chromatograms under certain conditions

Some selected chromatograms under isothermal and isocratic conditions from real experiments are demonstrated in **Figure 6-1**. At the top, the chromatogram under the reference condition at $T_R=25$ °C and $x_{mod,R}=0.5$ is shown. The elution profile of these three components forms a typical partly lagged separation problem, where the last eluting component C7 falls much behind from others. The injection volume was adjusted to form touching bands separation with high a yield for the preparative purpose, i.e., all components are fully separated. Obviously, the cycle time is relatively long and it can be further improved. As aforementioned, the retention time can be reduced by accelerating migration velocity i.e., increasing temperature or modifier fraction. It can be expected that the cycle time is shorter at high temperature or high modifier fraction. The subfigure at middle shows the elution profile under high temperature at $T_H=60$ °C whereas the one at bottom shows that under high modifier fraction at $x_{mod,H}=0.7$. Despite the cycle time is reduced, the remixing occurs between the first two components and the touching band separation no longer maintains. To recover the touching band separation, the loading volume should be compromised, which leads to decrease in productivity. A better way is to utilise gradients appropriately to minimise the cycle time without rendering separations between components. Additionally, there were no remixing between the intermediate and the last components even at high temperature and modifier fraction, which means that the gradients should be deployed from the intermediate component to minimise the cycle time.

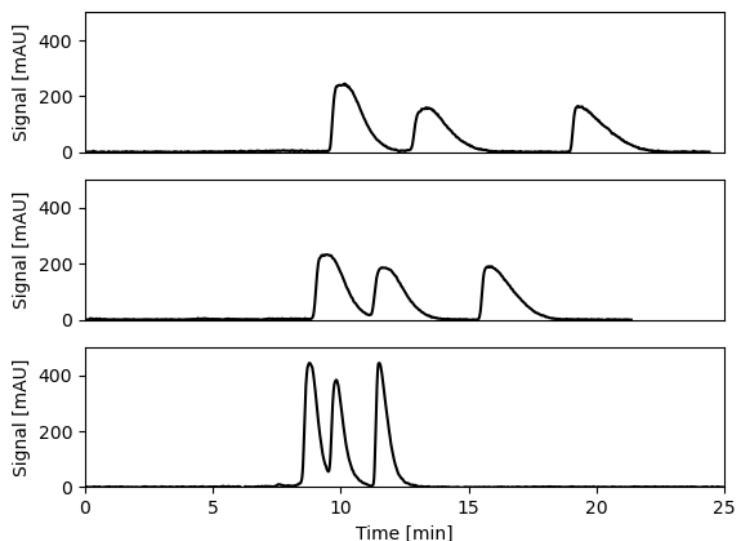


Figure 6-1 Illustration of chromatograms for three selected isothermal and isocratic conditions. Top: T_R and $x_{mod,R}$; Middle: T_H and $x_{mod,R}$; Bottom: T_R and $x_{mod,H}$.

6.2 Chromatograms under reference condition

The chromatograms under the reference condition at $T_R=25$ °C and $x_{mod,R}=0.5$ is shown in **Figure 6-2**, which corresponds to experimental profile in **Figure 6-1** (top) and the physical plane in **Figure 5-1**. The analytical profiles for EM and EDM were generated by using the methods described in section 5.5. The touching point between cycles in EDM is shifted as compared to that in EM due to the dispersion effect. It is also influenced by the threshold concentration. The simulated profile was converted to the signal intensity using detector calibration factors and compared with the experimental profile. As a result, they were in a good agreement.

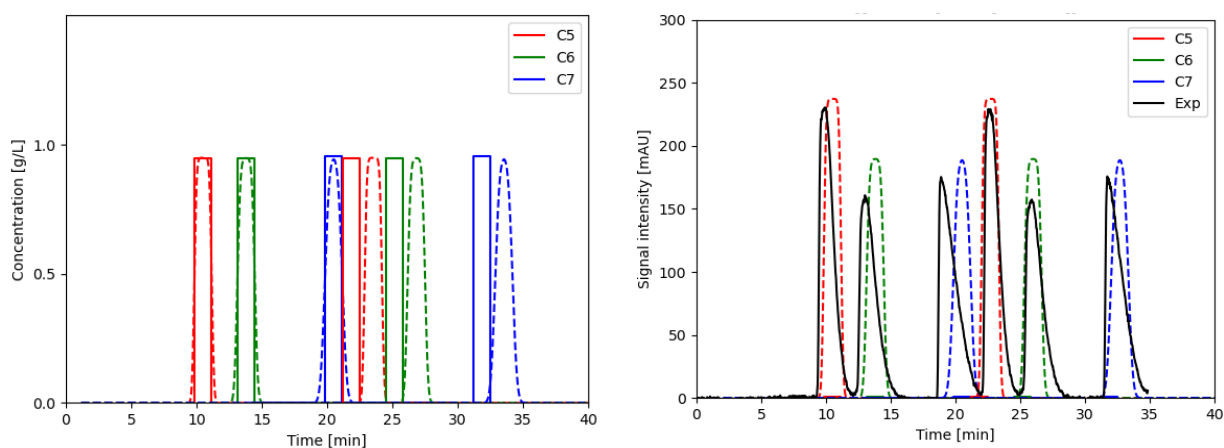


Figure 6-2 Chromatograms under isothermal and isocratic operation. Left: EM (solid line) and EDM (dashed line); Right: EDM (dashed line) and experimental profile (black solid line). The corresponding physical plane is in Figure 5-1. $T=T_R=25$ °C, $x_{mod}=x_{mod,R}=0.5$, $\dot{V}=0.3$ ml/min, $V_{inj}=400$ μ L. Henry's constants are from Table 4-7.

6.3 Temperature gradients

The migration behaviours under temperature gradients in the physical plane are theoretically demonstrated by wide injection of single component and experimentally validated. The temperature gradients were then applied in the mixture separation.

6.3.1 Single component wide injection

In order to demonstrate the influence of temperature gradients on the chromatograms (c-t plot) and the profile inside the column (c-z plot) in an intuitive manner, the wide injection was used with a single component. In actual experiments, the injection volume should be big enough to generate the breakthrough plateaus. In this section, the injection volume $V_{inj}=1500 \mu\text{L}$ with the injection period $\Delta t_{inj}=5 \text{ min}$ is used to reach breakthrough and keep an enough interval for modulation.

6.3.1.1 Theoretical single component migration behaviour in the physical plane

As aforementioned, the physical plane illustrates the component specific migration pathways of adsorption and desorption fronts, i.e. front and rear bands. These pathways appeared to be straight lines under linear isotherms [81,82], and their corresponding slopes are migration velocities depending on temperature and modifier fraction, as defined in Eq. (2-17). In this study, increase in temperature leads to decrease in Henry's constant, i.e., the slope increases by heating and decreases by cooling. The temperature is modulated on the segment II. Essential features of an exemplar physical plane for a single component wide injection under a single-step temperature gradient in EM is depicted in **Figure 6-3**. In this figure, the isothermal and isocratic case at reference temperature T_R (green) is shown. While keeping the constant injection period and injection concentration, the migration behaviour upon a step change to a higher temperature T_H (red) or a lower temperature T_L (blue) at a certain switch time t^* is demonstrated. For different switch times, the resulting chromatograms are quite different, which depends on where, when and by which gradient course each of the front and rear bands are influenced. All other possible scenarios for different switch times are given in Appendix 1.

In this example, the switch time is located between the front and rear retention times, i.e. $t_R^f < t^* < t_R^r$. The temperature is switched when part of the solute has left the column outlet before end of the elution. Therefore, only the part of the solute inside the column

is influenced by the gradient, which leads to a splitting chromatogram characterised by two distinct concentration levels. In case of increase in temperature, the profile after the switch time changes to a narrower band with higher concentration. It is opposite in the case of decrease in temperature. In any cases, the total area of chromatograms are kept same.

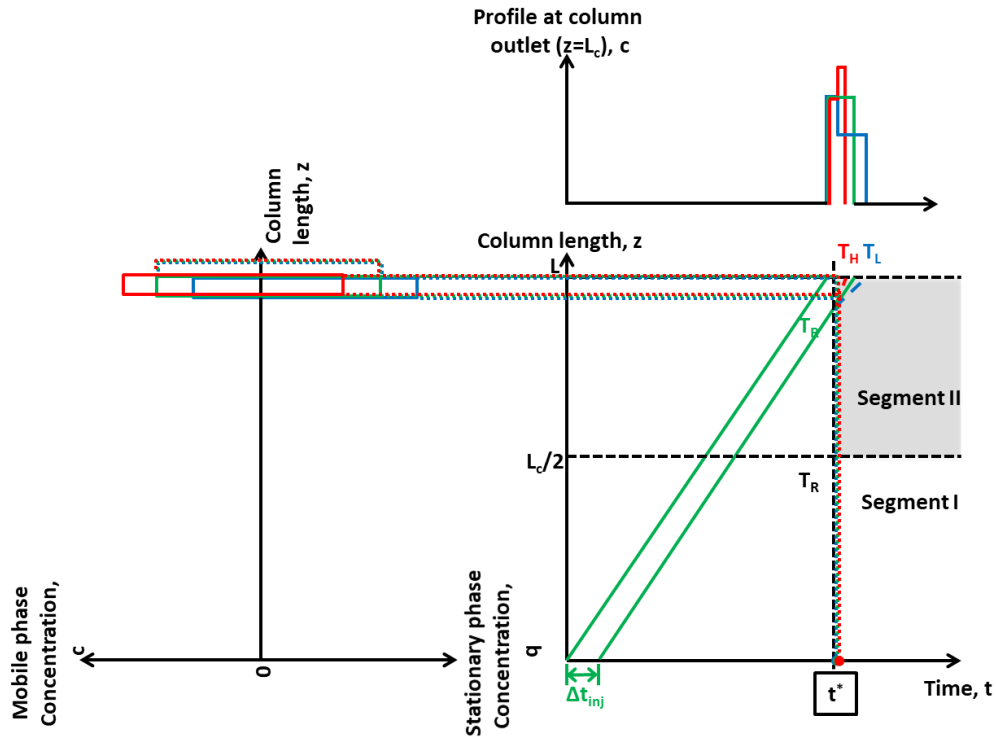


Figure 6-3 Migration behaviour under temperature gradients when $t_R^f < t^* < t_R^i$. Right bottom: physical plane. Green, blue and red colours refer to the temperature at T_R , T_L and T_H , respectively. The grey block indicates modulated temperature. Top: chromatogram at column outlet; Left: column internal profile showing solute distribution between mobile and stationary phases.

In all scenarios, the mass should be conserved. The injected mass is calculated as

$$m_{inj} = c_{inj} V_{inj} = c_{inj} \dot{V} \Delta t_{inj} \quad (6-1)$$

The mass along the column axis m_z at all time $\Delta t_{inj} < t < t_R$ is calculated as

$$m_z = A \varepsilon_t \{1 + F k_H [T(z)]\} \int_0^{L_c} c(t, z) dz \quad (6-2)$$

The mass along the time axis m_t at all positions $0 \leq z \leq L_c$ is calculated as

$$m_t = \dot{V} \int_0^{\infty} c(t, z) dt \quad (6-3)$$

6.3.1.2 Experimental validation of single component migration behaviour

The retention behaviours of single component wide injection are experimentally validated by different switch times in **Figure 6-4**. In the experiment, the feed of 0.1 vol% C7 dissolved in the reference modifier fraction was injected for $V_{inj}=1500 \mu\text{L}$ via pump. The corresponding injection period at $\dot{V}=0.3 \text{ ml/min}$ was 5 min. The lower temperature for cooling and the higher temperature for heating were set as $T_L=10 \text{ }^\circ\text{C}$ and $T_H=40 \text{ }^\circ\text{C}$.

The chromatograms for the scenario when $t^* = 0$ is shown in **Figure 6-4(a)** corresponding to **A. Fig. 1**. In this scenario, the temperature modulation is immediately activated from the beginning, i.e. each segment maintains its temperature all over the time. The front and rear band are influenced by the gradient at the same position but different times in difference of the injection period. On one hand, the bandwidth over time w_t and concentration height h in chromatograms are not changed upon gradients. On the other hand, the bandwidth over space w_z is changed while keeping the same height. Their total area of both phases are kept same. This behaviour is also valid when the switch time is very early or very late, i.e. $t^* < t_R^f(z = f_z L_c)$ or $t^* > t_R^r(z = L_c)$. In experimental chromatograms, the bandwidths and heights were not changed, which is in accordance with the theoretical demonstration.

The chromatograms for the scenario when $t_R^r(z = f_z L_c) < t^* \leq t_R^f(z = L_c)$ is shown in **Figure 6-4(b)** corresponding to **A. Fig. 3**. In this scenario, temperature switch happens after both front and rear bands fully enter the segment II before they reach the outlet. The front and rear bands are influenced by the gradient at the same time but different positions. This simultaneous change of both front and rear bands leads to unchanged w_z , but changed w_t and h . Thus, the chromatogram is compressed by heating and broadened by cooling. In the experiment, the switch time was set at $t^*=18 \text{ min}$ to satisfy this scenario. Consequently, the experimental chromatograms behaved in changed bandwidths and heights, which is consistent with the theory.

The chromatograms for the scenario when $t_R^f < t^* < t_R^r$ is shown in **Figure 6-4(c)** corresponding to **Figure 6-3**. As mentioned in the previous section, the chromatograms exhibit splitting behaviours in this scenario. In the experiment, the switch time was set at $t^*=24 \text{ min}$ to satisfy this scenario, where the solute is on the way leaving the column while the front band appeared on the detector at 22 min already. As expected, the experimental chromatograms showed the splitting behaviour upon temperature switch

since the part of solute inside the column is exposed to the gradient thereby causing changes in bandwidths and heights. Hence, this behaviour was successfully validated.

In all scenarios, the numerical solutions using EDM were plotted to compare with experimental profiles. As a result, the numerical solutions captured correct trends towards single-step temperature switches, which have relatively good agreements with the experimental profiles. Nonetheless, small deviations can be observed, which could be attributed to several factors. First, temperature inconsistency between two segments might exist due to different temperature controlling media, which can influence Henry's constant. Second, the nonideality of implementing step temperature profile can contribute to the deviation from the ideal profile used in the model. In reality, the temperature is modulated within a certain period towards a limited maximal value. Additionally, the uncertainties from thermostats should also be responsible for the nonideal profiles. Last, the model could be limited since thermal dispersions in axial and radial directions were neglected. The more detailed 2D model might provide a better agreement.

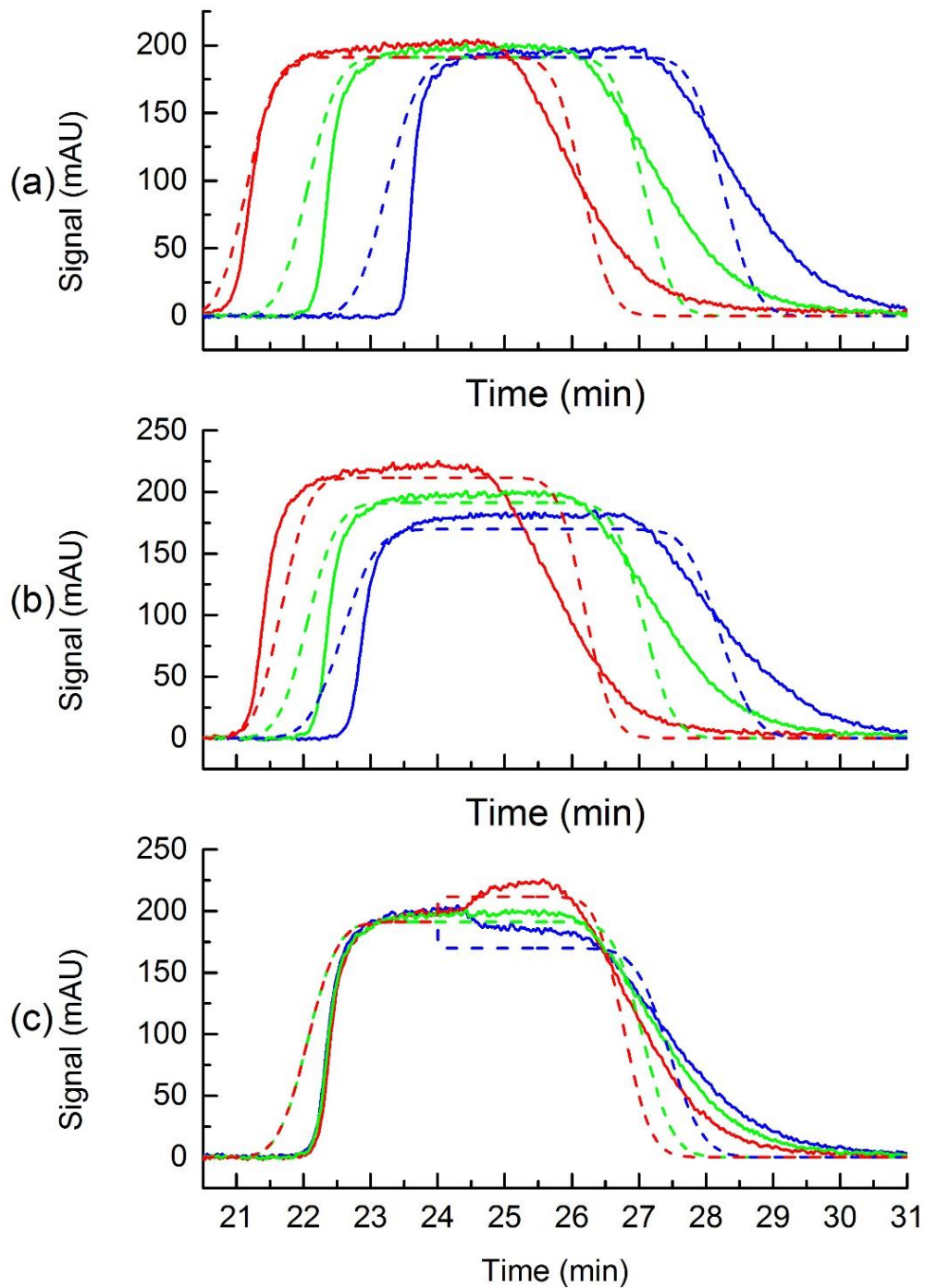


Figure 6-4 Experimental validation of single component (C7) retention behaviours under temperature gradients. Top: $t^* = 0$ corresponding to scenario in A. Fig. 1; Middle: $t_R^r(z = f_z L_c) < t^* \leq t_R^f(z = L_c)$ corresponding to scenario in A. Fig. 3; Bottom: $t_R^f < t^* < t_R^r$ corresponding to scenario in Figure 6-3. Solid lines: experimental profiles; dashed lines: numerical solutions. The lines in green, blue and red indicate the temperature at $T_R=25$ °C, $T_L=5$ °C and $T_H=60$ °C. $x_{mod}=0.5$, Henry's constants are from Table 4-7. $\dot{V}=0.3$ ml/min, $V_{inj}=1500$ μ L.

6.3.2 Ternary mixture separation

The ternary mixture separations under temperature gradients by designed operating regimes (section 5.3) were performed aiming at reducing the cycle time in a partly lagged separation problem. In the experiment, 0.1 vol% C5, C6 and C7 dissolved in the reference mobile phase in $V_{inj}=400\ \mu\text{L}$ were used as the mixture solution. This injection volume was chosen by finding the maximal loading to form touching bands without rendering separation quality for all components at the reference temperature. The ideal characteristic times were calculated by the analytical expressions in section 5.3 and used in analytical profiles. In experiments, it becomes more complicated since the plant dead time, actual band broadening and waiting times in the injector programming for consecutive injections should be considered. Thus, the characteristic times were determined by observed retention times using the same operating regimes. All determined characteristic times are summarised in Appendix 4. The analytical solutions in EM and numerical solutions in EDM were also given for comparison.

Ternary mixture separation experiments were carried out by the conservative regime described in section 5.3.1, and the result is shown in **Figure 6-5**. The first and second switch times were determined at observed $t_{R,1}^r$ and $t_{R,3}^r$ whereas the start time for next injection was determined by observed retention times by each individual segment in pre-experiments. The experimental cycle time was determined to be 11.4 min with an extra time of 4.1 min. As a result, its total production time (15.5 min) was even longer than that in the isothermal operation (12.7 min) due to the generated gap. As explained before, this gap in this regime is subjected to assure monotonic temperature modulation for each component. The analytical and numerical solutions were in a good agreement, though there was a shift in the second cycle. This shift is caused by the dispersion effect, which can influence the characteristic times and the cycle time. The numerical solution also fitted well with the experimental profile. The shift between profiles in the second cycle can be attributed to nonideal step gradient and different threshold criteria in simulations and experiments.

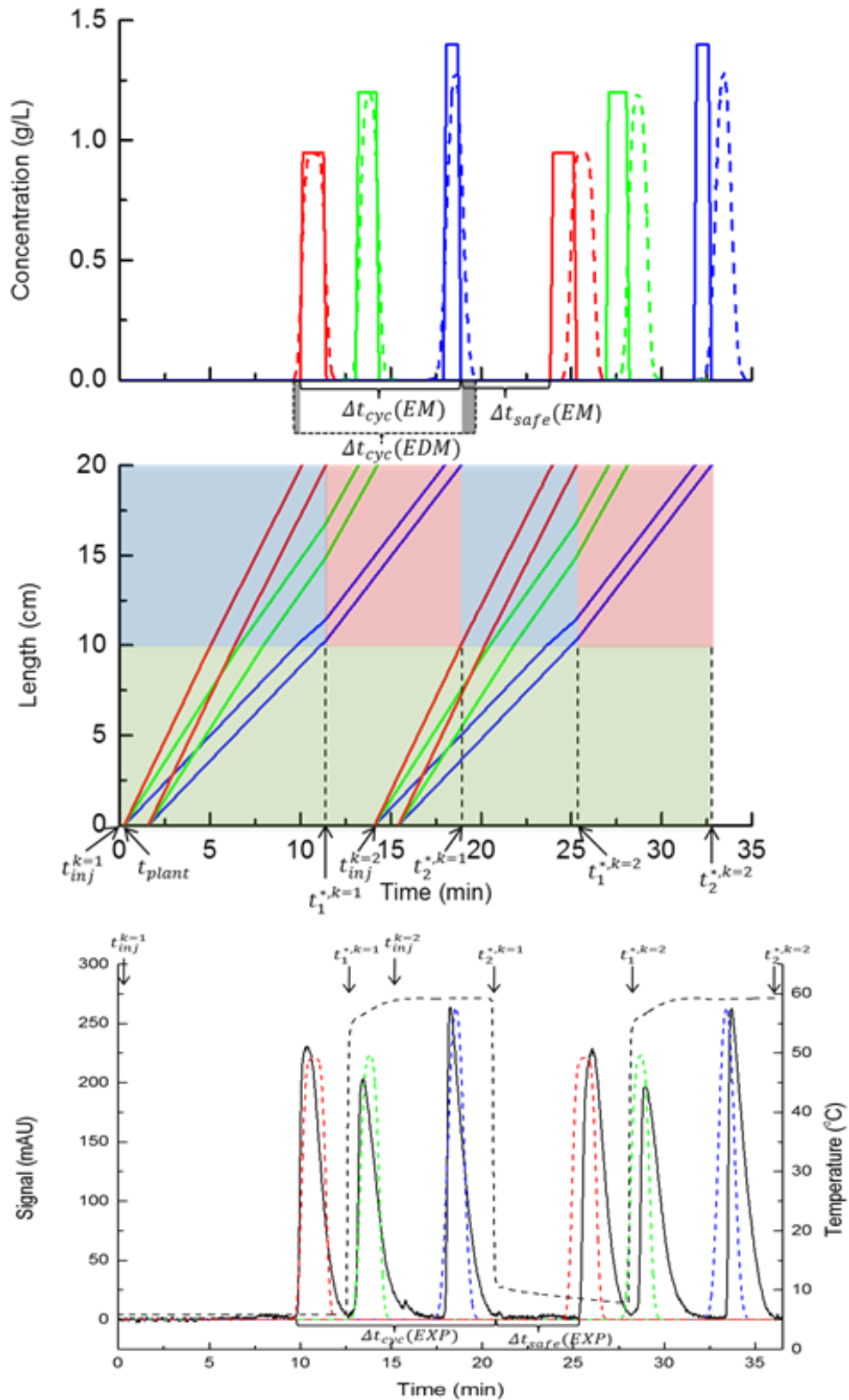


Figure 6-5 Experimental validation of ternary separation under temperature gradients by conservative regime. Lines in red, green and blue correspond to component C5, C6 and C7, respectively. Elution profiles: EM and EDM; Temperature profiles: ideal step gradients. Coloured solid lines: EM; Coloured dashed lines: EDM; Black solid lines: experiment (EXP). Top: profiles from EM and EDM; Middle: trajectories of chromatograms in the physical plane. The blocks in green, blue and red indicate the temperature at $T_R=25\text{ }^\circ\text{C}$, $T_L=5\text{ }^\circ\text{C}$ and $T_H=60\text{ }^\circ\text{C}$; Bottom: profiles from EDM and EXP. $x_{mod}=0.5$, Henry's constants are from Table 4-7. $\dot{V}=0.3\text{ ml/min}$, $V_{inj}=400\text{ }\mu\text{L}$.

Ternary mixture separation experiments were carried out by the improved regime described in section 5.3.1, and the result is shown in **Figure 6-6**. This figure was from the old work, where the repetitive improved regime actually starts from the second cycle like in Figure 5-6, whereas the same switch times in the conservative regime were used for the first cycle. All key information should be based on the second cycle. The only difference between two figures is the initial temperature modulation, though their calculation procedure for characteristic times are similar. The experimental characteristic times can be determined by observed retention times in additional single component experiments under the corresponding modulation. In this regime, the extra time was fully eliminated. The experimental cycle time was determined to be 11.1 min, which is equal to the total production time. It is shorter than that in the isothermal operation, which indicates improved productivity. As explained before, the reduction of the cycle time is attributed to the heating, whereas the cooling is for maintaining the resolution. The analytical and numerical profiles were compared, and the shift was caused by the dispersion effect in connection with the calculation of characteristic times. The numerical and experimental profiles were in a good agreement, and the deviation is from threshold criteria.

In order to confirm reproducibility and stability of this improved regime, four consecutive injections were carried out, as shown in **Figure 6-7**. The water temperature T_w (dashed line) and the measured outlet temperature T_{mes} (dotted line) are shown at the right axis. The nonideal temperature profile due to uncertainties from thermostats can be observed. The elution profiles from the second cycle were in a repeatable manner. Hence, the temperature gradient operation was verified to be reproducible and stable. All characteristic times are marked in the figure. Consecutive injections under isothermal condition was provide for comparison. The start times of next injections under the gradient operation were earlier than those under the isothermal operation due to the reduced cycle time. Additionally, the gradients obviously reduce the dispersion, especially the last eluting component.

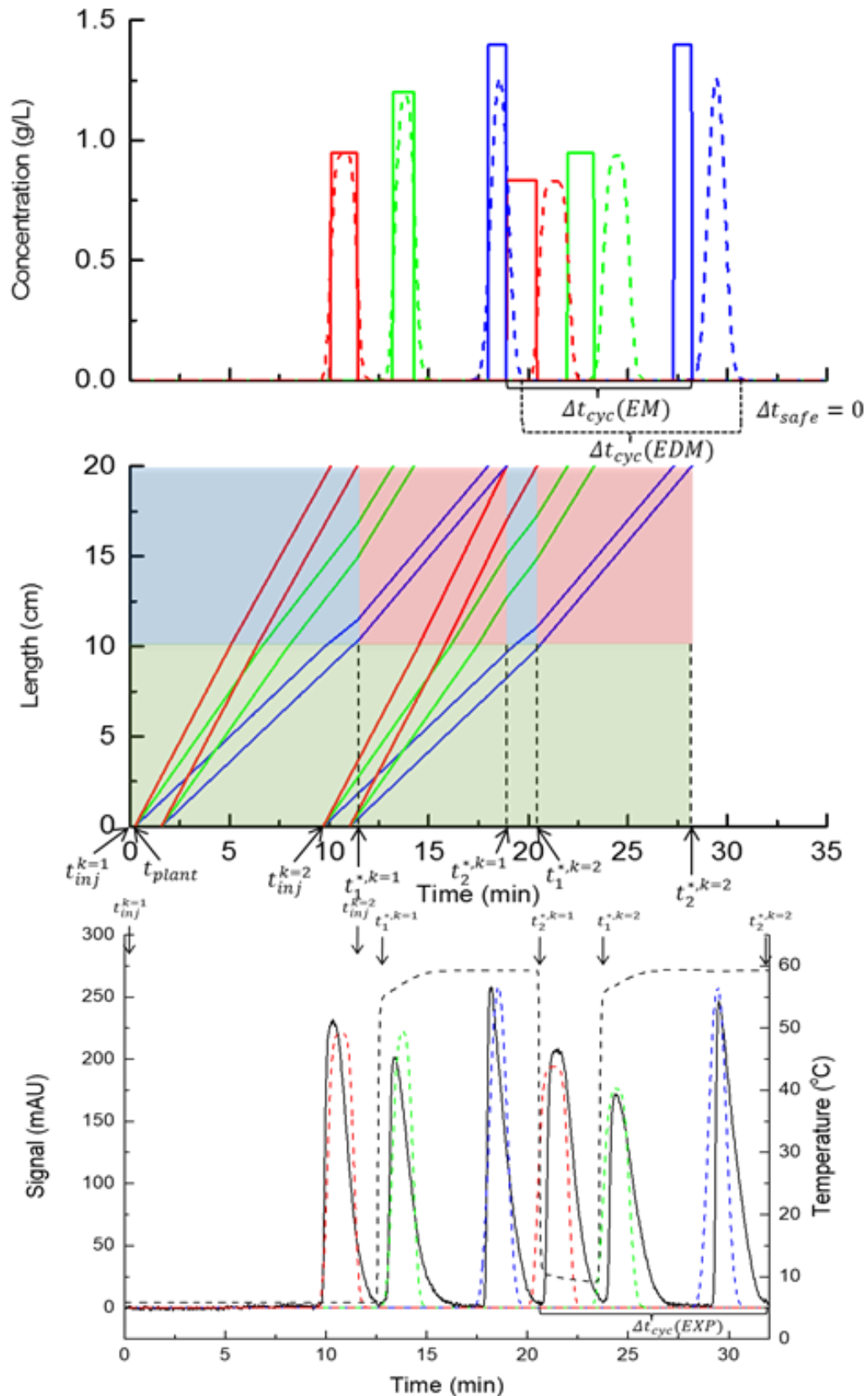


Figure 6-6 Experimental validation of ternary separation under temperature gradients by improved regime. Lines in red, green and blue correspond to component C5, C6 and C7, respectively. Elution profiles: EM and EDM; Temperature profiles: ideal step gradients. Coloured solid lines: EM; Coloured dashed lines: EDM; Black solid lines: experiment (EXP). Top: profiles from EM and EDM; Middle: trajectories of chromatograms in the physical plane. The blocks in green, blue and red indicate the temperature at $T_R=25$ °C, $T_L=5$ °C and $T_T=60$ °C; Bottom: profiles from EDM and EXP. $x_{mod}=0.5$, Henry's constants are from Table 4-7. $\dot{V}=0.3$ ml/min, $V_{inj}=400$ μ L.

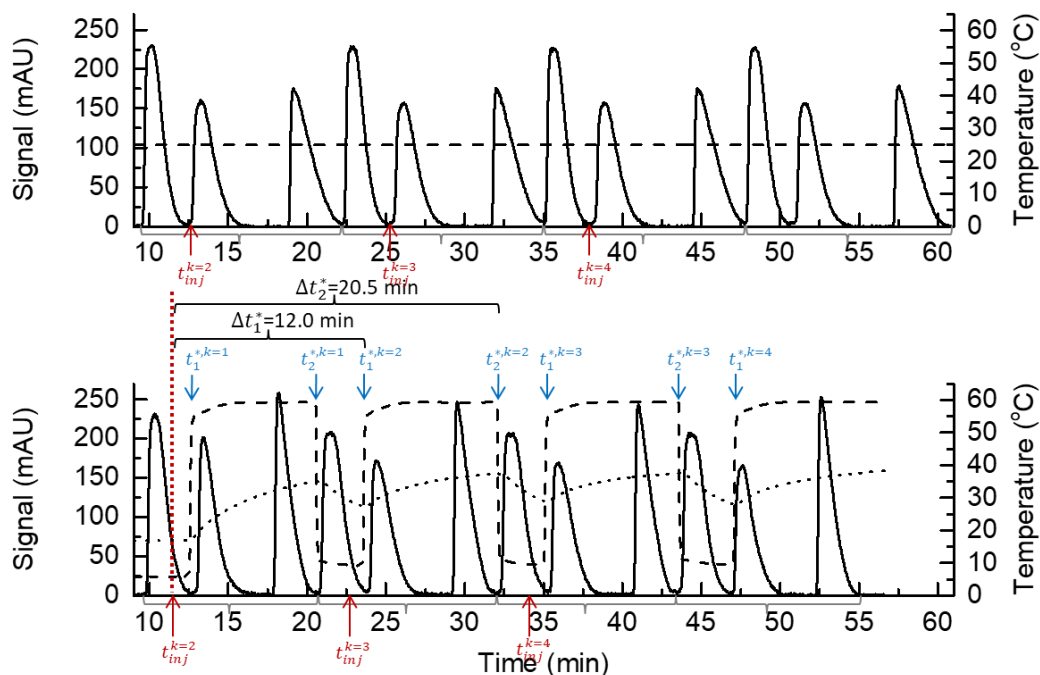


Figure 6-7 Elution profiles for consecutive four injections under isothermal condition and temperature gradient by improved regime. Top: isothermal operation at T_R ; Bottom: gradient operation by improved regime, $T_R=25$ °C, $T_L=5$ °C and $T_H=60$ °C. The solid line corresponds to chromatogram at left axis. The dashed and dotted lines at right axis correspond to measured temperature T_w and T_{mes} , respectively. The cycle time is the difference between $t_{inj}^{k=2}$ and $t_{inj}^{k=3}$. $x_{mod}=0.5$, $\dot{V}=0.3$ ml/min, $V_{inj}=400$ μ L.

6.4 Solvent gradients

The migration behaviour of a single component wide injection under the solvent gradient is demonstrated in **A. Fig. 4**. It is quite similar as that under the temperature gradient, where the chromatograms are changed characterised by the bandwidth and concentration height. The only difference is that the gradient line is inclined with the slope of intestinal velocity u .

The ternary mixture separation experiment by 2-step solvent gradient was carried out, and the result is shown in **Figure 6-8**. The modifier fractions were set in the ascending level of [0.5, 0.7]. As mentioned in section 6.1, the last two components were not remixed by the higher limit of elution strength at $x_{mod,H}$. Hence, the gradient can be deployed from the second eluting component to more effectively minimise the cycle time, though it accompanies the risk of remixing. As described in 5.4.1, two switch times in the 2-step solvent gradient are connected to the retention times of the first and last eluting component. The determined characteristic times are summarised in Appendix 4. The profiles in EM and EDM were in a good agreement. The ideal cycle time was determined to be 3.9 min with the extra time 3.6 min. The total production time was then

7.5 min, which is much shorter than that under the isocratic condition. However, safety margins for the switch times should be applied in the real experiment in order to avoid the remixing between the first two eluting components. With additional safety margin, the actual experimental profile was shifted with a longer total production time of 9.4 min.

The ternary mixture separation experiment by 3-step solvent gradient was carried, and the result is shown in **Figure 6-9**. The modifier fractions were set in the ascending level of [0.5, 0.6, 0.7]. In this case, three switch times are connected to retention times of each component. The determined characteristic times are summarised in Appendix 4. The profiles in EM and EDM were in a good agreement. Similarly, the safety margins were applied to the switch times in the real experiment to avoid the remixing, which leads to the shift of the experimental profile. The total production times from ideal and experiment profiles were determined to be 8.4 min and 10.1 min, respectively. As compared to 2-step gradient, 3-step has longer cycle time since the elution strength is partially reduced for a period. Meanwhile the band break between the first two components is bigger, which provides the merit of avoiding remixing.

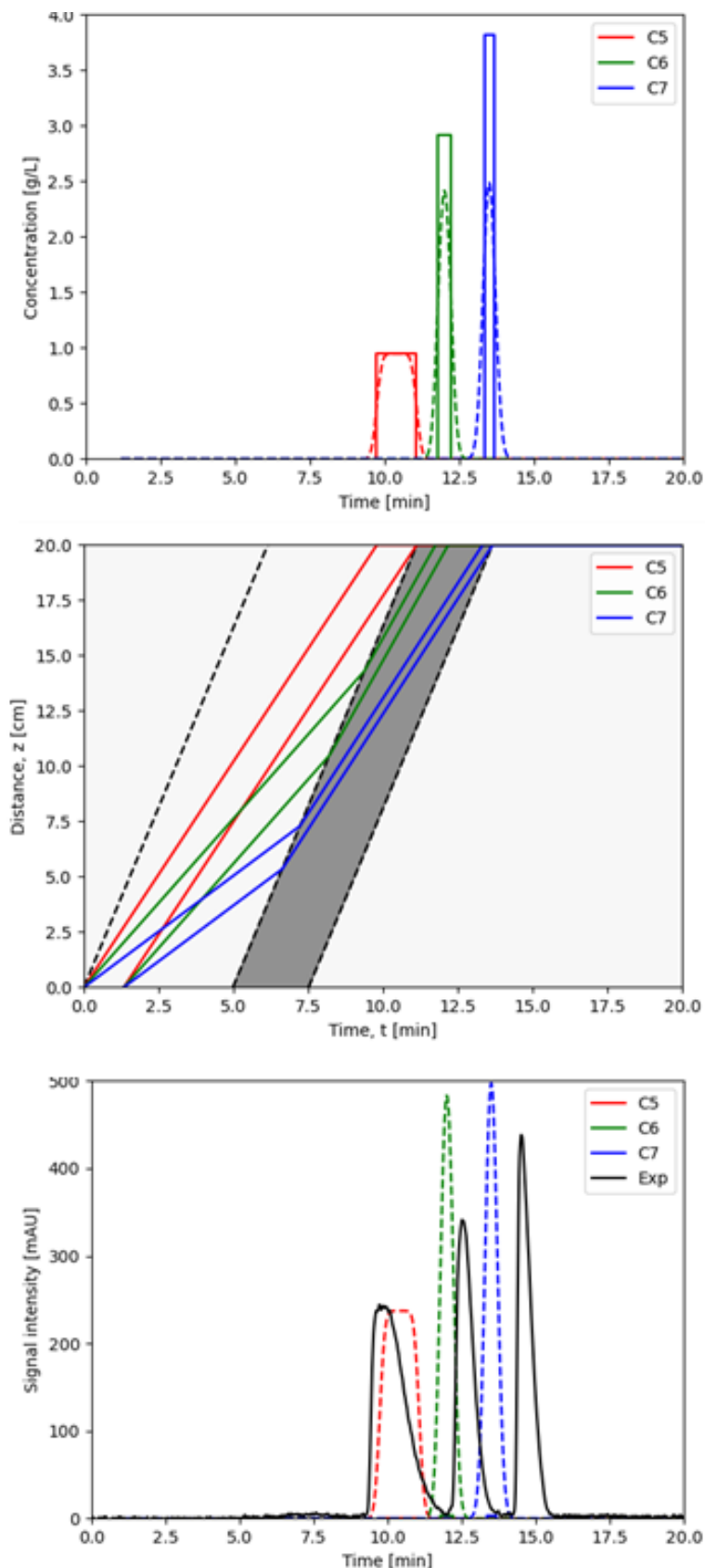


Figure 6-8 Experimental validation of ternary separation under 2-step solvent gradients. Lines in red, green and blue correspond to component C5, C6 and C7, respectively. Elution profiles: EM and EDM; Solvent profiles: ideal step gradients. Coloured solid lines: EM; Coloured dashed lines: EDM; Black solid lines: experiment (EXP). Top: profiles from EM and EDM; Middle: trajectories of chromatograms in the physical plane. The blocks in white and grey indicate the modifier fraction at 0.5 and 0.7; Bottom: profiles from EDM and EXP. No consecutive injections were carried out. $T=25\text{ }^{\circ}\text{C}$, Henry's constants are from Table 4-7. $\dot{V}=0.3\text{ ml/min}$, $V_{inj}=400\text{ }\mu\text{L}$.

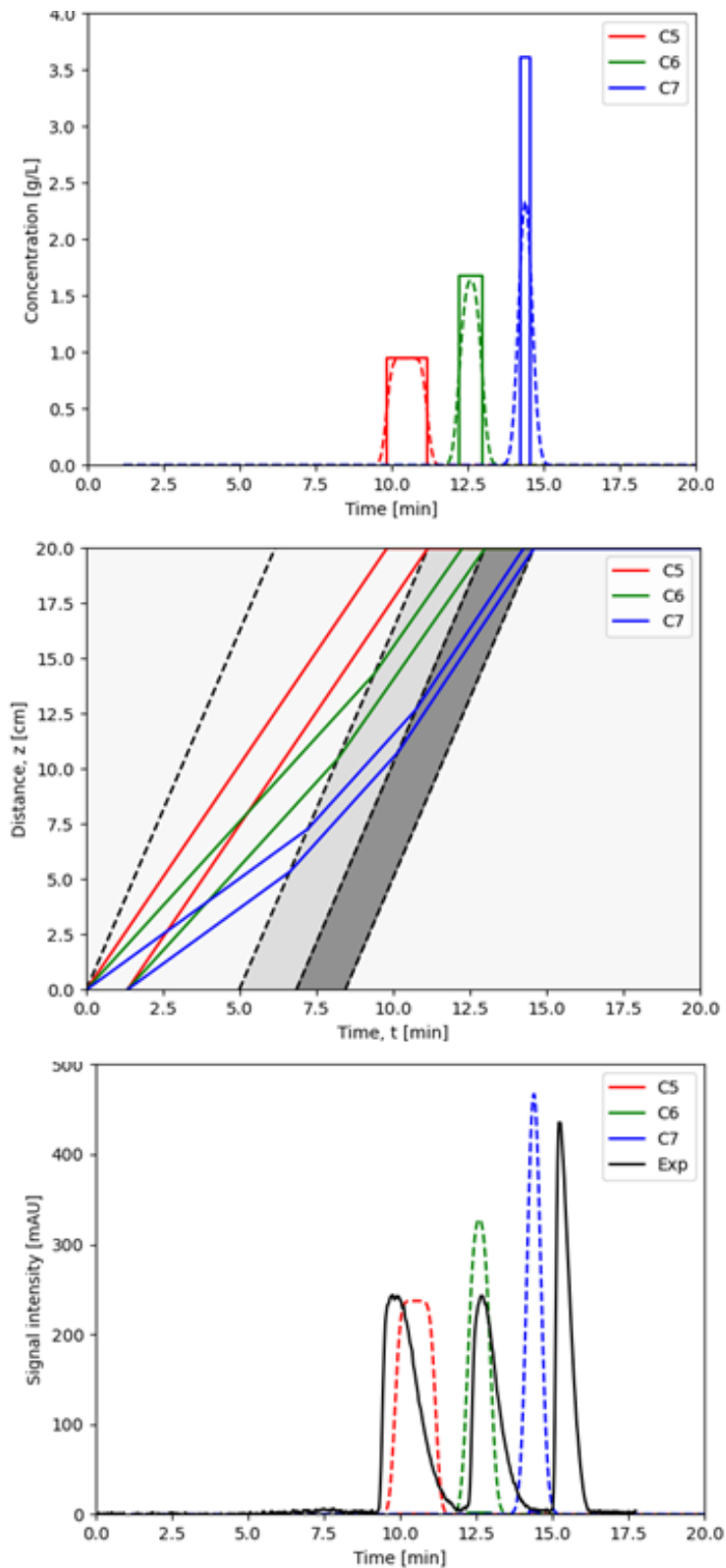


Figure 6-9 Experimental validation of ternary separation under 3-step solvent gradients. Lines in red, green and blue correspond to component C5, C6 and C7, respectively. Elution profiles: EM and EDM; Solvent profiles: ideal step gradients. Coloured solid lines: EM; Coloured dashed lines: EDM; Black solid lines: experiment (EXP). Top: profiles from EM and EDM; Middle: trajectories of chromatograms in the physical plane. The blocks in white, bright grey and dark grey indicate the modifier fraction at 0.5, 0.6 and 0.7; Bottom: profiles from EDM and EXP. No consecutive injections were carried out. $T=25\text{ }^{\circ}\text{C}$, Henry's constants are from Table 4-7. $\dot{V}=0.3\text{ ml/min}$, $V_{inj}=400\text{ }\mu\text{L}$.

6.5 Summary of performance evaluation

The performances in terms of the cycle time and the related productivity of all considered gradient operations of temperature and solvent for different models are summarised in **Table 6-1**.

As expected, the cycle times in EDM are longer than those in EM for the conditions investigated due to the dispersion effect, as described in Figure 2-13. The difference between them was ca. 0.8 min. The difference is not so big due to high column efficiency. The cycle times in experiments were found to be longer than those predicted by the EDM. The difference between them was ca. 1.5 min. On one hand, non-ideal tailing behaviour occurs in actual experiments. On the other hand, their threshold units are different, which may cause deviation. As comparison between EDM and experimental results, the EDM could predict the total production time very well. Furthermore, EM is also capable for providing a fast prediction.

In terms of total production time, the solvent gradients are shorter than temperature gradients. The total production time of isothermal operation in experiment was 12.7 min. It can be reduced to 11.1 min (ca. 12.6% decrease) under the temperature gradient by improved regime whereas reduced to 9.4 min (ca. 26.0% decrease) under the 2-step solvent gradient. The productivities of C6 in these cases were increased 14.5% and 35%, respectively. The 2-step solvent gradient has a shorter cycle time than 3-step due to the fact that the highest elution strength is imposed from the second eluting component.

In general, solvent gradients have shorter cycle time but accompanies with unavoidable extra times for regeneration. On the contrary, the temperature gradients can moderately reduce the cycle time and the extra time can be eliminated. It is proved the features that solvent gradients are stronger but a re-equilibration is required whereas the temperature gradients are weaker but more flexible. Hence, proper combination of both gradients could have a synergistic effect. However, it should be ensured that there is no remixing for the target component. More evaluation of gradients based on physical planes are discussed in the next chapter.

In this study, all components were considered as the targets and complete separation was aimed. In other cases, the constraint of remixing except for the target component

can be allowed, e.g. centre-cut separations, in order to increase the productivity of the target component further.

Table 6-1 Performance of temperature and solvent gradients.

Gradient	Regime	Profile*	Δt_{cyc}	Δt_{extra}	Δt_{tot}	$Pr_{n=C_6}$
			min Eq. (2-66)	min Eq. (2-67)	min Eq. (2-72)	g.hr ⁻¹ L ⁻¹ Eq. (2-71)
None (Reference)	Isothermal	EM	11.4	0.0	11.4	0.600
		EDM	12.2	0.0	12.2	0.561
	/Isocratic	EXP	12.7	0.0	12.7	0.539
Temperature	Conservative	EM	9.1	5.2	14.3	0.479
		EDM	9.9	6.0	15.9	0.431
		EXP	11.4	4.1	15.5	0.442
	Improved	EM	9.7	0.0	9.7	0.706
		EDM	10.5	0.0	10.5	0.652
		EXP	11.1	0.0	11.1	0.617
Solvent	2-step	EM	3.9	3.6	7.5	0.913
		EDM	4.6	4.3	8.9	0.769
		EXP	6.2	3.2	9.4	0.728
	3-step	EM	4.8	3.6	8.4	0.815
		EDM	5.6	4.4	10.0	0.685
		EXP	6.9	3.2	10.1	0.678

*EM: equilibrium model; EM: equilibrium dispersion model; EXP: experimental profile.

Chapter 7. Further improvements and productivity comparison

In this chapter, further possible improvements of gradients in chromatographic processes are explored based on evaluating the trajectories in the physical plane. The potential of combined gradients of temperature and solvent is illustrated. Then the performances of all gradient designs considered in this thesis are compared in terms of productivity. Their advantages and disadvantages are addressed.

7.1 Improved gradients based on simulation

(a) Temperature gradients

As mentioned in improved regime (section 5.3.1), the cycle time can be reduced within heating zones while the cooling zones aim at maintaining separation quality. According to this strategy, this regime can be further optimised, i.e. extended heating periods in the first segment with adjusted cooling periods in the second segment, as shown in **Figure 7-1**. The entire physical plane is initially set to a temperature corresponding to the heating zone including the first segment. The cooling zones are established between the first two eluting components to the maximal extent, i.e. from $t_{R,1}^f$ to $t_{R,2}^f$. They should be deployed where potential remixing happens, which can be multiple periods depending on separation problems. By this regime, all components can be accelerate via heating zones for the most time. Thus, the cycle time can be reduced without remixing. The resulting reduced cycle time for the described scenario is 8.9 min, which is shorter than the above described improved regime (9.7 min).

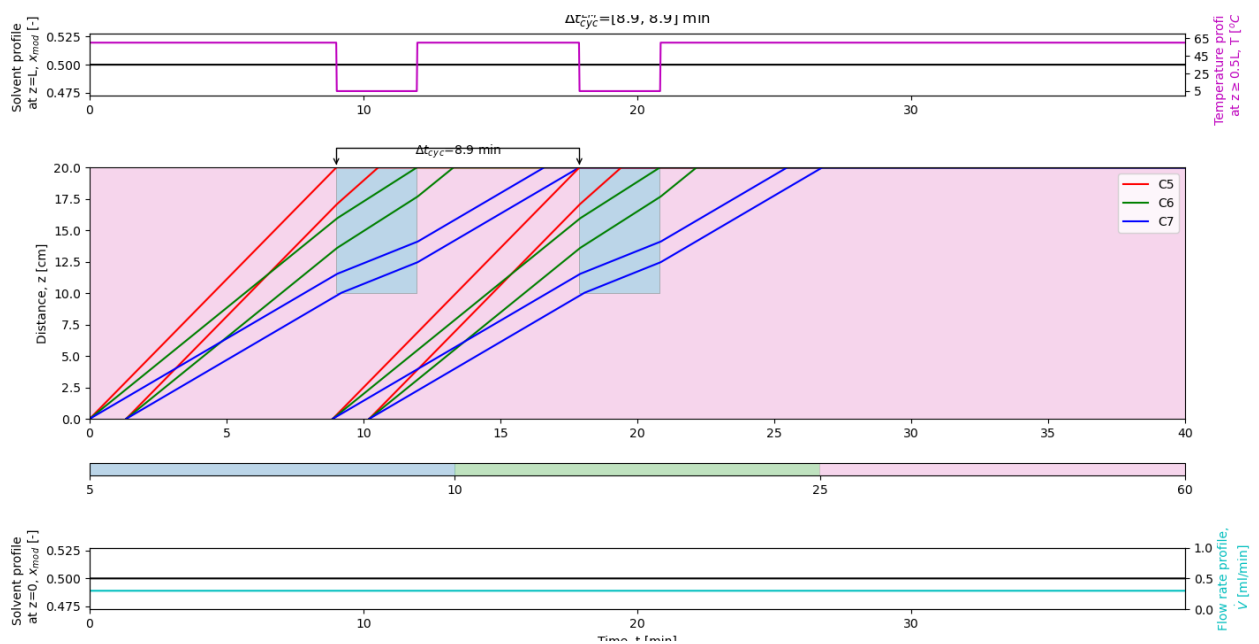


Figure 7-1 Optimal regime of temperature gradients. $T=[5, 60]$ °C, $x_{mod}=0.5$, $t_i^*=[0, 9, 12, 17.9, 20.8]$ min, $\Delta t_b=[1.4, 3.3, 0, 1.4, 3.3]$ min, $\Delta t_{cyc}=8.9$ min.

The described regime has the drawback that the cooling zone slows down the last eluting component, where cooling is not desirable. Therefore, the cooling zone can be spatially contracted by altering the segmentation ratio, as shown in **Figure 7-2**. By adjusting it to $f_z = 0.8$, the last eluting component travels in the course of heating only. Consequently, the cycle time can be further reduced to 8 min, which is considered as the best temperature gradient regime for the presented case study.

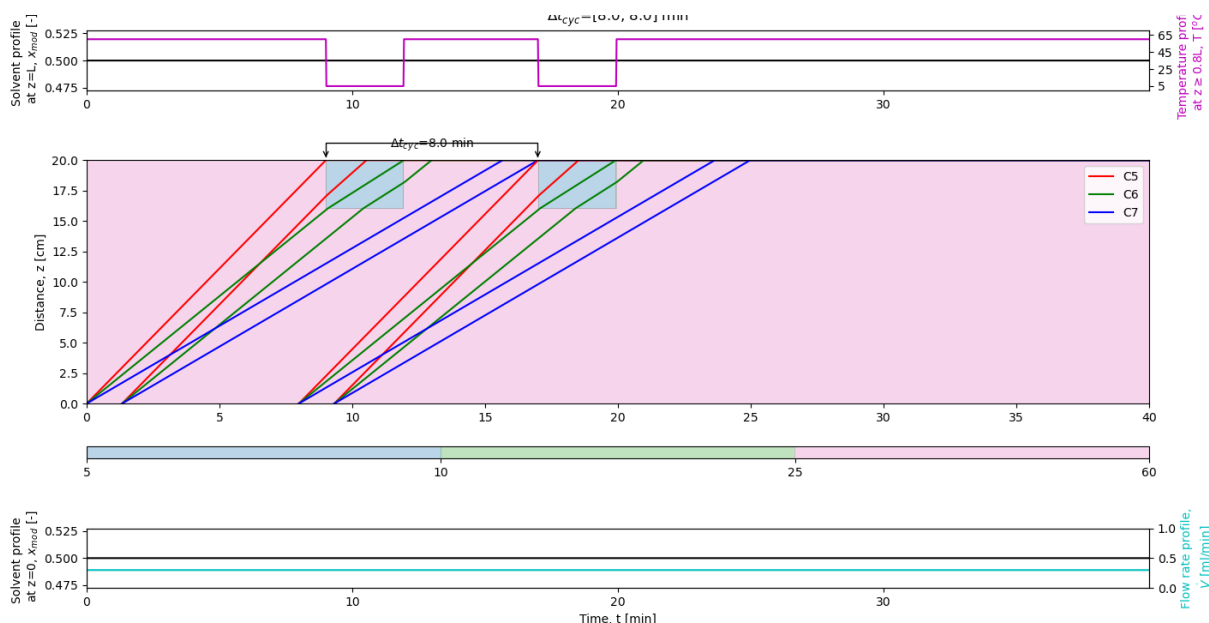


Figure 7-2 Optimal regime of temperature gradients with modified spatial segmentation. $f_z = 0.8$, $T = [5, 60]$ °C, $x_{mod} = 0.5$, $t_i^* = [0, 9, 11.9, 17, 19.9]$ min, $\Delta t_b = [1.4, 2.7, 0, 1.4, 2.7]$ min, $\Delta t_{cyc} = 8$ min.

(b) Solvent gradients

Modifying the cooling zones can improve the separation quality. The same effect can be expected for solvent gradients with reduced elution strength. With respect to this, a regime using negative solvent gradients (instead of the cooling zone in temperature gradients) is designed, as shown in **Figure 7-3**. The entire physical plane is initially set at the heating zone temperature ($T = T_H$) and a zone for negative solvent gradients is set from $t_{R,1}^f$ to $t_{R,1}^r$. In this regime, instantaneous fine tunings are not possible since all segments are influenced with a delay time by the negative solvent gradients. The resulting cycle time is 8.9 min, which is the same as the described optimal regime of temperature gradients. However, this solvent gradient regime has a higher risk for remixing the first two eluting components.

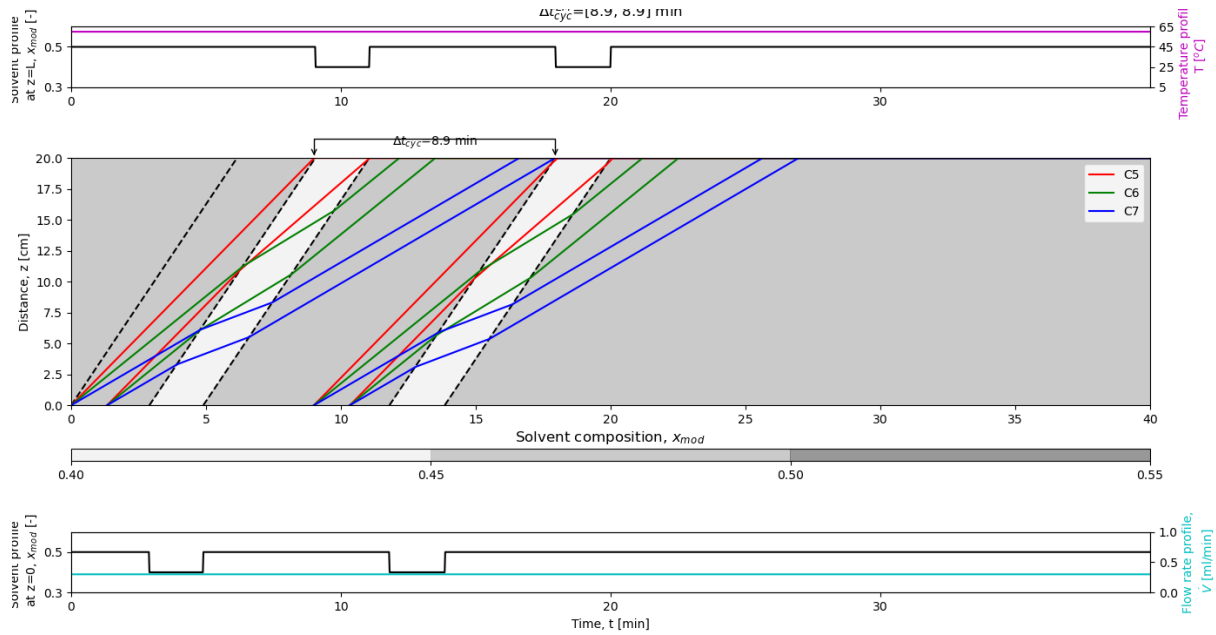


Figure 7-3 Modified negative solvent gradients at high temperature. $T=60\text{ }^{\circ}\text{C}$, $x_{mod}=[0.4, 0.5]$, $t_i^*=[10, 12.8, 17.3, 19.1, 21.8, 26.3]$ min, $\Delta t_b=[1.1, 3.1, 0, 1.1, 3.1]$ min, $\Delta t_{cyc}=8.9$ min.

(c) Combination of gradient options

As aforementioned, a proper combination of temperature and solvent gradients can generate a synergistic effect. A corresponding regime based on **Figure 7-1** and complemented by a positive solvent gradient is designed, as shown in **Figure 7-4**. In this regime, the positive solvent gradient counteracts the undesired cooling of the last eluting component instead of the possible adjustment of the segmentation ratio. The start time of the solvent gradient is connected to the end time of cooling. However, the duration of this solvent gradient should not be too long in order not to interfere with the next injection. The duration is limited to the extent where touching concentration profiles at outlet can be ensured between cycles. Although the solvent gradient is only shortly deployed, it can significantly reduce the cycle time. The finally predicted cycle time is 6.8 min, which is the shortest cycle time among all gradient designs quantified in this work.

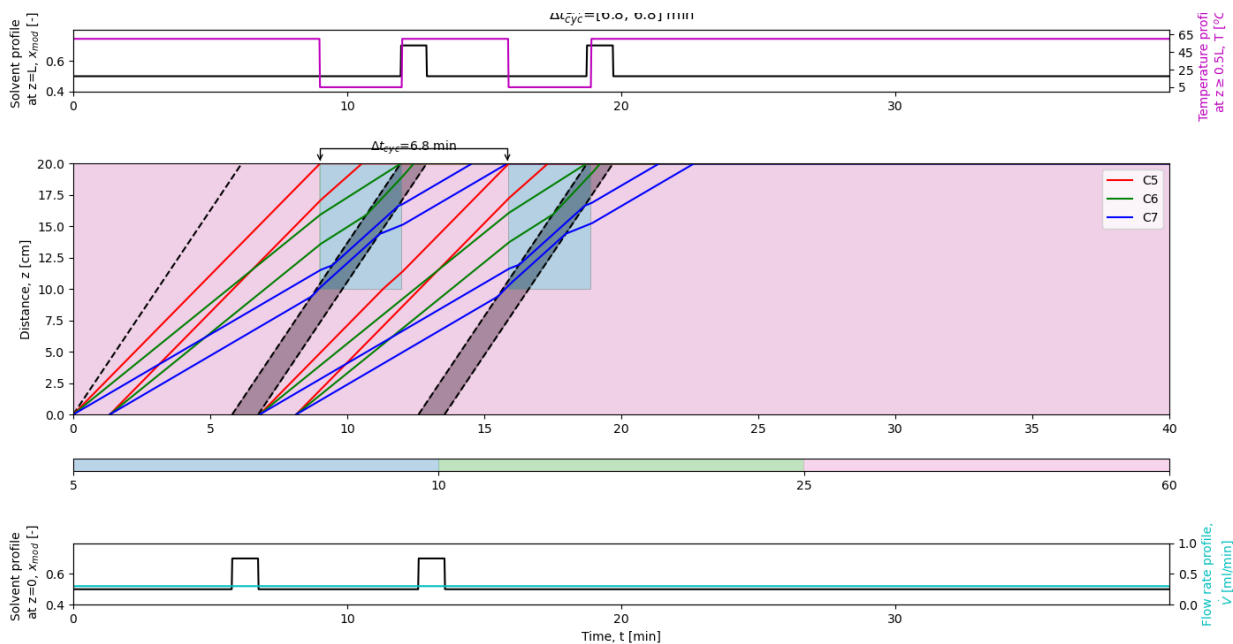


Figure 7-4 Combined temperature and solvent gradients. $T=[5, 60]$ °C, $x_{mod}=[0.5, 0.7]$, $t_i^*(T)=[0, 9, 12, 15.9, 18.9]$ min, $t_i^*(x_{mod})=[0, 5.8, 6.8, 12.6, 13.6]$ min, $\Delta t_b=[1.4, 2.1, 0, 1.4, 2.1]$ min, $\Delta t_{cyc}=6.8$ min.

It was found that, due to the larger number of degrees of freedom, the combined temperature and solvent gradients has the best performance. All gradients designs investigated in this work are compared in the following section.

7.2 Overall performance comparison

The performances of all studied gradient types based on results of the EM are summarised in **Table 7-1**. The productivity for producing C6, $Pr_{n=C_6}$, is calculated by Eq. (2-71) in terms of the regime specific cycle time Δt_{cyc} and extra time Δt_{extra} . An indexed normalised value $Pr_{n=C_6}^*$ according to Eq. (2-75) is also provided to account for the input of additional energy (temperature gradients) and material (solvent gradients), where equal weights of both gradient changes can be assumed, i.e. $w_1 = w_2 = 1$ for equal weights. To evaluate real processes, these weights can be different, depending on the specific case study.

Another important performance indicator to account for separation quality is the band break between easily remixed components, i.e. $\Delta t_b^{(1,2)}$ shown in Eq. (2-67) and Figure 2-13. From experimental observations for run 8 (solvent gradients), remixing happens between the first two eluting components if $\Delta t_b^{(1,2)} < 1.1$ min. For a center-cut separation, gradient designs, which cannot satisfy this constraint, are not applicable even when the productivities are improved.

In this study, $T=25$ °C and $x_{mod}=0.5$ at $\dot{V}=0.3$ ml/min was chosen as the reference condition. This reference condition might be different for other problems. The productivity in reference condition was determined to be 0.6 g.hr⁻¹L⁻¹ and the corresponding normalised productivity is 0. The highest productivity of 1.007 g.hr⁻¹L⁻¹ was achieved by the combined solvent and temperature gradient in run 10 (combined gradients) with an acceptable band break, which confirms their synergistic effect. Its productivity was increased ca. 67.8% compared to the reference condition. The highest normalised productivity of 1.38 g.hr⁻¹L⁻¹ and the second highest productivity of 0.856 g.hr⁻¹L⁻¹ was achieved by the optimal temperature regime with adjusted segmentation in run 6 (temperature gradients), where the productivity is increased ca. 42.7% by the least investment compared to the reference condition. The other runs with a high productivity are not applicable due to the constraint of band break, like run 2 and run 7.

It can be concluded in general that gradients should be designed by considering their key features that temperature gradients are weaker but instantaneous whereas solvent gradients are strong but delayed. Proper combinations can be powerful and versatile for various problems. It can be even combined with other gradients, like pH, stationary phase, flow rate, etc. In case of the flow rate gradient, its combination with solvent gradient could be very complicated since solvent migration and injection period are dependent of the flow rate. However, it can also be designed based on the physical plane using the developed tools.

Table 7-1 Summary of predicted performance of all gradients in EM (parts already in Table 6-1).

#	Gradient	Regime	x_{mod}	T °C	f_z	Δt_{cyc} min Eq. (2-66)	Δt_{extra} min Eq. (2-67)	Δt_{tot} min Eq. (2-72)	$Pr_{n=C6}$ g.h ⁻¹ L ⁻¹ Eq. (2-71)	$\Delta t_b^{(1,2)}$ min Eq. (2-68)	$\Delta Pr_{n=C6}^*$ g.h ⁻¹ L ⁻¹ Eq. (2-75)	Figure
1	Isothermal, Isocratic	$T=T_R,$ $x_{mod}=x_{mod,R}$	0.5	25	0.5	11.4	0.0	11.4	0.600	2.0	0.00	Figure 5-1
2	Isothermal, Isocratic	$T=T_H,$ $x_{mod}=x_{mod,R}$	0.5	60	0.5	8.0	0.0	8	0.856	1.0	2.17	Figure 5-2
3	Temperature	Conservative	0.5	5, 25, 60	0.5	9.1	5.2	14.3	0.479	1.8	-0.66	Figure 5-4
4	Temperature	Improved	0.5	5, 25, 60	0.5	9.7	0.0	9.7	0.706	1.6	0.57	Figure 5-6
5	Temperature	Optimal	0.5	5, 60	0.5	8.9	0.0	8.9	0.769	1.4	0.91	Figure 7-1
6	Temperature	Optimal with adjusted segmentation	0.5	5, 60	0.8	8.0	0.0	8	0.856	1.4	1.38	Figure 7-2
7	Solvent	2 step	0.5, 0.7	25	0.5	3.9	3.6	7.5	0.913	0.6	0.78	Figure 5-11
8	Solvent	3 step	0.5, 0.6, 0.7	25	0.5	4.8	3.6	8.4	0.815	1.1	0.54	Figure 5-12
9	Solvent	Negative step at $T=T_H$	0.4 , 0.5	60	0.5	8.9	0.0	8.9	0.769	1.1	0.53	Figure 7-3
10	Solvent + temperature	Combined	0.5, 0.7	5, 60	0.5	6.8	0.0	6.8	1.007	1.4	0.69	Figure 7-4

Chapter 8. Conclusion and outlook

Chromatography has become a popular separation technology through decades and applied in extensive applications. However, in many cases, classical isothermal or isocratic chromatographic operations are not adequate to achieve desired performance characterised by a compromise between productivity, purity and yield. It is well known that gradients can provide additional degrees of freedom for chromatographic processes. Hence, gradient techniques are attractive options to meet the requirements in a rather simple way. As conventional techniques, temperature and solvent gradients are widely used in gas and liquid chromatography, respectively. In this study, the application on temperature gradients in liquid chromatography was investigated followed by comparisons with traditional solvent gradients and those gradient combinations. All gradient conditions were designed to minimise the cycle time and, thus, to maximise the productivity for a specific model problem of a partly lagged ternary separation.

In this study, trajectories of chromatograms in the physical plane were introduced to illustrate the individual migration path of component under influence of gradients. Gradients can be rapidly designed by generating these physical planes assuming ideal equilibrium conditions just with thermodynamic data as input. This study assumed furthermore that the isotherms are linear and characterised by component specific Henry's constants. In the specific case study considered, temperature effects appeared to be more sensitive within the lower range of modifier fraction, which provides a potential for reducing solvent consumption. However, there might be a trade-off with energy input needed to realise the temperature gradients.

For linear isotherms and instantaneously implementable step gradients, the migration paths are straight lines. From physical planes, intersections between migration paths with the column boundary for isocratic/isothermal or gradient conditions can be identified. This provides key information of characteristic times required for designing repetitive batch chromatography, including the switch times, the start times for next injection and the retention times. Once the retention times are known, ideal repetitive (periodic) performance in terms of the cycle time or productivity can be determined. The results showed that the performance highly depends on how the gradients are designed, i.e. in particular, how the switch times are specified. In case of single gradients, the

switch times and the start times for next injection can be easily described by analytical expressions. In practice, these ideal times should be corrected by adding safety margins. For more complicated gradients, migration paths, switch times and cycle times can be numerically determined. Moreover, a segmentation factor or horizontal gradient line plays an important role in fine-tuning of the performance to avoid any unnecessary temperature modulation.

More realistic prediction can be made by generating chromatograms using the equilibrium dispersion model, which implies additional kinetic data as an input. All kinetic effects can be lumped into a single apparent dispersion coefficient or a corresponding theoretical plate number. This plate number can be determined classically from measured elution profiles assuming ideal Gaussian distributions. These plate numbers appeared to be linearly correlated with modifier fraction whereas no clear trend with temperature. For simplicity, average plate numbers over all ranges of components, modifier fractions and temperatures were used. Chromatograms simulated in this way were closer to actual elution profiles. Nevertheless, this kind of approach is still rather rough. To analyse the kinetics more precisely, more detailed methods should be used.

To get closer to the reality, nonidealities of step gradients were addressed. Non-ideal temperature profiles can be approximated by evaluating the first moments of measured temperature responses, which are correlated to a parameter X_2 in the short-cut energy balance introduced in this work. The other parameter X_1 , which is connected with X_2 , was validated using the physical data for the model system investigated. These two parameters are related to the heat capacity ratio of the chromatographic system and the space velocity. Their values can provide first insight into the range of heat transfer. Nonidealities of step solvent gradients can be approximated by steep linear gradients using a measurable gradient deviation time. Both suggested modifications can provide rapid estimations of nonideality of temperature and solvent step gradients.

Temperature gradients are especially beneficial for temperature sensitive chromatographic systems. They have potential to improve and solve separation problems in a non-contact manner. However, sufficient heat transfer rates can be the main challenging issue in a practical point of view. To overcome limitations of heat transfer rates, usually thermally conductive adsorbents can be used, e.g., carbon-based instead of silica-based adsorbents. To improve heat transfer area or surface to volume

ratio, the columns with large length to diameter ratios should be used. For example, bundled slim columns in a water jacket (similar to hollow fibre membrane modules) can be designed for applications in larger scale processes.

Temperature gradients trigger typically slower responses compared to solvent gradients. The latter modulate elution strength strongly but with unavoidable re-equilibration and delay times. Although only one specific case study was investigated, this work has shown that temperature gradients can be attractive. However, the simple model approach taken needs to be further refined to be more precise.

Combined temperature and solvents gradients can offer synergistic effects. For combined gradients, solvent gradients should be utilised at proper timings to reduce the cycle time, whereas temperature gradients should be imposed for fine-tuning of resolutions, where necessary. Proper combinations could be promising for maximising productivity. However, the design is complex and requires tackling a trade-off between productivity improvement and investments of energy and material.

Temperature and solvent gradients were studied in this thesis both theoretically and experimentally for a specific separation problem. Some of the trends may be generalised to other problems. The developed tool using the trajectories of chromatograms in the physical plane was powerful and versatile to generate rapidly gradient designs and performance predictions. To construct the physical planes, only thermodynamic parameters are needed as input. The general approach can be extended to other gradient types or combinations, e.g. pH, flow rate, stationary phase gradients.

References

- [1] J.L. Humphrey, G.E. Keller II, *Separation Process Technology: Performance, Selection, Scaleup*, McGraw Hill. (1997).
- [2] C.F. Poole, *The Essence of Chromatography*, Elsevier B.V., 2003. <https://doi.org/10.1016/B978-0-444-50198-1.X5013-7>.
- [3] S. Fanali, B. Chankvetadze, P.R. Haddad, C.F. Poole, M.-L. Riekkola, *Liquid Chromatography: Fundamentals and Instrumentation*, Elsevier, 2023.
- [4] P. Atkins, J. de Paula, *Physikalische Chemie*, Wiley-VCH, 2005.
- [5] D.M. Ruthven, *Principles of Adsorption and Adsorption Processes*, John Wiley & Sons, 1984.
- [6] K. Sakodynskii, The life and scientific workds of Michael Tswett, *J. Chromatogr. A.* 73 (1972) 303–360. [https://doi.org/10.1016/S0021-9673\(01\)91213-0](https://doi.org/10.1016/S0021-9673(01)91213-0).
- [7] G. Guiochon, S. Ghodbane, S. Golshan-Shirazi, J.X. Huang, A. Katti, B.C. Lin, Z. Ma, Nonlinear chromatography Recent theoretical and experimental results, *Talanta.* 36 (1989) 19–33. [https://doi.org/10.1016/0039-9140\(89\)80079-7](https://doi.org/10.1016/0039-9140(89)80079-7).
- [8] T. Fornstedt, P. Forssén, D. Westerlund, Basic HPLC Theory and Definitions: Retention, Thermodynamics, Selectivity, Zone Spreading, Kinetics, and Resolution, *Anal. Sep. Sci.* (2015) 1–24. <https://doi.org/10.1002/9783527678129.ASSEP001>.
- [9] L.S. Ettre, Nomenclature for chromatography, *Pure Appl. Chem.* 65 (1993) 819–872. <https://doi.org/10.1351/PAC199365040819>.
- [10] A.J.P. Martin, Summarizing paper, *Discuss. Faraday Soc.* 7 (1949) 332–336. <https://doi.org/10.1039/DF9490700332>.
- [11] P.C. Wankat, The relationship between one-dimensional and two-dimensional separation processes, *AIChE J.* 23 (1977) 859–867. <https://doi.org/10.1002/AIC.690230612>.
- [12] A. Thiele, T. Falk, L. Tobiska, A. Seidel-Morgenstern, Prediction of elution profiles in annular chromatography, *Comput. Chem. Eng.* 25 (2001) 1089–1101. [https://doi.org/10.1016/S0098-1354\(01\)00684-6](https://doi.org/10.1016/S0098-1354(01)00684-6).
- [13] C.G.G. Donald, B Broughton, Continuous sorption process employing fixed bed of sorbent and moving inlets and outlets, US Patent 2 985 589, 1961.
- [14] A. Rajendran, G. Paredes, M. Mazzotti, Simulated moving bed chromatography for the separation of enantiomers, *J. Chromatogr. A.* 1216 (2009) 709–738. <https://doi.org/10.1016/j.chroma.2008.10.075>.
- [15] D.B. Broughton, Production-Scale Adsorptive Separations of Liquid Mixtures by

Simulated Moving-Bed Technology,
<https://doi.org/10.1080/01496398408068590>. 19 (2006) 723–736.
<https://doi.org/10.1080/01496398408068590>.

- [16] A. Seidel-Morgenstern, L.C. Keßler, M. Kaspereit, New developments in simulated moving bed chromatography, *Chem. Eng. Technol.* 31 (2008) 826–837. <https://doi.org/10.1002/ceat.200800081>.
- [17] D. Antos, A. Seidel-Morgenstern, Two-step solvent gradients in simulated moving bed chromatography: Numerical study for linear equilibria, *J. Chromatogr. A.* 944 (2002) 77–91. [https://doi.org/10.1016/S0021-9673\(01\)01365-6](https://doi.org/10.1016/S0021-9673(01)01365-6).
- [18] M. Juza, M. Mazzotti, M. Morbidelli, Simulated moving-bed chromatography and its application to chirotechnology, *Trends Biotechnol.* 18 (2000) 108–118. [https://doi.org/10.1016/S0167-7799\(99\)01419-5](https://doi.org/10.1016/S0167-7799(99)01419-5).
- [19] S. Jermann, S. Katsuo, M. Mazzotti, Intermittent simulated moving bed processes for chromatographic three-fraction separation, *Org. Process Res. Dev.* 16 (2012) 311–322. <https://doi.org/10.1021/op200239e>.
- [20] S. Jermann, M. Meijssen, M. Mazzotti, Three column intermittent simulated moving bed chromatography: 3. Cascade operation for center-cut separations, *J. Chromatogr. A.* 1378 (2015) 37–49. <https://doi.org/10.1016/j.chroma.2014.12.011>.
- [21] J. Nowak, D. Antos, A. Seidel-Morgenstern, Theoretical study of using simulated moving bed chromatography to separate intermediately eluting target compounds, *J. Chromatogr. A.* 1253 (2012) 58–70. <https://doi.org/10.1016/j.chroma.2012.06.096>.
- [22] D. Kiwala, J. Mendrella, D. Antos, A. Seidel-Morgenstern, Center-cut separation of intermediately adsorbing target component by 8-zone simulated moving bed chromatography with internal recycle, *J. Chromatogr. A.* 1453 (2016) 19–33. <https://doi.org/10.1016/j.chroma.2016.04.083>.
- [23] F.V. Santos da Silva, A. Seidel-Morgenstern, Evaluation of center-cut separations applying simulated moving bed chromatography with 8 zones, *J. Chromatogr. A.* 1456 (2016) 123–136. <https://doi.org/10.1016/j.chroma.2016.05.060>.
- [24] J.W. Lee, Expanding Simulated Moving Bed Chromatography into Ternary Separations in Analogy to Dividing Wall Column Distillation, *Ind. Eng. Chem. Res.* 59 (2020) 9619–9628. <https://doi.org/10.1021/acs.iecr.0c00572>.
- [25] G. Agrawal, Y. Kawajiri, Comparison of various ternary simulated moving bed separation schemes by multi-objective optimization, *J. Chromatogr. A.* 1238 (2012) 105–113. <https://doi.org/10.1016/j.chroma.2012.03.064>.

- [26] T.K. Kim, C. Botti, J. Angelo, X. Xu, S. Ghose, Z.J. Li, M. Morbidelli, M. Sponchioni, Experimental Design of the Multicolumn Countercurrent Solvent Gradient Purification (MCSGP) Unit for the Separation of PEGylated Proteins, *Ind. Eng. Chem. Res.* 60 (2021) 10764–10776. <https://doi.org/10.1021/acs.iecr.1c01345>.
- [27] R. Gorczyca, W. Marek, R. Bochenek, W. Piątkowski, D. Antos, Protein separation in carousel multicolumn setup. Performance analysis and experimental validation, *J. Chromatogr. A.* 1460 (2016) 40–50. <https://doi.org/10.1016/j.chroma.2016.06.080>.
- [28] G. Guiochon, A. Felinger, D.G. Shirazi, A.M. Katti, *Fundamentals of Preparative and Nonlinear Chromatography*, 2nd ed., Academic Press, 2006.
- [29] H. Schmidt-Traub, M. Schulte, A. Seidel-Morgenstern, *Preparative Chromatography: Second Edition*, 2013. <https://doi.org/10.1002/9783527649280>.
- [30] R.M. Nicoud, *Chromatographic processes: Modeling, simulation and design*, Cambridge University Press, 2015. <https://doi.org/10.1017/CBO9781139998284>.
- [31] B. Sreedhar, A. Seidel-Morgenstern, Preparative separation of multi-component mixtures using stationary phase gradients, *J. Chromatogr. A.* 1215 (2008) 133–144. <https://doi.org/10.1016/j.chroma.2008.11.003>.
- [32] L.N. Jeong, S.C. Rutan, Simulation of Elution Profiles in Liquid Chromatography - III. Stationary Phase Gradients, *J. Chromatogr. A.* submitted (2018) 128–136. <https://doi.org/10.1016/j.chroma.2018.06.007>.
- [33] G. Carta, A. Jungbauer, *Protein Chromatography: Process Development and Scale-Up*, Wiley-VCH, 2010. <https://doi.org/10.1002/9783527630158>.
- [34] C.A. Martínez Cristancho, A. Seidel-Morgenstern, Purification of single-chain antibody fragments exploiting pH-gradients in simulated moving bed chromatography, *J. Chromatogr. A.* 1434 (2016) 29–38. <https://doi.org/10.1016/j.chroma.2016.01.001>.
- [35] T.M. Pabst, D. Antos, G. Carta, N. Ramasubramanyan, A.K. Hunter, Protein separations with induced pH gradients using cation-exchange chromatographic columns containing weak acid groups, *J. Chromatogr. A.* 1181 (2008) 83–94. <https://doi.org/10.1016/j.chroma.2007.12.054>.
- [36] T.J. Trinklein, D. V. Gough, C.G. Warren, G.S. Ochoa, R.E. Synovec, Dynamic pressure gradient modulation for comprehensive two-dimensional gas chromatography, *J. Chromatogr. A.* 1609 (2020) 1–9. <https://doi.org/10.1016/j.chroma.2019.460488>.
- [37] P. Jandera, J. Churáček, Gradient elution in column liquid chromatography: theory and practice, *J. Chromatogr. Libr.* 31 (1985) 1–510.

- [38] L. Aumann, M. Morbidelli, A Continuous Multicolumn Countercurrent Solvent Gradient Purification (MCSGP) Process, *Biotechnol. Bioeng.* 98 (2007) 1043–1055. <https://doi.org/10.1002/bit>.
- [39] A. Damtew, B. Sreedhar, A. Seidel-Morgenstern, Evaluation of the potential of nonlinear gradients for separating a ternary mixture, *J. Chromatogr. A.* 1216 (2009) 5355–5364. <https://doi.org/10.1016/j.chroma.2009.05.026>.
- [40] G. Carta, W.B. Stringfield, Analytic solution for volume-overloaded gradient elution chromatography, *J. Chromatogr. A.* 605 (1992) 151–159. [https://doi.org/10.1016/0021-9673\(92\)85232-l](https://doi.org/10.1016/0021-9673(92)85232-l).
- [41] J. Vanova, D. Malinak, R. Andrys, M. Kubat, T. Mikysek, E. Rousarova, K. Musilek, T. Rousar, P. Cesla, Optimization of Gradient Reversed Phase High Performance Liquid Chromatography Analysis of Acetaminophen Oxidation Metabolites using Linear and Non-linear Retention Model, *J. Chromatogr. A.* 1669 (2022) 462956. <https://doi.org/10.1016/j.chroma.2022.462956>.
- [42] R.S. Alm, R.J.P. Williams, A. Tiselius, Gradient elution analysis, *Acta Chem. Scand.* 6 (1952) 826–836. <https://doi.org/10.1039/AN9527700905>.
- [43] D.C. Fenimore, Gradient temperature programming of short capillary columns, *J. Chromatogr. A.* 112 (1975) 219–227. [https://doi.org/10.1016/S0021-9673\(00\)99955-2](https://doi.org/10.1016/S0021-9673(00)99955-2).
- [44] A. Peng, R. Li, J. Hu, L. Chen, X. Zhao, H. Luo, H. Ye, Y. Yuan, Y. Wei, Flow rate gradient high-speed counter-current chromatography separation of five diterpenoids from *Triperygium wilfordii* and scale-up, *J. Chromatogr. A.* 1200 (2008) 129–135. <https://doi.org/10.1016/J.CHROMA.2008.05.041>.
- [45] S. Horváth, F. Gritti, K. Horváth, Theoretical study of the efficiency of liquid chromatography columns with particle size gradient, *J. Chromatogr. A.* 1651 (2021) 462331. <https://doi.org/10.1016/j.chroma.2021.462331>.
- [46] A.P. Schellinger, P.W. Carr, Isocratic and gradient elution chromatography: A comparison in terms of speed, retention reproducibility and quantitation, *J. Chromatogr. A.* 1109 (2006) 253–266. <https://doi.org/10.1016/j.chroma.2006.01.047>.
- [47] L.R. SNYDER, J.W. DOLAN, *High-performance gradient elution*, Wiley & Sons, Inc., 2007.
- [48] S. Fekete, A. Murisier, J.M. Nguyen, M.A. Lauber, D. Guillarme, Negative gradient slope methods to improve the separation of closely eluting proteins, *J. Chromatogr. A.* 1635 (2021) 461743. <https://doi.org/10.1016/j.chroma.2020.461743>.

- [49] Y. Shan, A. Seidel-Morgenstern, Optimization of gradient elution conditions in multicomponent preparative liquid chromatography, *J. Chromatogr. A.* 1093 (2005) 47–58. <https://doi.org/10.1016/j.chroma.2005.07.047>.
- [50] A.D. Hamza, Analysis of the potential of nonlinear solvent gradients in preparative chromatography, 2010.
- [51] T. Greibrokk, T. Andersen, High-temperature liquid chromatography, *J. Chromatogr. A.* 1000 (2003) 743–755. [https://doi.org/10.1016/S0021-9673\(02\)01963-5](https://doi.org/10.1016/S0021-9673(02)01963-5).
- [52] G. Vanhoenacker, P. Sandra, High temperature and temperature programmed HPLC: Possibilities and limitations, *Anal. Bioanal. Chem.* 390 (2008) 245–248. <https://doi.org/10.1007/s00216-007-1671-7>.
- [53] B.W. Wenclawiak, S. Giegold, T. Teutenberg, High-temperature liquid chromatography, *Anal. Lett.* 41 (2008) 1097–1105. <https://doi.org/10.1080/00032710802053955>.
- [54] T. Teutenberg, High temperature liquid chromatography – a brief review about an emerging technique, *Chromatogr. Today.* (2010) 3–6.
- [55] T. Greibrokk, Heating or cooling: Ignoring temperature in LC columns, *Anal. Chem.* 74 (2002) 374A-378A.
- [56] K. Nagase, T. Okano, Thermoresponsive-polymer-based materials for temperature-modulated bioanalysis and bioseparations, *J. Mater. Chem. B.* 4 (2016) 6381–6397. <https://doi.org/10.1039/c6tb01003b>.
- [57] K. Wicht, M. Baert, N. von Doehren, G. Desmet, A. de Villiers, F. Lynen, Speeding up temperature-responsive \times reversed-phase comprehensive liquid chromatography through the combined exploitation of temperature and flow rate gradients, *J. Chromatogr. A.* 1685 (2022) 463584. <https://doi.org/10.1016/j.chroma.2022.463584>.
- [58] K. Nagase, H. Kanazawa, Temperature-responsive chromatography for bioseparations: A review, *Anal. Chim. Acta.* 1138 (2020) 191–212. <https://doi.org/10.1016/j.aca.2020.07.075>.
- [59] K. Nagase, K. Matsumoto, H. Kanazawa, Temperature-responsive mixed-mode column for the modulation of multiple interactions, *Sci. Rep.* 12 (2022) 1–13. <https://doi.org/10.1038/s41598-022-08475-8>.
- [60] K. Nagase, H. Takagi, H. Nakada, H. Ishikawa, Y. Nagata, T. Aomori, H. Kanazawa, Chromatography columns packed with thermoresponsive-cationic-polymer-modified beads for therapeutic drug monitoring, *Sci. Rep.* 12 (2022) 1–15. <https://doi.org/10.1038/s41598-022-16928-3>.

- [61] M. Baert, K. Wicht, Z. Hou, R. Szucs, F. Du Prez, F. Lynen, Exploration of the Selectivity and Retention Behavior of Alternative Polyacrylamides in Temperature Responsive Liquid Chromatography, *Anal. Chem.* 92 (2020) 9815–9822. <https://doi.org/10.1021/acs.analchem.0c01321>.
- [62] S. Qamar, N. Kiran, T. Anwar, S. Bibi, A. Seidel-Morgenstern, Theoretical Investigation of Thermal Effects in an Adiabatic Chromatographic Column Using a Lumped Kinetic Model Incorporating Heat Transfer Resistances, *Ind. Eng. Chem. Res.* 57 (2018) 2287–2297. <https://doi.org/10.1021/acs.iecr.7b04555>.
- [63] J.W. Lee, P.C. Wankat, Thermal simulated moving bed concentrator, *Chem. Eng. J.* 166 (2011) 511–522. <https://doi.org/10.1016/j.cej.2010.11.009>.
- [64] C. Migliorini, M. Wendlinger, M. Mazzotti, M. Morbidelli, Temperature gradient operation of a simulated moving bed unit, *Ind. Eng. Chem. Res.* 40 (2001) 2606–2617. <https://doi.org/10.1021/ie000825h>.
- [65] X. Jiang, L. Zhu, B. Yu, Q. Su, J. Xu, W. Yu, Analyses of simulated moving bed with internal temperature gradients for binary separation of ketoprofen enantiomers using multi-objective optimization: Linear equilibria, *J. Chromatogr. A.* 1531 (2018) 131–142. <https://doi.org/10.1016/j.chroma.2017.11.045>.
- [66] S. Qamar, F.A. Sattar, I. Batool, A. Seidel-Morgenstern, Theoretical analysis of the influence of forced and inherent temperature fluctuations in an adiabatic chromatographic column, *Chem. Eng. Sci.* 161 (2017) 249–264. <https://doi.org/10.1016/j.ces.2016.12.027>.
- [67] A. Brandt, G. Mann, W. Arlt, Temperature gradients in preparative high-performance liquid chromatography columns, *J. Chromatogr. A.* 769 (1997) 109–117. [https://doi.org/10.1016/S0021-9673\(97\)00235-5](https://doi.org/10.1016/S0021-9673(97)00235-5).
- [68] M. Baert, K. Wicht, A. Moussa, G. Desmet, K. Broeckhoven, F. Lynen, Implementations of temperature gradients in temperature-responsive liquid chromatography, *J. Chromatogr. A.* 1654 (2021) 462425. <https://doi.org/10.1016/j.chroma.2021.462425>.
- [69] P. Cao, T.K.H. Müller, B. Ketterer, S. Ewert, E. Theodosiou, O.R.T. Thomas, M. Franzreb, Integrated system for temperature-controlled fast protein liquid chromatography . II . Optimized adsorbents and ‘ single column continuous operation ,’ *J. Chromatogr. A.* 1403 (2015) 118–131. <https://doi.org/10.1016/j.chroma.2015.05.039>.
- [70] R. De Pauw, M. Pursch, G. Desmet, Using the column wall itself as resistive heater for fast temperature gradients in liquid chromatography, *J. Chromatogr. A.* 1420 (2015) 129–134. <https://doi.org/10.1016/j.chroma.2015.10.005>.

- [71] W. Jin, P.C. Wankat, Thermal operation of four-zone simulated moving beds, *Ind. Eng. Chem. Res.* 46 (2007) 7208–7220. <https://doi.org/10.1021/ie070047u>.
- [72] S. Wiese, T. Teutenberg, T.C. Schmidt, A general strategy for performing temperature-programming in high performance liquid chromatography-Prediction of segmented temperature gradients, *J. Chromatogr. A.* 1218 (2011) 6898–6906. <https://doi.org/10.1016/j.chroma.2011.08.022>.
- [73] S. Teramachi, H. Matsumoto, T. Kawai, Direction of temperature gradient for normal-phase temperature gradient interaction chromatography in polystyrene fractionation, *J. Chromatogr. A.* 1100 (2005) 40–44. <https://doi.org/10.1016/j.chroma.2005.09.023>.
- [74] I.L. Skuland, T. Andersen, R. Trones, R.B. Eriksen, T. Greibrokk, Determination of polyethylene glycol in low-density polyethylene by large volume injection temperature gradient packed capillary liquid chromatography, *J. Chromatogr. A.* 1011 (2003) 31–36. [https://doi.org/10.1016/S0021-9673\(03\)01186-5](https://doi.org/10.1016/S0021-9673(03)01186-5).
- [75] J.J. Heiland, C. Lotter, V. Stein, L. Mauritz, D. Belder, Temperature Gradient Elution and Superheated Eluents in Chip-HPLC, *Anal. Chem.* 89 (2017) 3266–3271. <https://doi.org/10.1021/acs.analchem.7b00142>.
- [76] K. Horváth, S. Horváth, D. Lukács, Effect of axial temperature gradient on chromatographic efficiency under adiabatic conditions, *J. Chromatogr. A.* 1483 (2017) 80–85. <https://doi.org/10.1016/j.chroma.2016.12.063>.
- [77] J. Leppert, L.M. Blumberg, M. Wüst, P. Boeker, Simulation of the effects of negative thermal gradients on separation performance of gas chromatography, *J. Chromatogr. A.* 1640 (2021). <https://doi.org/10.1016/j.chroma.2021.461943>.
- [78] J. Leppert, P.J. Müller, M.D. Chopra, L.M. Blumberg, P. Boeker, Simulation of spatial thermal gradient gas chromatography, *J. Chromatogr. A.* 1620 (2020) 460985. <https://doi.org/10.1016/j.chroma.2020.460985>.
- [79] J.A. Contreras, A. Wang, A.L. Rockwood, H.D. Tolley, M.L. Lee, Dynamic thermal gradient gas chromatography, *J. Chromatogr. A.* 1302 (2013) 143–151. <https://doi.org/10.1016/j.chroma.2013.06.008>.
- [80] K. Kaczmarek, M. Chutkowski, Impact of changes in physicochemical parameters of the mobile phase along the column on the retention time in gradient liquid chromatography. Part A – Temperature gradient, *J. Chromatogr. A.* 1655 (2021) 462509. <https://doi.org/10.1016/j.chroma.2021.462509>.
- [81] A. Hayat, X. An, S. Qamar, G. Warnecke, A. Seidel-Morgenstern, Theoretical analysis of forced segmented temperature gradients in liquid chromatography, *Processes.* 7 (2019) 1–19. <https://doi.org/10.3390/pr7110846>.

- [82] H.-K. Rhee, R. Aris, N.R. Amundson, On the Theory of Multicomponent Chromatography, *Philos. Trans. R. Soc. London. Ser. A, Math. Phys. Sci.* 267 (1970) 419–455. <https://doi.org/10.1007/BF01018308>.
- [83] X. An, A. Hayat, J.W. Lee, S. Qamar, G. Warnecke, A. Seidel-Morgenstern, Analysis and experimental demonstration of temperature step gradients in preparative liquid chromatography, *J. Chromatogr. A.* 1665 (2022) 462831. <https://doi.org/10.1016/j.chroma.2022.462831>.
- [84] L.M. Blumberg, Chromatographic parameters: Characteristic parameters of solute retention – an insightful description of column properties, *J. Chromatogr. A.* 1685 (2022) 463594. <https://doi.org/10.1016/j.chroma.2022.463594>.
- [85] L.M. Blumberg, Theory of linear focusing in chromatographic columns with exponential retention . Part 1 : Basic solutions, *J. Chromatogr. A.* 1696 (2023) 463967. <https://doi.org/10.1016/j.chroma.2023.463967>.
- [86] S. Giegold, T. Teutenberg, J. Tuerk, T. Kiffmeyer, B. Wenclawiak, Determination of sulfonamides and trimethoprim using high temperature HPLC with simultaneous temperature and solvent gradient, *J. Sep. Sci.* 31 (2008) 3497–3502. <https://doi.org/10.1002/jssc.200800330>.
- [87] F. Gritti, Combined solvent- and non-uniform temperature-programmed gradient liquid chromatography. I – A theoretical investigation, *J. Chromatogr. A.* 1473 (2016) 38–47. <https://doi.org/10.1016/j.chroma.2016.09.026>.
- [88] A. Ndiripo, A. Albrecht, H. Pasch, Advanced Liquid Chromatography of Polyolefins Using Simultaneous Solvent and Temperature Gradients, *Anal. Chem.* 92 (2020) 7325–7333. <https://doi.org/10.1021/acs.analchem.0c01095>.
- [89] A. Ndiripo, P.Z. Ndlovu, A. Albrecht, H. Pasch, Improving temperature gradient interaction chromatography of polyolefins by simultaneous use of different stationary phases, *J. Chromatogr. A.* 1653 (2021) 462416. <https://doi.org/10.1016/j.chroma.2021.462416>.
- [90] F. Houdiere, P.W.J. Fowler, N.M. Djordjevic, Combination of Column Temperature Gradient and Mobile Phase Flow Gradient in Microcolumn and Capillary Column High-Performance Liquid Chromatography, *Anal. Chem.* 69 (1997) 2589–2593. <https://doi.org/10.1021/ac9612741>.
- [91] M. Mouellef, F.L. Vetter, S. Zobel-Roos, J. Strube, Fast and versatile chromatography process design and operation optimization with the aid of artificial intelligence, *Processes.* 9 (2021). <https://doi.org/10.3390/pr9122121>.
- [92] M. Mouellef, F.L. Vetter, J. Strube, Benefits and Limitations of Artificial Neural Networks in Process Chromatography Design and Operation, *Processes.* 11

- (2023). <https://doi.org/10.3390/pr11041115>.
- [93] B. Huygens, K. Efthymiadis, A. Nowé, G. Desmet, Application of evolutionary algorithms to optimise one- and two-dimensional gradient chromatographic separations, *J. Chromatogr. A.* 1628 (2020) 461435. <https://doi.org/10.1016/j.chroma.2020.461435>.
- [94] F. Gritti, N. Trebel, A. Hölzel, U. Tallarek, Prediction of surface excess adsorption and retention factors in reversed-phase liquid chromatography from molecular dynamics simulations, *J. Chromatogr. A.* 1685 (2022) 463627. <https://doi.org/10.1016/j.chroma.2022.463627>.
- [95] C.H. Giles, D. Smith, A. Huitson, A general treatment and classification of the solute adsorption isotherm. I. Theoretical, *J. Colloid Interface Sci.* 47 (1974) 755–765. [https://doi.org/10.1016/0021-9797\(74\)90252-5](https://doi.org/10.1016/0021-9797(74)90252-5).
- [96] M. Khalfaoui, S. Knani, M.A. Hachicha, A. Ben Lamine, New theoretical expressions for the five adsorption type isotherms classified by BET based on statistical physics treatment, *J. Colloid Interface Sci.* 263 (2003) 350–356. [https://doi.org/10.1016/S0021-9797\(03\)00139-5](https://doi.org/10.1016/S0021-9797(03)00139-5).
- [97] F. Gritti, G. Guiochon, Overload behavior and apparent efficiencies in chromatography, *J. Chromatogr. A.* 1254 (2012) 30–42. <https://doi.org/10.1016/j.chroma.2012.07.015>.
- [98] S. Javeed, S. Qamar, A. Seidel-Morgenstern, G. Warnecke, Parametric study of thermal effects in reactive liquid chromatography, *Chem. Eng. J.* 191 (2012) 426–440. <https://doi.org/10.1016/j.cej.2012.02.040>.
- [99] R. Chromatography, I.I. Preparative, R. Jost, B. Bornschein, M. Kaspereit, Separation of Molar Weight-Distributed Polyethylene Glycols, (2023) 1–16.
- [100] L.R. SNYDER, J.J. KIRKLAND, J.W. DOLAN, Introduction to modern liquid chromatography, John Wiley & Sons, Inc., 2010.
- [101] S. Qamar, N. Rehman, G. Carta, A. Seidel-Morgenstern, Analysis of gradient elution chromatography using the transport model, *Chem. Eng. Sci.* 225 (2020) 115809. <https://doi.org/10.1016/j.ces.2020.115809>.
- [102] H.-K. Rhee, R. Aris, N.R. Amundson, Theory and Application of Hyperbolic Systems of Quasilinear Equations, Prentice-Hall, 1986.
- [103] A. Seidel-Morgenstern, Rapid Estimation of the Breakthrough Behavior of Competing Adsorbing Components, *Chemie-Ingenieur-Technik.* 92 (2020) 323–330. <https://doi.org/10.1002/cite.202000008>.
- [104] A. Rajendran, M. Mazzotti, Local equilibrium theory for the binary chromatography of species subject to a generalized langmuir isotherm. 2. Wave interactions and

- chromatographic cycle, *Ind. Eng. Chem. Res.* 50 (2011) 352–377.
<https://doi.org/10.1021/ie1015798>.
- [105] M. Mazzotti, A. Rajendran, Equilibrium theory - Based analysis of nonlinear waves in separation processes, *Annu. Rev. Chem. Biomol. Eng.* 4 (2013) 119–141.
<https://doi.org/10.1146/annurev-chembioeng-061312-103318>.
- [106] P. V. Danckwerts, Continuous flow systems: Distribution of residence times, *Chem. Eng. Sci.* 2 (1953) 1–13. [https://doi.org/10.1016/0009-2509\(53\)80001-1](https://doi.org/10.1016/0009-2509(53)80001-1).
- [107] P. Rouchon, M. Schonauer, P. Valentin, G. Guiochon, Numerical Simulation of Band Propagation in Nonlinear Chromatography, *Sep. Sci. Technol.* 22 (1987) 1793–1833. <https://doi.org/10.1080/01496398708057614>.
- [108] G. Guiochon, B. Lin, *Modeling for Preparative Chromatography*, Academic Press, 2003.
- [109] K. Meyer, J.K. Huusom, J. Abildskov, High-order approximation of chromatographic models using a nodal discontinuous Galerkin approach, *Comput. Chem. Eng.* 109 (2018) 68–76.
<https://doi.org/10.1016/j.compchemeng.2017.10.023>.
- [110] S. Javeed, S. Qamar, A. Seidel-Morgenstern, G. Warnecke, Efficient and accurate numerical simulation of nonlinear chromatographic processes, *Comput. Chem. Eng.* 35 (2011) 2294–2305.
<https://doi.org/10.1016/j.compchemeng.2010.10.002>.
- [111] S. Javeed, S. Qamar, A. Seidel-Morgenstern, G. Warnecke, A discontinuous Galerkin method to solve chromatographic models, *J. Chromatogr. A.* 1218 (2011) 7137–7146. <https://doi.org/10.1016/j.chroma.2011.08.005>.
- [112] K. Kaczmarek, M. Chutkowski, Note of solving Equilibrium Dispersive model with the Craig scheme for gradient chromatography case, *J. Chromatogr. A.* 1629 (2020) 461504. <https://doi.org/10.1016/J.CHROMA.2020.461504>.
- [113] J.W. Lee, A. Seidel-Morgenstern, Solving hyperbolic conservation laws with active counteraction against numerical errors: Isothermal fixed-bed adsorption, *Chem. Eng. Sci.* 207 (2019) 1309–1330.
<https://doi.org/10.1016/J.CES.2019.07.053>.
- [114] R.J. LeVeque, *Finite Volume Methods*, in: *Finite Vol. Methods Hyperbolic Probl.*, Cambridge University Press, 2002: pp. 64–86.
<https://doi.org/10.1017/CBO9780511791253.005>.
- [115] L. Lapidus, N.R. Amundson, Mathematics of adsorption in beds, *J. Phys. Chem.* 56 (1952) 984–988.
- [116] J.J. van Deemter, F.J. Zuiderweg, A. Klinkenberg, Longitudinal diffusion and

- resistance to mass transfer as causes of nonideality in chromatography, *Chem. Eng. Sci.* 5 (1956) 271–289. [https://doi.org/10.1016/0009-2509\(56\)80003-1](https://doi.org/10.1016/0009-2509(56)80003-1).
- [117] L.C. Craig, Identification of small amounts of organic compounds by distribution studies. II. Separation by counter-current distribution, *J. Biol. Chem.* 155 (1944) 519–534. [https://doi.org/10.1016/S0021-9258\(18\)51183-2](https://doi.org/10.1016/S0021-9258(18)51183-2).
- [118] S. Qamar, S. Bashir, S. Perveen, A. Seidel-Morgenstern, Relations between kinetic parameters of different column models for liquid chromatography applying core-shell particles, *J. Liq. Chromatogr. Relat. Technol.* 42 (2019) 16–30. <https://doi.org/10.1080/10826076.2019.1570522>.
- [119] O. Kaltenbrunner, A. Jungbauer, Simple model for blending aqueous salt buffers: Application to preparative chromatography, *J. Chromatogr. A.* 769 (1997) 37–48. [https://doi.org/10.1016/S0021-9673\(97\)00161-1](https://doi.org/10.1016/S0021-9673(97)00161-1).
- [120] J.W. Lee, K.H. Row, Determination of retention factors of aromatic compounds by gradient-elution reverse-phase high performance liquid chromatography, *Korean J. Chem. Eng.* 19 (2002) 978–985. <https://doi.org/10.1007/BF02707220>.
- [121] Y. Shan, A. Seidel-Morgenstern, Analysis of the isolation of a target component using multicomponent isocratic preparative elution chromatography, *J. Chromatogr. A.* 1041 (2004) 53–62. <https://doi.org/10.1016/J.CHROMA.2004.04.061>.
- [122] B. Sreedhar, A. Wagler, M. Kaspereit, A. Seidel-Morgenstern, Optimal cut-times finding strategies for collecting a target component from overloaded elution chromatograms, *Comput. Chem. Eng.* 49 (2013) 158–169. <https://doi.org/10.1016/j.compchemeng.2012.09.009>.
- [123] P. Suvarov, Robust control methods for Simulated Moving Bed chromatographic separation processes, 2016.
- [124] J. Siitonen, T. Sainio, Steady state recycling chromatography with solvent removal—Effect of solvent removal constraints on process operation under ideal conditions, *J. Chromatogr. A.* 1341 (2014) 15–30. <https://doi.org/10.1016/J.CHROMA.2014.03.039>.
- [125] I. Poplewska, W. Piątkowski, D. Antos, Effect of temperature on competitive adsorption of the solute and the organic solvent in reversed-phase liquid chromatography, *J. Chromatogr. A.* 1103 (2006) 284–295. <https://doi.org/10.1016/j.chroma.2005.11.038>.
- [126] J. Siitonen, T. Sainio, A. Rajendran, Design of batch chromatography for separation of binary mixtures under reduced purity requirements, *J. Chromatogr. A.* 1286 (2013) 55–68. <https://doi.org/10.1016/J.CHROMA.2013.02.051>.

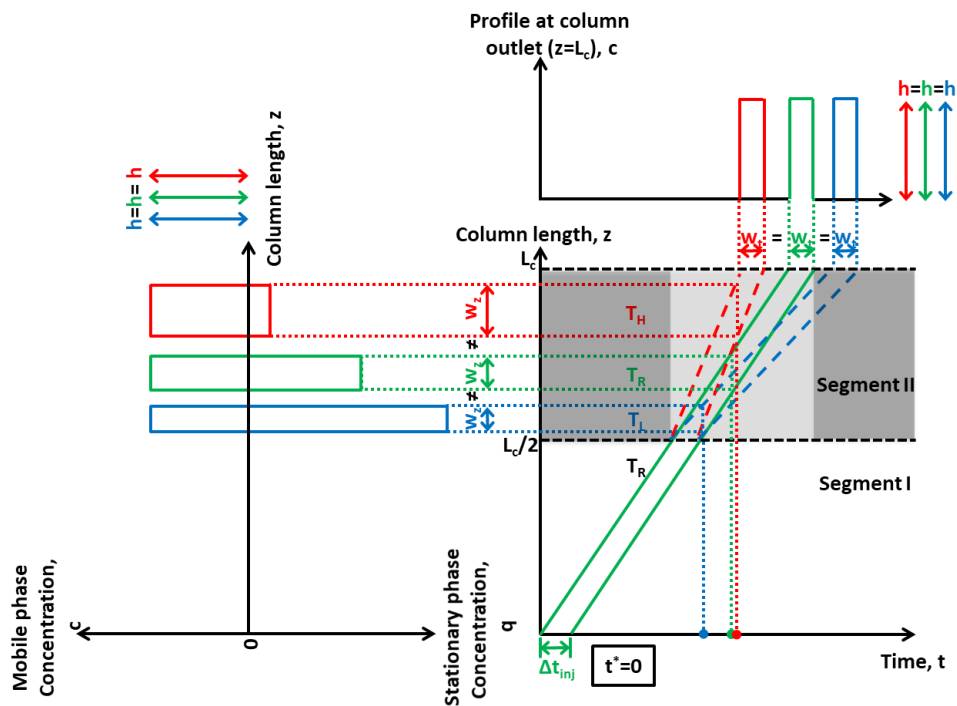
- [127] S. Li, Y. Kawajiri, J. Raisch, A. Seidel-Morgenstern, Optimization of startup and shutdown operation of simulated moving bed chromatographic processes, *J. Chromatogr. A.* 1218 (2011) 3876–3889. <https://doi.org/10.1016/J.CHROMA.2011.04.051>.
- [128] H. Schramm, M. Kaspereit, A. Kienle, A. Seidel-Morgenstern, Simulated moving bed process with cyclic modulation of the feed concentration, *J. Chromatogr. A.* 1006 (2003) 77–86. [https://doi.org/10.1016/S0021-9673\(03\)00327-3](https://doi.org/10.1016/S0021-9673(03)00327-3).
- [129] D.A. Wellings, *A Practical Handbook of Preparative HPLC*, Elsevier Ltd, 2006. <https://doi.org/10.1016/B978-1-85617-466-4.X5000-2>.
- [130] V.J. Barwick, Strategies for solvent selection — a literature review, *TrAC Trends Anal. Chem.* 16 (1997) 293–309. [https://doi.org/10.1016/S0165-9936\(97\)00039-3](https://doi.org/10.1016/S0165-9936(97)00039-3).
- [131] R.H. Perry, D.W. Green, J.O. Maloney, *Perry's chemical engineers' handbook.*, (1997).
- [132] V.R. Meyer, *Practical High-Performance Liquid Chromatography*, John Wiley and Sons, 2010. <https://doi.org/10.1002/9780470688427>.
- [133] J.W. Lee, K.H. Row, Method to predict the bandwidth of elution profile under the linear gradient elution in reversed-phase HPLC, *J. Sep. Sci.* 32 (2009) 221–230. <https://doi.org/10.1002/jssc.200800535>.

Appendix

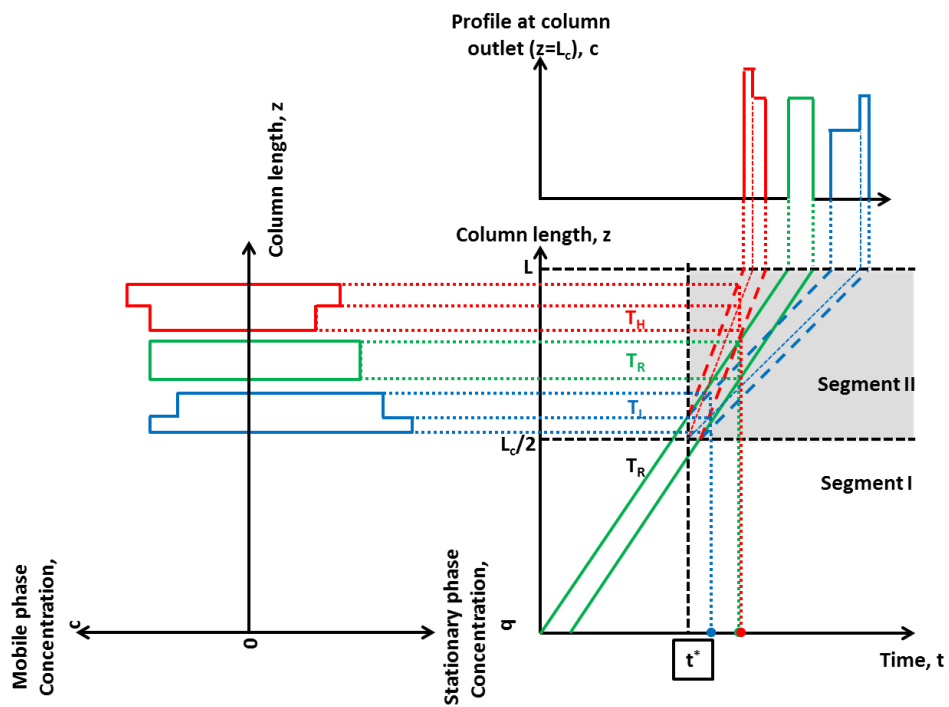
Five appendices are given below to provide supplementary information in different sections.

Appendix 1 Single component behaviour under gradient conditions

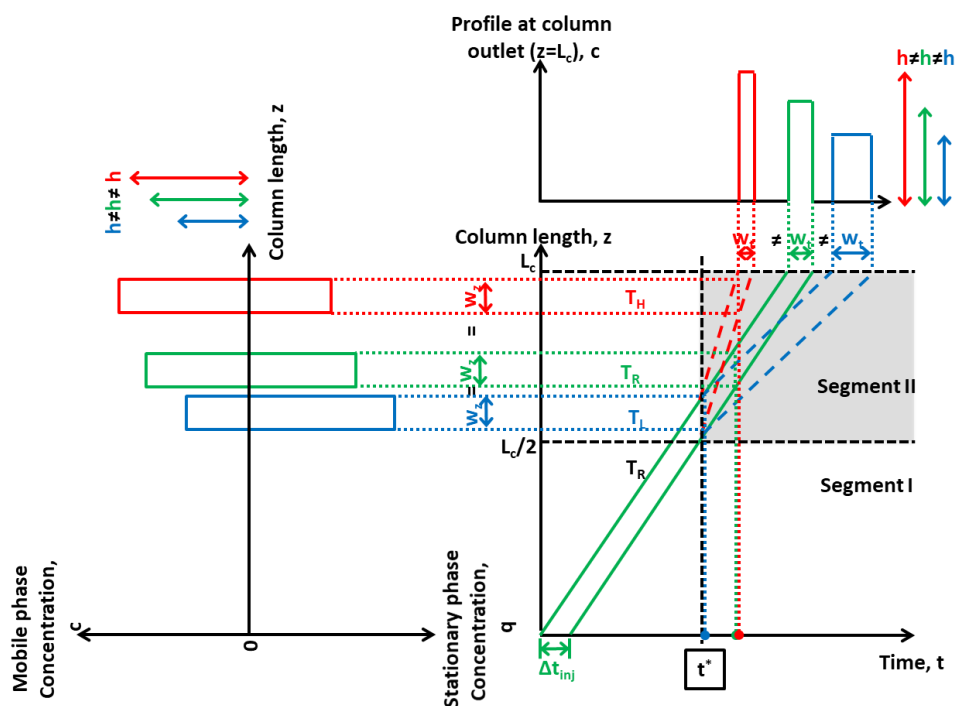
In this appendix, complementary plots of single component behaviours in the physical plane under influence of temperature gradients mentioned in section 6.3.1 are provided. Depending on switch time, the resulting chromatograms are quite different. An additional plot for solvent gradients is given in A. Fig. 4.



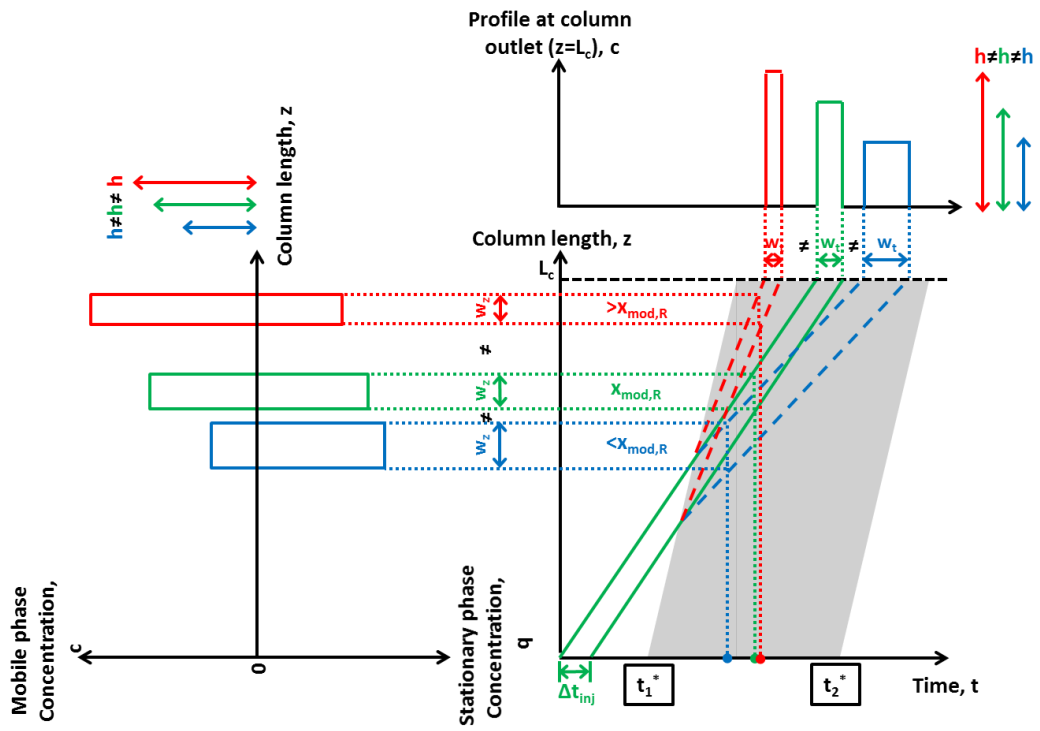
A. Fig. 1 Physical plane of single component migration behaviour under temperature gradients when $t^* = 0$. Green, blue and red colours refer to at temperature T_R , T_L and T_H , respectively. The grey block indicates modulated temperature. Dark grey block indicates invalid zone for switch time in the case at T_R . The chromatogram characterised by the bandwidth over time w_t and concentration height h is shown on the top. The local distributions between the two phases characterised by the bandwidth over space w_z at a certain time is shown on the left.



A. Fig. 2 Physical plane of single component migration behaviour under temperature gradients when $t_R^f(z = f_z L_c) < t^* \leq t_R^r(z = f_z L_c)$. Green, blue and red colours refer to at temperature T_R , T_L and T_H , respectively. The grey block indicates modulated temperature.



A. Fig. 3 Physical plane of single component migration behaviour under temperature gradients when $t_R^r(z = f_z L_c) < t^* \leq t_R^f(z = L_c)$. Green, blue and red colours refer to at temperature T_R , T_L and T_H , respectively. The grey block indicates modulated temperature.



A. Fig. 4 Physical plane of single component migration behaviour under solvent gradients. Green, blue and red colours refer to at modifier fraction $X_{mod,R}$, $X_{mod,L}$ and $X_{mod,H}$, respectively. The grey block indicates modulated modifier fraction.

Appendix 2 Henry's constants

In this appendix, the full data of experimentally determined Henry's constants in a function of temperature and modifier fraction in Eq. (2-9) are provided, which are calculated from retention times in Eq. (3-5).

Henry's constants of C5

T (°C) \ X_{mod}	0.3	0.4	0.5	0.6	0.7
5.88	2.155	1.305	0.794	0.544	0.386
10.72	2.105	1.254	0.765	0.530	0.374
15.55	1.995	1.216	0.738	0.514	0.370
20.42	1.926	1.180	0.730	0.501	0.355
25.24	1.868	1.151	0.692	0.480	0.341
30.11	1.793	1.108	0.686	0.466	0.331
34.99	1.716	1.078	0.659	0.450	0.319
39.91	1.663	1.042	0.638	0.437	0.306
44.74	1.618	0.992	0.600	0.419	0.292
49.60	1.525	0.949	0.595	0.403	0.281
54.50	1.477	0.910	0.570	0.385	0.269
59.35	1.427	0.891	0.552	0.369	0.256

Henry's constants of C6

T (°C) \ X_{mod}	0.3	0.4	0.5	0.6	0.7
5.88	5.539	2.983	1.589	0.969	0.619
10.72	5.317	2.839	1.509	0.938	0.597
15.55	4.937	2.721	1.448	0.906	0.586
20.42	4.754	2.589	1.431	0.880	0.563
25.24	4.572	2.544	1.347	0.839	0.543
30.11	4.329	2.373	1.315	0.812	0.525
34.99	4.074	2.299	1.253	0.781	0.504
39.91	3.922	2.195	1.206	0.749	0.487
44.74	3.738	2.047	1.139	0.716	0.463
49.60	3.478	1.959	1.105	0.691	0.446
54.50	3.270	1.876	1.055	0.661	0.427
59.35	3.130	1.786	1.012	0.634	0.408

Henry's constants of C7

T ($^{\circ}\text{C}$) \ x_{mod}	0.3	0.4	0.5	0.6	0.7
5.88	14.038	6.793	3.223	1.769	1.024
10.72	13.173	6.431	3.046	1.700	0.982
15.55	12.175	6.079	2.880	1.633	0.960
20.42	11.657	5.724	2.808	1.580	0.919
25.24	11.306	5.529	2.634	1.488	0.880
30.11	10.377	5.121	2.552	1.434	0.850
34.99	9.572	4.871	2.403	1.368	0.813
39.91	9.170	4.618	2.282	1.311	0.784
44.74	8.533	4.263	2.127	1.238	0.745
49.60	7.830	4.020	2.063	1.185	0.713
54.50	7.322	3.806	1.945	1.128	0.678
59.35	6.901	3.628	1.854	1.073	0.650

Appendix 3 Derivation of analytical solution for short-cut energy balance

In this appendix, the derivation procedure of the analytical solution of temperature profile in Eq. (2-57) is shown.

The Eq. (2-56) is transformed by

$$\frac{\partial T}{\partial \tau} = a \frac{\partial T}{\partial x} - bX_2 + c \quad (\text{A. 1})$$

where $a = -X_1$, $b = -t_0X_2$ and $c = t_0X_2T_w$. The initial and boundary conditions are

$$T(\tau = 0, x) = T_0 \quad (\text{A. 2})$$

$$T(\tau, x = 0) = T_0 \quad (\text{A. 3})$$

By forward transformation

$$sY - T_0 = a \frac{dY}{dx} + bY + \frac{c}{s} \quad (\text{A. 4})$$

By rearranging

$$\frac{dY}{dx} = \frac{s-b}{a}Y + \frac{-T_0 - c/s}{a} = AY + B \quad (\text{A. 5})$$

where $A = (s-b)/a$, $B = -[T_0/a + c/(sa)]$, and thus $B/A = -T_0(s-b) - c/[s(s-b)]$.

By rearranging and integrating both sides

$$\int_{T_0/s}^{Y(x,s)} \frac{dY(x,s)}{AY + B} = \int_0^1 dx \quad (\text{A. 6})$$

By solving and rearranging

$$Y(x,s) = -\frac{B}{A} + \left(\frac{T_0}{s} + \frac{B}{A}\right)e^{Ax} \quad (\text{A. 7})$$

By substituting A and B, it finally becomes

$$Y(x,s) = \frac{T_0}{s-b} + \frac{c}{s(s-b)} + \left[\left(T_0 + \frac{c}{b}\right)e^{-\frac{b}{a}x}\right] \frac{e^{\frac{x}{a}s}}{s} - \left[\left(T_0 + \frac{c}{b}\right)e^{-\frac{b}{a}x}\right] \frac{e^{\frac{x}{a}s}}{s-b} \quad (\text{A. 8})$$

By backward transformation

$$T(\tau, x) = \begin{cases} T_w - (T_w - T_0)e^{-t_0X_2\tau} & \tau \leq \frac{x}{X_1} \\ T_w - (T_w - T_0)e^{-t_0\frac{X_2}{X_1}x} & \tau \geq \frac{x}{X_1} \end{cases} \quad (\text{A. 9})$$

In section 4.5, the determination method for X_1 and X_2 is described.

Appendix 4 Characteristic times

In this appendix, switch times and the start time for next injection according to different operating regimes in section 6.3.2 and section 6.4 are summarised.

Gradient	Regime	Profile*	$t_{1}^{*,k=1}$	$t_{2}^{*,k=1}$	$t_{3}^{*,k=1}$	$t_{1}^{*,k=2}$	$t_{2}^{*,k=2}$	$t_{inj}^{k=2}$
			min	min	min	min	min	min
Temperature	Conservative	EM	11.2	18.6	-	25.0	32.7	13.9
	(Figure 6-5)	EXP	12.5	20.5	-	28.0	35.8	15.5
	Improved	EM	11.2	18.6	-	20.2	28.2	9.5
	(Figure 6-6)	EXP	12.5	20.5	-	23.5	32.0	11.5
Solvent	2-step	EM	5.0	7.5	-	-	-	7.5
	(Figure 6-8)	EXP	6.6	9.6	-	-	-	9.6
	3-step	EM	5.0	6.8	8.4	-	-	8.4
	(Figure 6-9)	EXP	6.6	8.6	10.3	-	-	10.3

*EM: equilibrium model; EXP: experimental profile.